Magneto-Spatial Dispersion Phenomena

Photonic Band Gaps and Chirality in Magneto-Optics

Dissertation

zur Erlangung des akademischen Grades des
Doktors der Naturwissenschaften
an der Universität Konstanz
Fachbereich Physik

vorgelegt von

Clemens Koerdt

geboren in Werl

Tag der mündlichen Prüfung: 1.10.2004

Referent: Prof. Dr. P. Wyder (Grenoble)
Referent: Prof. Dr. G. Schatz

Konstanz, 2004

Contents

List of Figures

List of Tables

General Introduction

During the last century, the knowledge acquired about electrons and their behavior in matter has brought about a boost of technology that proved revolutionary for mankind. This success has put scientific research on such a level of importance, that in every major industrialized country research and development now constitute a sizable share of the economy.

More scientific breakthroughs are expected to follow suit. If many people think of biology to take up the torch in the long run, in the medium term industries related to modern optical technology are expected to have one of the highest growth rates, with actual markets already the size of hundreds of billions of dollars. A sound knowledge in photon-matter interaction is essential. Basic research thus plays the underlying part that will keep the process going.

Optics is an already old and important part of physics, that has recently rejuvenated, mainly due to the invention of the laser. Modern research in the field of optics aims to control the flow of light. Exiting new technologies are being developed to produce high-end optical components for a wide spectrum of industries, from electronics and telecommunications to healthcare. The complexity of the involved optical effects has considerably increased the interest in a sound understanding of classical optics and special topics therein, like magneto-optics.

Magneto-optics deals with phenomena arising as a result of interaction between light and matter that is subject to a magnetic field. The dispersion curves of the medium are changed by the presence of a magnetic field and leads to the appearance or modification of optical anisotropy. Optical anisotropy can be interpreted as the lifting of the degeneracy of the two possible polarization states of the light. Their energy level splits up in an external magnetic field due to the Zeeman effect. The optical anisotropy manifests itself as dichroism, i.e. the difference between the absorption coefficients for the two orthogonal polarizations, and birefringence, that is the difference between the refractive indices.

The Faraday effect can be seen in the rotation of the plane of polarization of linearly polarized light that has propagated through a medium in the presence of a magnetic field. This is the result from a difference of the refractive indices between right- and left-circularly polarized light and the fact that linearly polarized light can be constructed as the sum of a right- and a left-circularly polarized light beam.

The same rotation of polarization happens phenomenologically in optical activity. The birefringence here is the result of a molecular helical structure in optically active substances and needs no magnetic field.

The Faraday effect and optical activity are known for a hundred years. However, new optical effects are still found in our days. An examples is the magneto-

chiral anisotropy, observed in dichroism (Rikken and Raupach, 1997 [RR97]) and in birefringence (Valet et al., 2001 [KW98, VGF+01]). The magneto-chiral anisotropy can be regarded as a cross-effect of the Faraday effect and optical activity. With the help of the magneto-chiral anisotropy, magnetic fields can discriminate between media that have a right- or left-handed helical structure, and that regardless of the polarization state of the light. The dielectric constant for a chiral medium with an applied magnetic field will differ depending if the light travels parallel or antiparallel to the magnetic field.

Symmetry considerations play an important part and have been used to predict theoretically this new effect [BZ79]. The possible symmetry groups of a crystal in the presence of a magnetic field not only contain the usual rotations, reflections and translations, but also the time reversal symmetry. An external magnetic field breaks this time reversal symmetry. Optically active substances lack the mirror symmetry. And it is this symmetry breaking that is at the origin of new phenomena. During the work of this thesis, I studied systems, where the time reversal symmetry was broken and in combination with other fundamental symmetries broken: the mirror symmetry and the translational symmetry.

An interesting new form of optical materials can be found in so called photonic crystals. Their design is based on the principle to construct for photons the same periodic spatial pattering in the potential energy that electrons encounter in an ordinary crystal lattice. The forbidden energy gap of electronic states in a semiconductor is the result of a coherent superposition of electron wave functions that are scattered at the regular array of nuclei. This coherent scattering is Bloch's theorem. The same theorem holds for the electromagnetic case in a periodic potential. Photonic crystals achieve just that by a variation of the refractive index on a length scale that is of the order of the light's wavelength. An incident wave is diffracted by the periodic structure and forms optical modes that have the periodicity of the lattice. For certain frequencies the incident light is Bragg reflected and cannot enter the crystal. The absence of extended light modes for those frequencies is called a photonic band gap following the corresponding term of the electronic case. Photonic crystals no longer have the continuous translational symmetry of a homogeneous material. They conserve however a discrete translational symmetry.

Photonic crystals can manipulate the flow of light, making them attractive materials for new types of optical components [JVF97].

There was a lack of both experimental and theoretical studies on photonic crystals subject to an external magnetic field. So we considered it is time to study the magneto-optics of those materials.

Photonic Band Gaps in Magneto-optics is the second chapter of this thesis. I developed a simulation method, by which it was possible to study transmission and Faraday rotation, as well as other magneto-optical properties of one dimensional photonic crystals. The simulations revealed a derivative type spectral shape of the Faraday rotation around the photonic band gap with peaks of opposite signs at the edges of the band gap. It was also observed that around specially designed defects the Faraday rotation peaks very sharply and that the peak splits into two peaks for high magnetic fields. So far there is no method to simulate numerically magneto-optical effects in three dimensional photonic crystals and I turned to measurements

instead. Different kind of photonic crystals samples, that were kindly provided by several contacted groups, had been examined and I made efforts to produce some of my own. I show how I prepared magneto-optically active samples and how a highly sensitive experiment was set up, with which it was possible to measure the Faraday rotation even for frequencies inside the photonic band gap, for which transmission is extremely low. Numerous difficulties had to be overcome in order to detect the coherently scattered part of the transmitted light in a noisy background of diffusively scattered light. Finally, I was able to measure the Faraday rotation throughout the photonic band gap and beyond. This constitutes the first magneto-optical measurement on photonic crystals. I observed that the Faraday rotation outside the photonic band gap has the usual behavior of a paramagnetic liquid. For frequencies inside the photonic band gap, however, the Faraday rotation shows a resonant enhancement. I interpret the result as being due to multiple internal reflections and the well-known fact that the Faraday rotation is cumulative under reflection. This result suggests that photonic crystals could replace the so far rather bulky Faraday rotators, as they are used in optical diodes, to build a more compact device for integrated optics. Apart from possible application, the obtained result calls for the development of a fully three dimensional scattering theory, that is able to work under a broken time reversal symmetry. Additionally, it can now be expected that similar resonant behavior occurs in other magneto-optical effects.

If a system lacks the mirror symmetry, it is called a *chiral* system. The study of chirality is an important and still hotly investigated part not only in physics, but also in chemistry and biology. An example here is the synthesization of purely homochiral[1] substances that is still a challenging technological undertaking in modern pharmacology. The need for purely homochiral substances is related to the fact that biological life itself is homochiral, i.e. only left-handed amino-acids and only right-handed sugars are found. The origin of this homochirality of life is still unknown and the existence of magneto-chiral anisotropy is discussed as one possibility of this imbalance [RR00].
However, the observed magnitude of the magneto-chiral anisotropy makes this hypothesis unlikely, unless there is additionally a process of amplification involved. *Chiral Symmetry Breaking in Photo-crystallization* is the third chapter of this thesis. In this chapter I show measurements that proof the existence of such an amplification mechanism in the crystallization of chiral substances influenced by light (photo-crystallization).

In the production of chiral substances from solutions the chiral symmetry is usually conserved in the way that both kinds of handedness are produced in statistically equal amounts. I found that by irradiating an aqueous solution of nickel sulfate, I was able to break this chiral symmetry. By changing between right- and left-circularly polarized light, I produce an excess of crystals with respectively right- or left-handed symmetry. So in contrast to a reported spontaneous chiral symmetry breaking in stirred solutions [KLA99], this one is controllable and induced.

The nickel sulfate crystals show optical activity and in so far present already

[1] Homochirality means *singlehandedness*, i.e. the absence of one out of two possible mirror images.

an anisotropy. The absorption anisotropy of the two mirror images is in the order of 8%, whereas the produced excesses come close to a complete elimination of one handedness. Therefore, photo-crystallization has been identified by us to act as an amplification mechanism for chiral anisotropy. The photo-crystallization experiment has been performed under a great variety of experimental conditions. The handling of the experiment is not easy and a proper preparation of the initial crystallization conditions is rather delicate.

I propose a model that is able to correctly predict the sign of the produced excesses.

I show further that the same mechanism should in principle work for the amplification of the magneto-chiral anisotropy instead of optical activity. To amplify the magneto-chiral anisotropy one has to use unpolarized light in combination with a surrounding magnetic field. The excess would then be controllable by the orientation of the magnetic field relative to the projected light beam.

Since very high magnetic fields in combination with unpolarized light can be found in the vicinity of neutron stars, the hypothesis of the magneto-chiral anisotropy being responsible for the evolution of the homochirality of life would be strengthened.

Further more, modern pharmacology can be interested in the photo-crystallization process for the technologically challenging production of homochiral substances, that have become the norm of new drugs reaching the market today.

Liquid crystals exhibit a state of order that is in between crystals and liquids. They combine the fluidity of a liquid - and have thus imperfect long range order - with anisotropic properties of a crystal, due to a certain molecular orientation. Liquid crystals in its form of cholesterics show a helical structure in their collective molecular orientation [DGG+98, KH80] and therefor lack mirror symmetry. I emphasize in this thesis that cholesteric liquid crystals can be considered as chiral photonic crystals, in which both the chiral symmetry and the continuous translational symmetry are broken. Along the optical axis of the cholesteric liquid crystals the structure is periodic and acts as a one dimensional photonic crystal. The crystals exhibit a photonic band gap for wavelengths that correspond to the pitch of such helices. *Magneto-chiral anisotropy in Bragg scattering* is the fourth chapter of this thesis. In this chapter I show experimentally that light scattering in cholesteric liquid crystals shows strongly resonant magneto-chiral anisotropy near the Bragg resonance. The optical transmission of unpolarized light depends linearly on an external longitudinal magnetic field and on the handedness of the medium. I therefore found in resonant Bragg scattering another amplification mechanism for the magneto-chiral anisotropy. The main difficulty in this experiment was the preparation of high quality liquid crystal samples, especially those of the right-handed kind and to provide a sufficiently stable environment for the measurements.

A theoretical framework for the observed phenomena is presented in the first chapter of this thesis. I summarize in this chapter the main points surrounding the form of the dielectric constant and its symmetry following in most parts a well respected textbook [LLP84]. By the help of the presented theoretical framework I have been able to put all observed aspects of the present dissertation into a

common perspective and to provide the essential analytical tools.

The description of light interaction with dielectrics is essentially done by relating the electric and magnetic fields $\mathbf{E}, \mathbf{H}$ with the electric and magnetic inductions $\mathbf{D}, \mathbf{B}$. By avoiding ferromagnetic materials one can approximate the magnetic permeability by one $\mu = 1$. The whole magneto-optics can then be done by the sole study of the form of the dielectric function ε. The symmetry considerations are of particular importance in such a study. The dielectric constant becomes wavelength dependent if one takes into account (frequency) dispersion. To include anisotropies in the medium the dielectric constant becomes a tensor and its elements might be complex valued, if I wish to incorporate absorption. *Spatial dispersion* means the dielectric constant is also depending on the wavevector $\mathbf{k}$ and has at its origin a *non-local* relation between the electric induction $\mathbf{D}(\mathbf{r})$ and the electric fields at and around the point $\mathbf{r}$ in space. Usually, spatial dispersion is a very small effect. As I will show in the first chapter spatial dispersion is potentially much larger in photonic crystals. Finally, the term *magneto-spatial dispersion* is used, if the dielectric function is also dependent on an externally applied magnetic field [PB71, KZ77].

The title *Magneto-Spatial Dispersion Phenomena* was chosen because it nicely covers the three somewhat distinct parts of this thesis, which are *Photonic Band Gaps in Magneto-optics, Chiral Symmetry Breaking in Photo-crystallization, and Magneto-Chiral Anisotropy in Bragg Scattering.*

In general, situations were studied, in which one or several fundamental symmetries are broken; in chiral systems it is the *parity* that is broken; magnetic fields break the *time reversal symmetry*; and a periodic dielectric constant is breaking a *continuous translational symmetry* into a discrete one. Apart from a reduced symmetry, one encounters problems related to *nonlocality*, i.e. spatial dispersion, as well as resonance phenomena.

Chapter 1

Magneto-Spatial Dispersion: Theoretical Framework

This section introduces the theoretical framework of magneto-spatial dispersion. It is largely based on Landau and Lifshitz' *Electrodynamics of Continuous Media* [LLP84].

1.1 Dielectric properties of matter

Dielectrics are called media in which no steady current can flow, in contrast to *conductors*. The microscopic fields follow the Maxwell equations and are usually averaged in media to allow for a macroscopic description of the electrodynamics.

$$\nabla \cdot \mathbf{B} = 0 \qquad (1.1), \qquad \nabla \times \mathbf{E} + \frac{1}{c}\frac{\partial \mathbf{B}}{\partial t} = 0 \qquad (1.2)$$

$$\nabla \cdot \mathbf{D} = 0 \qquad (1.3), \qquad \nabla \times \mathbf{H} - \frac{1}{c}\frac{\partial \mathbf{D}}{\partial t} = 0 \qquad (1.4)$$

Together with Maxwell's equations in matter Eqs. (1.1)-(1.4), the description of dielectrics is then completed by the following equations relating the electric field $\mathbf{E}$ to the *electric induction* $\mathbf{D}$ and the magnetic field $\mathbf{H}$ to the *magnetic induction* $\mathbf{B}$:

$$\mathbf{D} = \mathbf{E} + 4\pi\mathbf{P} = \varepsilon\mathbf{E} \qquad (1.5)$$

$$\mathbf{B} = \mathbf{H} + 4\pi\mathbf{M} = \mu\mathbf{H} \qquad (1.6)$$

$\mathbf{P}$ is called the *(dielectric) polarization* and $\mathbf{M}$ is the *magnetization*. The polarization is the density of the *electric moment* of the dielectric, whereas the magnetization is the density of the *magnetic moment*.

Instead of dealing with the densities of the electric and magnetic moments, it is convenient to introduce the *dielectric constant* ε[1]and the *magnetic permeability* μ.

The reason for this formulation lies in the fact that in a great majority of cases the dielectric and magnetic permeabilities do not depend on the fields. The

[1]Other common names for ε are *permittivity*, *dielectric permeability*, or *dielectric function*.

relations between the fields and the inductions are then simply linear, which significantly simplifies any calculation. This approximation is justified, if the external fields are small compared to the internal molecular fields. It then corresponds to the first term of an expansion of the permeabilities in powers of the fields. For a finer approximation higher order terms should then be taken into account.

For ordinary diamagnetic and paramagnetic media, the magnetic permeability μ is very close to one and can therefore be approximated by that value.

1.2 The form of the dielectric *constant*

Only in the simplest case can the dielectric constant be regarded as a simple scalar. Apart from the condition–as mentioned above–that the relation between the electric induction $\mathbf{D}$ and the electric field $\mathbf{E}$ be linear, the dielectric also has to be isotropic. Additionally, the involving fields should be static or at least *quasistatic*, that means they should change *sufficiently slow* over time. In any other case the form of the dielectric constant becomes more complicated. This will be discussed in the following subsections.

1.3 Frequency dispersion

In case of rapidly varying electromagnetic fields, whose frequencies are not restricted to be small in comparison with the eigenfrequencies of the molecular vibrations or the electronic transitions, *dispersion* occurs.

For very high frequencies ω the wavelength $\lambda = c/\omega$ approaches microscopic dimensions a, where the macroscopic description is no longer valid. If still $\lambda \gg a$, one can continue using the macroscopic theory, but has to introduce dispersion phenomena. The polarization cannot keep pace with a rapidly varying electromagnetic field and $\mathbf{D}$ is not instantaneously following $\mathbf{E}$, but depends also on fields at previous times:

$$\mathbf{D}(t) = \mathbf{E}(t) + \int_0^\infty f(\tau)\mathbf{E}(t-\tau)\,d\tau \tag{1.7}$$

If Fourier transformed, this states:

$$\mathbf{D}(\omega) = \varepsilon(\omega)\mathbf{E}(\omega) \quad \text{with} \quad \varepsilon(\omega) \equiv 1 + \int_0^\infty f(\tau)e^{i\omega\tau}\,d\tau \tag{1.8}$$

The dependence of ε on the frequency is called the *dispersion relation*. In this case $\varepsilon(\omega)$ is mostly referred to as the *dielectric function*.

1.4 Absorbing media

The dielectric function $\varepsilon(\omega)$ is generally complex valued:

$$\varepsilon(\omega) = \varepsilon(\omega)' + i\varepsilon(\omega)'' \tag{1.9}$$

In such a way, absorbing media can be included in the description. The relation to the *refractive index* n and the *absorption coefficient* κ, which gives the rate of damping of an electromagnetic wave inside this medium, is:

$$\sqrt{\varepsilon} = n + i\kappa \tag{1.10}$$
$$\varepsilon' = n^2 - \kappa^2 \tag{1.11}$$
$$\varepsilon'' = 2n\kappa \tag{1.12}$$

However, damping of a wave ($\kappa \neq 0$) can be present even without true absorption ($\varepsilon'' \neq 0$).

1.5 Analytical properties of the dielectric function

The real and imaginary part of the dielectric function are not completely independent, but are related by the *Kramers-Kronig formula*:

$$\varepsilon'(\omega) - 1 = \frac{1}{\pi}\mathcal{P}\int_{-\infty}^{+\infty} \frac{\varepsilon''(\omega')}{\omega' - \omega} d\omega' \tag{1.13}$$

$$\varepsilon''(\omega) = -\frac{1}{\pi}\mathcal{P}\int_{-\infty}^{+\infty} \frac{\varepsilon'(\omega') - 1}{\omega' - \omega} d\omega'. \tag{1.14}$$

Other properties are

$$\varepsilon(-\omega) = \varepsilon^*(\omega), \tag{1.15}$$
$$\varepsilon(\omega) \geq 1, \tag{1.16}$$
$$\varepsilon(\omega \to \infty) \to 1. \tag{1.17}$$

1.6 Anisotropic media

In an anisotropic medium the vectors $\mathbf{D}$ and $\mathbf{E}$ are not necessarily collinear. ε then takes the form of a tensor of rank two and is called the *dielectric tensor*, whose elements ε_{ik} are given by:

$$D_i = \varepsilon_{ik} E_k \tag{1.18}$$

Without an external magnetic field, the dielectric tensor is symmetrical:

$$\varepsilon_{ik}(\omega) = \varepsilon_{ki}(\omega) \tag{1.19}$$

By a suitable choice of coordinates, the tensor can be diagonalized and only three independent values ε_x, ε_y and ε_z remain.

Crystals are said to be *biaxial* if all three principal values of the dielectric tensor are different. This is the case for crystals of *triclinic*, *monoclinic* and *orthorhombic* symmetries.

Uniaxial crystals have only two independent quantities. They are of the *tetragonal*, *rhombohedral* and *hexagonal* types.

Cubic systems behave like *isotropic* bodies, and the dielectric tensor is then determined by only one single scalar (or function for dispersive media).

1.7 Magneto-optical effects

Applying an external magnetic field $\mathbf{B}$ changes the symmetry of the dielectric tensor. In fact, in the presence of an external magnetic field, the time-reversal symmetry in no longer valid.

The symmetry of $\hat{\varepsilon}(\omega, \mathbf{B})$ with respect to the field is:

$$\hat{\varepsilon}_{ik}(\mathbf{B}) = \hat{\varepsilon}_{ki}(-\mathbf{B}) \tag{1.20}$$

Even without absorption, $\varepsilon(\omega, \mathbf{B})$ now has an imaginary part and takes the form:

$$\hat{\varepsilon}(\omega, \mathbf{B}) = \hat{\varepsilon}'(\omega) + i\hat{\varepsilon}''(\omega) + i\hat{\varepsilon}'''(\omega, \mathbf{B}) \tag{1.21}$$

The tensors $\hat{\varepsilon}'$ and $\hat{\varepsilon}''$ are symmetrical, whereas $\hat{\varepsilon}'''$ is anti-symmetrical. The reason for the latter is that for any axial vector, like $\mathbf{B}$, one can find an equivalent anti-symmetrical tensor of rank two[2].

The principal magneto-optical effects are discussed later in section 2.3.

1.8 Spatial dispersion

Spatial dispersion is connected with a *non-local* relation between the induction $\mathbf{D}(t, \mathbf{r})$ and the electric fields at and around the point $\mathbf{r}$ in space. Together with the frequency dispersion (1.7) one obtains:

$$\mathbf{D}_i(t, \mathbf{r}) = \mathbf{E}_i(t, \mathbf{r}) + \int_0^\infty \int f_{ik}(\tau, \mathbf{r}, \mathbf{r}')\mathbf{E}_k(t - \tau, \mathbf{r}')\, d\tau\, d\mathbf{r}' \tag{1.22}$$

Fourier transformed with the use of a full set of monochromatic plane waves of the form $\mathbf{E}(t, \mathbf{r}) = \int\int \mathbf{E}(\omega, \mathbf{k}) e^{i(\mathbf{k}\cdot\mathbf{r} - \omega t)}\, d\mathbf{k}\, d\omega$, the dielectric tensor can be defined as

$$\varepsilon_{ik}(\omega, \mathbf{k}) = \delta_{ik} + \int_0^\infty \int f_{ik}(\tau, \mathbf{r}, \mathbf{r}') e^{i(\mathbf{k}\cdot\mathbf{r}' - \omega\tau)}\, d\tau\, d\mathbf{r}', \tag{1.23}$$

so that the relation now reads $\mathbf{D}_i(\omega, \mathbf{k}) = \varepsilon_{ik}(\omega, \mathbf{k})\mathbf{E}_k(\omega, \mathbf{k})$.

Spatial dispersion is present when the macroscopic properties of a medium depend on the spatial inhomogeneity of the electromagnetic field. One principal manifestation is that the wave vector $\mathbf{k}$ now defines a distinctive direction in the medium and reduces the symmetry of the dielectric tensor accordingly.

In general, the magnitude of spatial dispersion is not very important. But the changed symmetry brings with it new physical phenomena. One of those is for example *natural optical activity*, which is treated in some detail in Sec. 3.3.

For wavelengths in the vicinity of an absorption peak, spatial dispersion can become quite large.

[2]However, $\hat{\varepsilon}'''$ is not *exactly* a corresponding anti-symmetrical tensor to $\mathbf{B}$.

1.9 Inhomogeneous media

The statements of the preceding sections are, strictly speaking, only valid for homogeneous and infinitely extended media. In inhomogeneous media one has to deal with phenomena like scattering, or reflection and refraction on interfaces. If the inhomogeneities are on a macroscopic scale l that is large with respect to the wavelength $l \gg \lambda$, the theory is still applicable. One has just the additional task of calculating (separately) the fields (incoming fields as well as scattered, reflected, and refractive fields) for each homogeneous part in a piecewise fashion.

The situation is different when the inhomogeneities are on a scale that is comparable to the wavelength. A treatment for such a case is difficult to incorporate into the formalism. There is however a special case, the one of periodic inhomogeneities. Photonic crystals (see chapter 2), for example, fall into that category. They can be interpreted as homogeneous media that exhibits large spatial dispersion (Sec. 1.8). So instead of dielectric function for each component one is dealing with a single one, but one that is now depending on the wavevector $\mathbf{k}$.

1.10 Magneto-spatial dispersion

Is, additionally to spatial dispersion, an external magnetic field present, the dielectric tensor needs an anti-symmetrical component to compensate the axial vector $\mathbf{B}$. A generalized form of Eq. (1.21) gives

$$\hat{\varepsilon}(\omega, \mathbf{k}, \mathbf{B}) = \hat{\varepsilon}'(\omega, \mathbf{k}) + i\hat{\varepsilon}''(\omega, \mathbf{k}) + i\hat{\varepsilon}'''(\omega, \mathbf{k}, \mathbf{B}). \tag{1.24}$$

Again, the tensors $\hat{\varepsilon}'$ and $\hat{\varepsilon}''$ are symmetrical, whereas $\hat{\varepsilon}'''$ is anti-symmetrical.

1.11 The dielectric tensor and its expansion in k and B

It was shown that the dielectric tensor for non-magnetic media in presence of magneto-spatial dispersion is a function of frequency, the wave propagation vector and the external magnetic field, $\hat{\varepsilon}(\omega, \mathbf{k}, \mathbf{B})$.

The influence of spatial dispersion and not too high magnetic fields can be treated as perturbations, which allows to expand the dielectric tensor in powers of $\mathbf{k}$ and $\mathbf{B}$ [PB71]:

$$\begin{aligned} \varepsilon_{ik}(\omega, \mathbf{k}, \mathbf{B}) &= \varepsilon_{ik}(\omega) + \alpha_{ikl}(\omega)k_l + \beta_{ikl}(\omega)B_l \\ &+ \gamma_{iklm}(\omega)k_l B_m + \chi_{iklm}(\omega)k_l k_m + \xi_{iklm}(\omega)B_l B_m \end{aligned} \tag{1.25}$$

The zero order term is the dielectric tensor for a uniform electromagnetic field ($k \to 0$) and for a vanishing external magnetic field ($\mathbf{B} = 0$). The tensors $\hat{\alpha}, \hat{\beta}, \hat{\gamma}, \hat{\chi}$ and $\hat{\xi}$ are material parameters and reflect the underlying symmetry of the system (crystal group + wave propagation direction).

Chapter 2

Photonic Band Gaps in Magneto-Optics

2.1 Introduction

The field of photonic crystals (or photonic band gap materials: PBG) is a rather new one, but it has developed quickly during the last decade. Interest is high and there are challenges to be found in abundance. When my project was started, there were no reports of experiments that connect photonic crystals with magnetic fields, nor was there any theory. The major challenge was still the fabrication of those crystals and the control of their optical properties.

The effects of magnetic fields on the propagation of light in photonic crystals are still unresolved. The usual methods to calculate dispersion relations and transmission [PK92, HCS90] fail, when time-symmetry is broken by an applied magnetic field. Even the simple case of light scattering by single spheres in magnetic fields has only recently been calculated for the first time [LvTRS98].

The interface between two dielectric media with different dielectric constants constitutes a dispersive element for a wave packet. When it comes to photonic band gap materials, there are a lot of these interfaces and the effects can be particularly high for waves, whose wavelength is commensurate to the interface periodicity and are thus able to coherently interact with the whole structure. A magnetic field will destroy the time reversal symmetry and as such is having its impact on the coherence of the wave scattering.

At the resonance wavelength, where the Bragg condition holds, light will be subject to multiple internal refraction as much as in a Fabry-Pérot resonator [LOT97]. High Faraday effects could then be expected for photonic crystals subject to a magnetic field and with a Faraday active component. Colloidal photonic crystals (also called opals) were supposed to be easily infiltrated by liquids, which contain rare earth elements. An elucidation of the spectral behavior of Faraday rotation in photonic crystals should then help to predict the outcome of other magneto-optical effects. One of those is, for example, a suspected increased transverse diffusion of light in such periodic structures (s. [RvT96]).

After an introduction into the concept of photonic crystals and stating the related fundamental magneto-optical equations I present here my simulations in

one dimensional PBGs. From this I talk about the design of my experiment in three dimensional samples. I present the Faraday rotation and magnetic circular dichroism measurements, that are discussed in some detail. Some considerations are given at the end of the chapter that should be taken into account when it comes to the construction of a theory incorporating effects of external magnetic fields in the magneto-optics of photonic crystals.

2.2 Photonic band gaps

In recent years, photonic crystals have been the subject of intensive theoretical and experimental studies. Their periodic dielectric structure (see Fig. 2.2) result in Bloch-like electro-magnetic waves inside the crystal with a stopband in their frequency spectrum for certain propagation directions and sometimes even a genuine gap with a vanishing density of states.

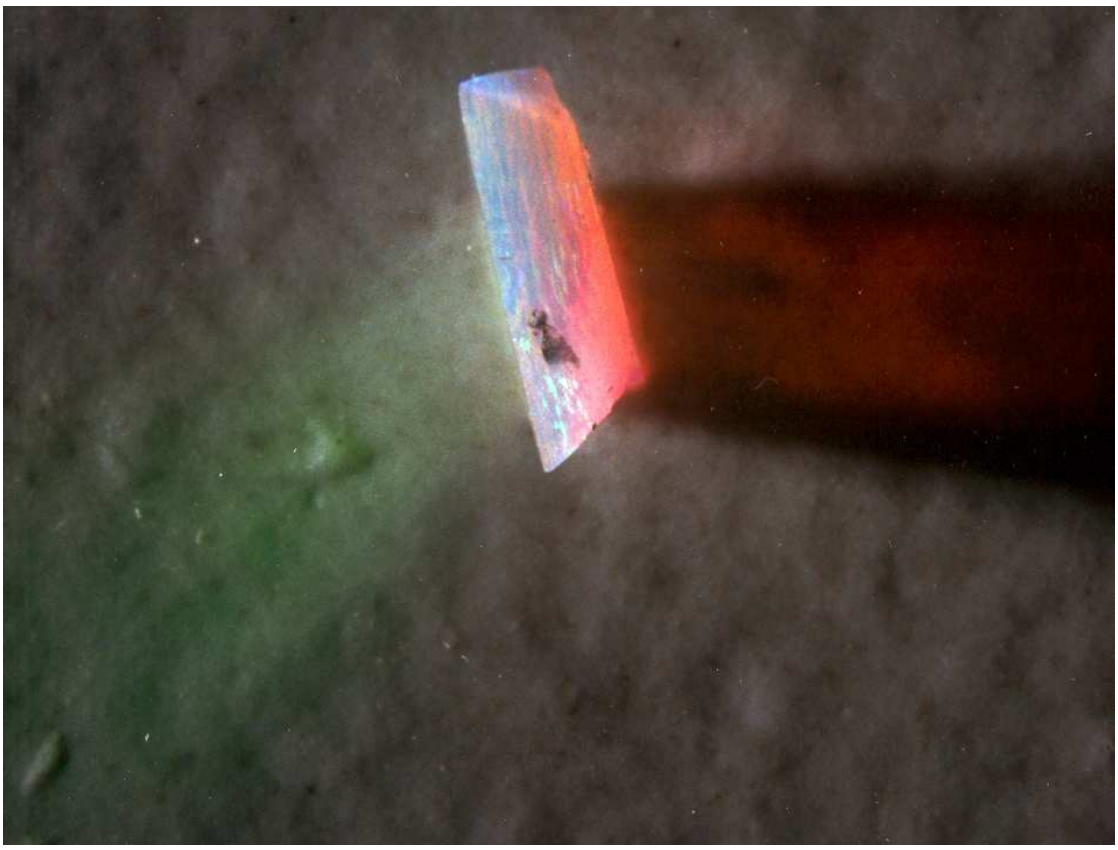

Figure 2.1: *Photonic crystal with a stopband in the green wavelength region when illuminated from the left with white light.*

Fig. 2.1 is a photography of one of my photonic crystals. It has its stopband in the green wavelength region. White light is falling on the sample from the left. The transmitted light is red, since the the green component is not allowed to enter

the crystal and is reflected. The borders appear blue, this is due to scattering of light on defects, which is more pronounced for waves having a short wavelength.

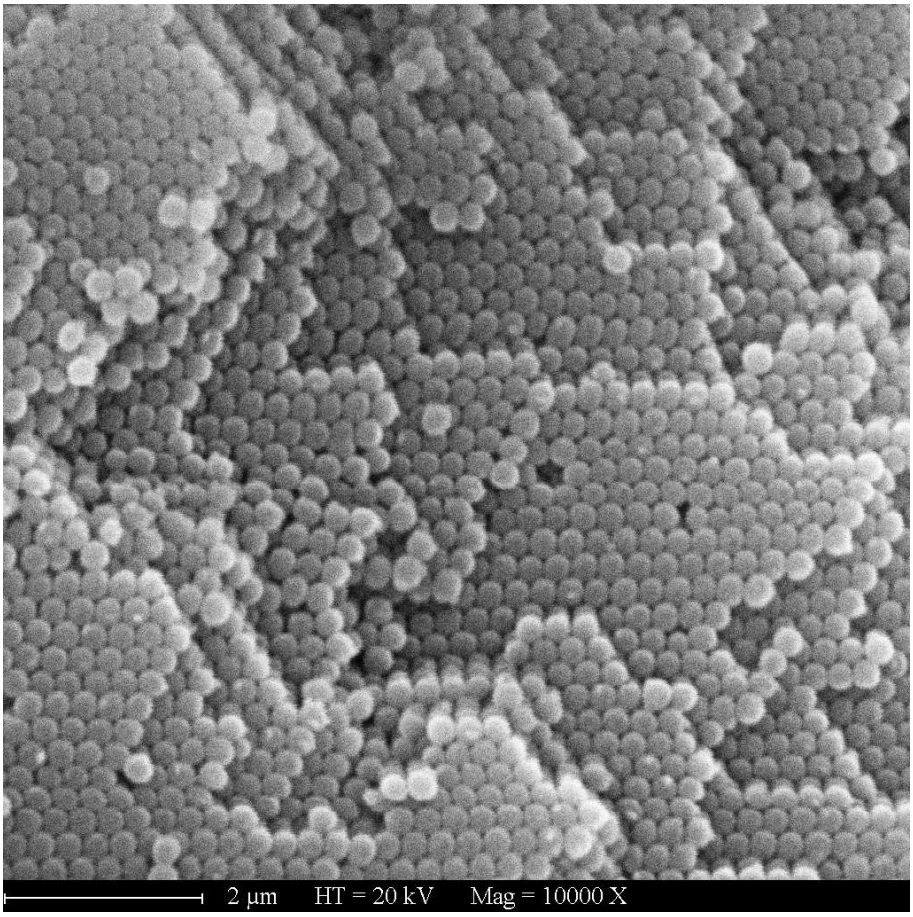

Figure 2.2: *Scanning Electron Microscopy (SEM) image of my colloidal photonic crystal, which shows the silica beads of a diameter of 295 nm forming an fcc lattice.*

2.2.1 The concept

The concept behind photonic crystals is to mimic for photons what is happening to electrons in a real crystal. Because the ions in a perfect crystal are arranged in a regular periodic array, one typically considers the problem of an electron in a potential $U(\mathbf{r})$ having the periodicity of the underlying Bravais lattice. For photons the potential depends on the dielectric tensor ε, which now has a periodic structure:

$$\varepsilon(\mathbf{r} - \mathbf{R}) = \varepsilon(\mathbf{r}), \quad \forall\, \mathbf{R} \in \mathcal{R}. \tag{2.1}$$

The set $\mathcal{R} = \{n_1\mathbf{a}_1 + n_2\mathbf{a}_2 + n_3\mathbf{a}_3; (n_1, n_2, n_3) \in \mathbb{Z}^3\}$ of lattice vectors $\mathbf{R}$ is generated by the primitive translations $\mathbf{a}_i$ that describe the structure of the photonic crystal.

Applying Bloch's theorem, one can construct the eigenvectors (*Bloch photons*) in form of plane waves times a function with the periodicity of the lattice.

The essential difference on one hand are that photons are bosons, whereas electrons are fermions. In fact it simplifies the problem, since photon-photon interaction normally needs not being dealt with. On the other hand electromagnetic waves are vector functions, whereas the electron wavefunction is a scalar one.

2.2.2 Photonic band gaps and magneto-spatial dispersion

How does the concept of photonic crystals now fits into the framework of this thesis. This is shown by treating the periodically varying dielectric constant as a single homogeneous one with additionally taking into account spatial dispersion (see section 1.9).

expanding $\varepsilon(\mathbf{r})$ in a Fourier series

The periodicity of the dielectric constant Eq. (2.1) implies being able to write Eq. (1.23) as

$$\varepsilon_{ik}(\omega, \mathbf{k}) = \delta_{ik} + \frac{1}{\Omega} \int_{WSC} \int_0^\infty \varepsilon_{ik}(\tau, \mathbf{r}') e^{i(-\mathbf{G}\cdot\mathbf{r}' - \omega\tau)} \, d\tau \, d^3r'. \tag{2.2}$$

$\mathbf{G}$ corresponds here to one of the possible reciprocal lattice vectors of the lattice vector $\mathbf{R}$ in real space (see, e.g., [Sak01, BJ99]) and Ω is the volume of the Wigner-Seitz cell (WSC).

2.2.3 Band gap structure

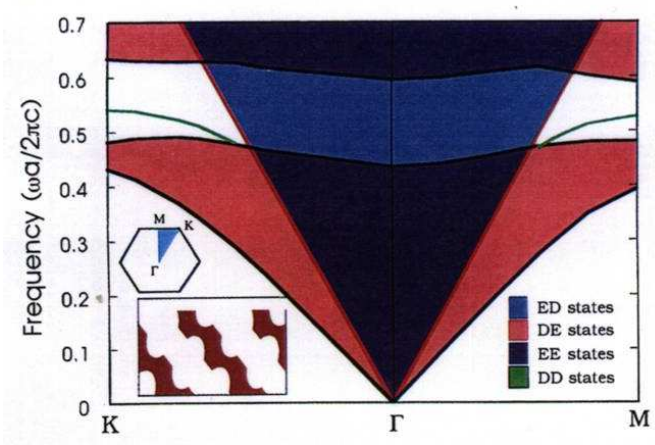

Figure 2.3: *Photonic band structure with band gap in a two dimensional photonic crystal (from: [JMW95])*

In order to better understand the interaction of electromagnetic waves with a photonic crystal, the main features will be discussed on the basis of Fig. 2.3. It depicts the photonic band structure of a two dimensional periodic structure (see inset of Fig. 2.3). I can restrict myself to the irreducible Brillouin zone as

a direct result of the crystal's periodicity. There are two bands (red area) and between those bands is the *photonic band gap* (white), in which there can be no possible *extended state* for a wave inside the crystal. Exceptions can be designed by introducing defects (green lines).

There is also the light line[1]. Only states with an energy below this line can be excited inside the crystal with incoming light. The states above this line (blue area) are inaccessible by those means.

Light with a frequency within the forbidden gap cannot build up an *extended state*, but it can enter some way into the crystals in form of so called *evanescent waves*. The amplitude decays exponentially from the surface to the inside of the crystal, but the creation of localized evanescent light modes can be possible around defects.

2.2.4 The Master equation

The similarities in the phenomenon of a band gap naturally leads to the question if concepts that had been developed for the case of electrons can not be translated into the case of photons. Electromagnetic problems are covered by the Maxwell equations (2.3)-(2.6), whereas quantum mechanical problems are basically associated with solving the corresponding Schrödinger equation.

$$\nabla \cdot \mathbf{H}(\mathbf{r},t) = 0 \qquad (2.3), \qquad \nabla \times \mathbf{E}(\mathbf{r},t) + \frac{1}{c}\frac{\partial \mathbf{H}(\mathbf{r},t)}{\partial t} = 0 \qquad (2.4)$$

$$\nabla \cdot \varepsilon(\mathbf{r})\mathbf{E}(\mathbf{r},t) = 0 \qquad (2.5), \qquad \nabla \times \mathbf{H}(\mathbf{r},t) - \frac{\varepsilon(\mathbf{r})}{c}\frac{\partial \mathbf{E}(\mathbf{r},t)}{\partial t} = 0 \qquad (2.6)$$

It can be shown that for my (special) electromagnetic case, I can construct an equation that resembles the Schrödinger equation:

$$\Theta\mathbf{H}(\mathbf{r}) \equiv \nabla \times \left(\frac{1}{\varepsilon(\mathbf{r})}\nabla \times \mathbf{H}(\mathbf{r})\right) = \left(\frac{\omega}{c}\right)^2 \mathbf{H}(\mathbf{r}) \qquad (2.7)$$

The master equation here determines $\mathbf{H}(\mathbf{r})$. The electric field $\mathbf{E}(\mathbf{r})$ is then given by

$$\mathbf{E}(\mathbf{r}) = \left(\frac{-ic}{\omega\varepsilon(\mathbf{r})}\right) \nabla \times \mathbf{H}(\mathbf{r}). \qquad (2.8)$$

2.3 Basic magneto-optical effects

Magneto-optics is about light interacting with matter that is subject to a magnetic field. The presence of a magnetic field changes the dispersion curves of the medium and creates or modifies an optical anisotropy. For two orthogonal polarization modes the absorption and refraction can be different and is called *dichroism* in the former and *birefringence* in the latter case. In general, one can classify magneto-optical effects into circular or linear polarization effects. Depending on the direction of the magnetic field, there are two basic geometries. If the

[1] meaning the dispersion relation for light in vacuum: $\omega = ck$

magnetic field and the light beam are parallel, it is called the *Faraday geometry*, for perpendicular fields it is called the *Voigt geometry*.

2.3.1 Faraday effect

The *magnetic circular birefringence* was discovered by Michael Faraday and is generally known as the *Faraday effect* [Man99, ZK97]. It has to be separated from *natural circular birefringence* (see *optical activity* in Sec. 3.3). The birefringence here is the result of a parallel magnetic field that creates a difference in the refractive index for the two circular polarization modes. The direction of polarization of linearly polarized light is rotated. The rotation angle θ is given by Eq. (2.9), where B is the magnetic field, d the propagation distance and the material parameter V is called the Verdet constant.

$$\theta = V \cdot B \cdot d \tag{2.9}$$

The Verdet constant is a material parameter that depends on the frequency of the light and on the temperature.

Another notation involves the *magneto-optical parameter* Q (more in Sec: 2.5.1):

$$\theta = -\frac{\pi n}{\lambda} Q d \tag{2.10}$$

The sense of rotation depends on the direction of the magnetic field. For a beam reflected at the end of the medium, the sense of rotation is not reversed. The rotation angle doubles, when a wave goes forth and back through the medium. This is in contrast to *natural circular birefringence*.

The circular anisotropy of the medium is the result of the splitting of the electronic energy levels into different values for different eigenvalues of the angular momentum. In the simplest case, the magnetic field induces Larmor precession of the electron orbits. This can be seen in a splitting of the refractive index n into n_+ and n_- for the two circular polarization modes of the light, which are here the eigenstates of the system:

$$n_\pm(\omega) \approx n(\omega) \pm \frac{dn}{d\omega} \frac{eB}{2mc} \tag{2.11}$$

The Verdet constant can then be estimated by the Becquerel formula:

$$V = \frac{e}{2mc^2} \lambda \frac{dn}{d\lambda} \tag{2.12}$$

Eq. (2.12) is consistent with data for diamagnetic media.

The terms *diamagnetic* and *paramagnetic* are also used to describe the magneto-optical properties of media. In contrast to the well-known properties of diamagnetic or paramagnetic susceptibilities, in magneto-optics both the diamagnetic and the paramagnetic type can be of positive and negative sign.

For the paramagnetic type the dispersion of magneto-optical effects is governed by the magnetization of the ion. In case of a weak magnetic field the magnetization

in turn is connected to the paramagnetic susceptibility. In this case the Verdet constant is inversely proportional to the temperature T:

$$V \propto T^{-1} \tag{2.13}$$

Its wavelength dependence is approximately given by:

$$V \propto (\lambda^2 - \lambda_0^2)^{-1} \tag{2.14}$$

The parameter λ_0 is the wavelength that indicates the nearest absorption resonance in the medium.

A quantum-mechanical description of the Faraday effect can be found in Ref. [ZK97].

2.3.2 Magnetic circular dichroism

If a medium exhibits absorption, then the absorption coefficients of the right- and left-handed circularly polarized light are different in the presence of a longitudinal magnetic field.

Absorption can be introduced in the formalism as an additional imaginary part of the refractive index:

$$\hat{n} = n + i\kappa \tag{2.15}$$

The dichroism results in different refractive indices for the two circular polarization modes:

$$\hat{n}_\pm(\omega) \approx n_\pm(\omega) + i\left(\kappa(\omega) \pm \frac{d\kappa}{d\omega}\frac{eB}{2mc}\right) \tag{2.16}$$

The term $n_\pm$ corresponds to the formula for the Faraday rotation in Eq. (2.11) is a real number without absorption $\hat{n} = n$.

As a consequence linearly polarized light becomes elliptically polarized when traveling in this medium alongside the magnetic field. The major axis of the ellipse is oriented at the angle

$$\theta = -\frac{\pi n\, d}{\lambda} Q' \tag{2.17}$$

and has an ellipticity

$$\psi = -\frac{\pi n\, d}{\lambda} Q'' \tag{2.18}$$

The magneto-optical parameter $Q = Q' + iQ''$.

The above fromula are only valid exactly for centro-symmetric materials, this excludes effects of natural optical activity (s. Sec. 3.3.1).

2.3.3 Magneto-optical Kerr effect, Cotton-Mouton effect, and magnetic linear dichroism

The *magneto-optical Kerr effect* designates the influence of the magnetization of a medium on the reflected light. One distinguishes between three types depending on the relative orientation of the magnetization direction to the reflective surface and to the plane of polarization for the incident light beam: *polar*, *longitudinal* and *transverse Kerr effect*.

- **polar**: magnetic field direction is perpendicular to the surface and parallel to the plane of polarization
- **longitudinal**: magnetic field direction is parallel to the surface and perpendicular to the plane of polarization
- **transverse**: magnetic field direction is parallel to the surface and parallel to the plane of polarization

The Kerr effect is generally small.

For the Voigt configuration, where the magnetic field is perpendicular to the direction of the light beam, the encountered anisotropy is 'linear'. That means the normal modes inside the medium are two orthogonal linearly polarized waves.

The *magnetic linear birefringence* is habitually known by the name *Cotton-Mouton effect*. It is strongest in materials, where the magnetically and optically anisotropic molecules can freely orientate themselves, notably liquids and gases, and align in the applied field direction. The effect is even in the magnetic field and depends usually quadratically on the magnetic field intensity.

In absorbing media, one has *magnetic linear dichroism* as well. The absorption coefficient differs for light that is polarized parallel or perpendicular to the magnetic field direction.

2.3.4 Higher order and inverse magneto-optical effects

The effects that were discussed in this section are the basic ones, that are in first order linear in the magnetic field. Magnetic linear dichroism is proportional to B^2, even in B, magnetic circular dichroism is odd in B. But there are also contributions in higher orders of the magnetic field that are usually small but can become predominant for high fields.

Another higher order effect that was recently discovered goes with the product of the wave vector $\mathbf{k}$ and the magnetic field $\mathbf{B}$, the *magneto-chiral anisotropy*. This effect is discussed in more detail in Sec. 3.3.

There are also the light-induced magneto-optical effects, where the light not only probes the magnetization, but also changes it.

The *inverse Faraday effect* is an example for a nonlinear magneto-optical effect. It describes the phenomenon that a medium becomes magnetized under the influence of an intense circularly polarized light beam.

Luminescence and emission can also be described by the dielectric constant, and are not essentially different from the effects in absorption or refraction.

2.4 Numerical methods employed for photonic crystals

In order to calculate light propagation in photonic crystals various methods are employed, of which I present here the most important. Basically, one has to solve the Maxwell equations (2.3)-(2.6) for an inhomogeneous and periodic medium.

The common approach is to use techniques that were successful in calculating the band structure for electrons in crystals, because of their close analogy to my electromagnetic(EM) case.

In the EM case, the great advantage is that the waves are generally superimposable and so one avoids many-body interaction problems and can easily transfer a result from one scale to another. But now one has to deal with vector waves and the dielectric constant can be very complicated: i) complex values, ii) strong dependence of wavelength, and iii) strong spatial variations. The most successful methods are the plane-wave expansion (PWE) method and the transfer matrix method (TMM). These are discussed in more detail below. Other methods that were successfully transfered from the corresponding electronic calculations are finite-difference time domain (FDTD) method [CYH95, Taf95] or Korringa-Kohn-Rostoker (KKR) method [BNM+01]. They have certain advantages in their scaling behavior (FDTD) or for systems that have been built from spherical particles (KKR).

2.4.1 Plane wave expansion method

From Eq. (2.7) and assuming $\varepsilon(\mathbf{r})$ to be periodic in space, $\varepsilon(\mathbf{r}+\mathbf{R}) = \varepsilon(\mathbf{r})$, one can apply Bloch's theorem and expand the magnetic field $\mathbf{H}(\mathbf{r})$ in plane waves of the form:

$$\mathbf{H}(\mathbf{r}) = \sum_{\mathbf{G}} \sum_{\lambda=1}^{2} \mathbf{h}_{\mathbf{G},\lambda} \hat{\mathbf{e}}_\lambda e^{i(\mathbf{k}+\mathbf{G})\cdot\mathbf{r}} \tag{2.19}$$

A plane wave expansion approach was employed by Ho et al. [HCS90] for the calculation of photonic band structures. Also possible is the expansion in spherical waves, this is then called the *spherical wave expansion method* (see, e.g., [SKM92]).

2.4.2 Transfer matrix method

A Transfer Matrix Method (TMM) for photonic phenomena was introduced by Pendry and McKinnon [PK92]. This on-shell scattering method is in general better suitable for the calculation of reflection and transmission coefficients. TMM is basically a finite-element method in which space is divided into a set of small cells with coupling between neighboring cells. A *transfer matrix* relates one side of a structure to the other side. Where the structure is the unit cell of a periodic array, the eigenvalues of the transfer matrix give the band structure of the system.

2.5 Simulations in one dimension

I applied the transfer matrix method (s. Sec. 2.4.2) to calculate transmission and Faraday rotation in the simplified case of a one dimensional photonic crystal. In Ref. [Yeh80] I found a basic algebra in form of a 4x4 matrix method to investigate plane wave propagation in an arbitrarily anisotropic medium. As will be seen later in this section it has to be modified considerably to allow for magneto-optical

properties [HS96]. An approach similar to mine was recently published by Kato et al. [KMTE03].

2.5.1 Dielectric and magneto-optically active multilayers

design of the one dimensional magneto-optic photonic crystal

The experimental situation I simulated is schematically depicted in Fig. 2.4. It

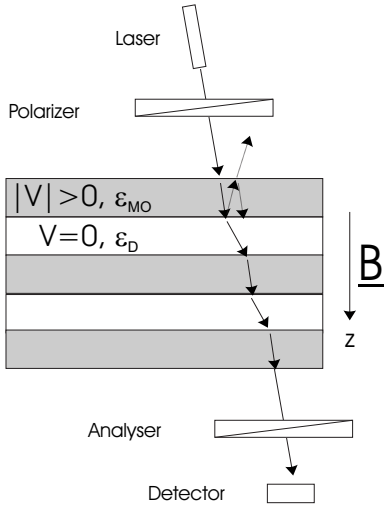

Figure 2.4: *The simulated case*

consists of a multilayer structure in the form $(M/G)^n$, i.e., alternating nonmagnetic dielectric(G) and magneto-optically active[2] dielectric layers(M) with repetition number n. Each layer was allowed to be anisotropic and its interaction with light is fully specified by the form and value of each dielectric tensor $\hat{\varepsilon}(\lambda)$, that is a function of wavelength λ. The magnetic permeability μ was approximated by 1 (no ferromagnetic layers).

[2] of the paramagnetic type

the dielectric tensors

The dielectric tensor of the dielectric layer has the form:

$$\hat{\varepsilon}_G = \begin{pmatrix} \varepsilon_x & 0 & 0 \\ 0 & \varepsilon_y & 0 \\ 0 & 0 & \varepsilon_z \end{pmatrix} \tag{2.20}$$

The dielectric tensor of the magneto-optically active layer:

$$\hat{\varepsilon}_M = \begin{pmatrix} \varepsilon_x & -iQ\varepsilon_{xy} & 0 \\ iQ\varepsilon_{xy} & \varepsilon_y & 0 \\ 0 & 0 & \varepsilon_z \end{pmatrix} \tag{2.21}$$

with

$$Q = \frac{\lambda}{\sqrt{\varepsilon_{xy}}\pi} V_M B_z \quad , \quad \varepsilon_{xy} = \frac{1}{2}(\varepsilon_x + \varepsilon_y) \tag{2.22}$$

where I restricted myself to an externally applied magnetic field B only in the z-direction. Q is called the *magneto-optic parameter*. V_M is the Verdet constant of the magneto-optically active layer. The Verdet constant of the dielectric layer is here set to zero: $V_G = 0$.

2.5.2 4x4 matrix formalism

the wave equation

The first task consists of solving the wave equation for each kind of layer.

$$\mathbf{k} \times (\mathbf{k} \times \mathbf{E}) + \omega^2 \varepsilon \mathbf{E} = 0 \tag{2.23}$$

The solution to this provides four generally complex values for the wavevector $\mathbf{k}_\sigma$, where $\sigma = 1, 2, 3, 4$.

For light traveling in the z-direction $\mathbf{k} = k_z$ of an isotropic medium ($\varepsilon_x = \varepsilon_x = \varepsilon$) :

$$k_z = \pm\omega\sqrt{\varepsilon(1 \pm Q)} \tag{2.24}$$

So I have one forth and one back traveling wave with two *polarization eigenstates* each. For isotropic media these polarization eigenstates are circular.

From these I can construct the four *polarization eigenvectors* $\hat{\mathbf{p}}_\sigma$ of the light's electric field $\mathbf{E}$. For the simple isotropic case, these are:

$$\hat{\mathbf{p}}_1 = \frac{1}{\sqrt{2}} \begin{pmatrix} 1 \\ i \\ 0 \end{pmatrix} \quad (2.25), \qquad \hat{\mathbf{p}}_2 = \frac{1}{\sqrt{2}} \begin{pmatrix} -1 \\ -i \\ 0 \end{pmatrix} \tag{2.26}$$

$$\hat{\mathbf{p}}_3 = \frac{1}{\sqrt{2}} \begin{pmatrix} 1 \\ -i \\ 0 \end{pmatrix} \quad (2.27), \qquad \hat{\mathbf{p}}_4 = \frac{1}{\sqrt{2}} \begin{pmatrix} -1 \\ i \\ 0 \end{pmatrix} \tag{2.28}$$

The distribution of the electric field **E** within each homogeneous anisotropic layer can be expressed as a sum of the four partial waves. The complex amplitudes of these four partial waves constitute the components of a column vector $A_\sigma(n), \sigma = 1, 2, 3, 4$. The electromagnetic field in the nth layer of the medium can thus be written as:

$$\mathbf{E} = \sum_{\sigma=1}^{4} A_\sigma(n)\mathbf{p}_\sigma(n) \exp\left[ik_\sigma(n)(z - z_n) - i\omega t\right] \tag{2.29}$$

$$\mathbf{H} = \sum_{\sigma=1}^{4} A_\sigma(n)\mathbf{q}_\sigma(n) \exp\left[ik_\sigma(n)(z - z_n) - i\omega t\right] \quad , \quad \mathbf{q}_\sigma = \frac{c}{\omega}\mathbf{k}_\sigma \times \mathbf{p}_\sigma \tag{2.30}$$

field continuity at the interfaces

Now, that I know the fields within each layer, I can turn my attention to the interfaces between them. At these interfaces the fields (components along the interface) have to be continuous:

$$E_x(n-1) = E_x(n) \quad , \quad E_y(n-1) = E_y(n) \tag{2.31}$$

$$H_x(n-1) = E_x(n) \quad , \quad H_y(n-1) = H_y(n). \tag{2.32}$$

Therefore the column vectors A_σ are not independent of each other, but each is related to those of its neighboring layers.

field continuity matrix equation

Putting Eqs. (2.29)-(2.30) into the Eqs. (2.31)-(2.32) leads to four equations, that can be written in matrix form:

$$\begin{bmatrix} A_1(n-1) \\ A_2(n-1) \\ A_3(n-1) \\ A_4(n-1) \end{bmatrix} = D^{-1}(n-1)D(n)P(n) \begin{bmatrix} A_1(n) \\ A_2(n) \\ A_3(n) \\ A_4(n) \end{bmatrix} \tag{2.33}$$

where

$$D(n) = \begin{bmatrix} \hat{\mathbf{x}}\cdot\hat{\mathbf{p}}_1(n) & \hat{\mathbf{x}}\cdot\hat{\mathbf{p}}_2(n) & \hat{\mathbf{x}}\cdot\hat{\mathbf{p}}_3(n) & \hat{\mathbf{x}}\cdot\hat{\mathbf{p}}_4(n) \\ \hat{\mathbf{y}}\cdot\hat{\mathbf{q}}_1(n) & \hat{\mathbf{y}}\cdot\hat{\mathbf{q}}_2(n) & \hat{\mathbf{y}}\cdot\hat{\mathbf{q}}_3(n) & \hat{\mathbf{y}}\cdot\hat{\mathbf{q}}_4(n) \\ \hat{\mathbf{y}}\cdot\hat{\mathbf{p}}_1(n) & \hat{\mathbf{y}}\cdot\hat{\mathbf{p}}_2(n) & \hat{\mathbf{y}}\cdot\hat{\mathbf{p}}_3(n) & \hat{\mathbf{y}}\cdot\hat{\mathbf{p}}_4(n) \\ \hat{\mathbf{x}}\cdot\hat{\mathbf{q}}_1(n) & \hat{\mathbf{x}}\cdot\hat{\mathbf{q}}_2(n) & \hat{\mathbf{x}}\cdot\hat{\mathbf{q}}_3(n) & \hat{\mathbf{x}}\cdot\hat{\mathbf{q}}_4(n) \end{bmatrix} \tag{2.34}$$

$$\xrightarrow{\text{isotropic}} \frac{1}{\sqrt{2}} \begin{bmatrix} 1 & -1 & 1 & -1 \\ \sqrt{\varepsilon(1-Q)} & \sqrt{\varepsilon(1-Q)} & \sqrt{\varepsilon(1+Q)} & \sqrt{\varepsilon(1+Q)} \\ i & -i & -i & i \\ -i\sqrt{\varepsilon(1-Q)} & i\sqrt{\varepsilon(1-Q)} & i\sqrt{\varepsilon(1+Q)} & i\sqrt{\varepsilon(1+Q)} \end{bmatrix}$$

$D(n)$ is called the *dynamical matrix* and depends only on the eigenvectors $\hat{\mathbf{p}}_\sigma$ and $\hat{\mathbf{q}}_\sigma$.

$$P_{j\sigma}(n) \quad = \delta_{j\sigma} \exp\left(-i\,\hat{\mathbf{z}} \cdot \mathbf{k}_j\, d_n\right), \quad j, \sigma = 1, 2, 3, 4. \tag{2.35}$$

The *propagation matrix* $P(n)$ includes the thickness d_n of the layer n and describes the phase excursion for each partial wave.

transfer matrix

Going from layer 1 throughout the structure until layer N and enclosing it with interfaces to the surrounding medium (usually air) $D(0)$, one ends up with the transfer matrix:

$$\boxed{T = D^{-1}(0) \left(\prod_{n=1}^{N} D(n) P(n) D^{-1}(n) \right) D(0)} \tag{2.36}$$

transmission and reflection

Once the transfer matrix is calculated, the relation between incident (I), reflected (R) and transmitted light (T) for the two polarization states s and p is given by:

$$\begin{bmatrix} I_S \\ R_S \\ I_P \\ R_P \end{bmatrix} = T \begin{bmatrix} T_S \\ 0 \\ T_P \\ 0 \end{bmatrix} \tag{2.37}$$

The reflection and transmission coefficients are defined and expressed in term of the matrix elements as follows:

$$r_{ss} = \left(\frac{R_s}{I_s}\right)_{I_p=0} = \frac{T_{21}T_{33} - T_{23}T_{31}}{T_{11}T_{33} - T_{13}T_{31}}, \tag{2.38}$$

$$r_{sp} = \left(\frac{R_p}{I_s}\right)_{I_p=0} = \frac{T_{41}T_{33} - T_{43}T_{31}}{T_{11}T_{33} - T_{13}T_{31}}, \tag{2.39}$$

$$r_{ps} = \left(\frac{R_s}{I_p}\right)_{I_s=0} = \frac{T_{11}T_{23} - T_{21}T_{13}}{T_{11}T_{33} - T_{13}T_{31}}, \tag{2.40}$$

$$r_{pp} = \left(\frac{R_p}{I_p}\right)_{I_s=0} = \frac{T_{11}T_{43} - T_{41}T_{13}}{T_{11}T_{33} - T_{13}T_{31}}, \tag{2.41}$$

$$t_{ss} = \left(\frac{T_s}{I_s}\right)_{I_p=0} = \frac{T_{33}}{T_{11}T_{33} - T_{13}T_{31}}, \tag{2.42}$$

$$t_{sp} = \left(\frac{T_p}{I_s}\right)_{I_p=0} = \frac{-T_{31}}{T_{11}T_{33} - T_{13}T_{31}}, \tag{2.43}$$

$$t_{ps} = \left(\frac{T_s}{I_p}\right)_{I_s=0} = \frac{-T_{13}}{T_{11}T_{33} - T_{13}T_{31}}, \tag{2.44}$$

$$t_{pp} = \left(\frac{T_p}{I_p}\right)_{I_s=0} = \frac{T_{11}}{T_{11}T_{33} - T_{13}T_{31}}. \tag{2.45}$$

Faraday rotation

Finally, the Faraday rotation angle Θ and the ellipticity ψ are given by:

$$\Theta = \arg\left(\frac{T_{33}}{T_{11}}\right)\frac{90^\circ}{\pi} \tag{2.46}$$

$$\psi = \arctan\frac{1 - |\frac{T_{33}}{T_{11}}|}{1 + |\frac{T_{33}}{T_{11}}|} \tag{2.47}$$

2.6 Simulated transmission and Faraday rotation

In this section I show simulations for a structure composed of alternating layers of CeF_3 and CaF_2. These are materials that are commonly used in optics and can be grown in a standard fashion. Absorption is very low in these materials and is consequently put to zero in these simulations.

The external magnetic field was chosen to be $B = 33\,\mathrm{mT}$. The resulting magneto-optical parameter is $Q = 5 \cdot 10^{-7}$. Such a field can be easily obtained with small laboratory magnets.

CeF_3 has a refractive index $n_m = 1.62$ and its rare earth component makes it magneto-optically active $V_{633\,\mathrm{nm}} = 7.2 \cdot 10^4\,\mathrm{rad/Tm}$ (20 °C) [Lid03], whereas CaF_2 has $n_g = 1.42$ and has a negligible Verdet constant $V \sim 10\,\mathrm{rad/Tm}$ (633 nm, 20 °C). The refractive index contrast is 0.2.

The stopband was designed to occur around $\lambda_B = 570\,\mathrm{nm}$. For that end the condition

$$n_g \cdot d_g + n_m \cdot d_m = m \cdot \lambda_B/2 \quad , m = 1, 2, ... \tag{2.48}$$

has to be fulfilled. I chose $d_g = 89.4\,\mathrm{nm}$ and $d_g = 89.5\,\mathrm{nm}$. The Verdet constant for CeF_3 at 570 nm (and at room temperature) can be estimated by:

$$V_{\lambda_B} = V_{633\,\mathrm{nm}}\frac{(633\,\mathrm{nm})^2 - \lambda_0^2}{\lambda_B^2 - \lambda_0^2} \tag{2.49}$$

With $\lambda_0 = 300\,\mathrm{nm}$ in CeF_3: $V_{570\,\mathrm{nm}} = 9.5 \cdot 10^4\,\mathrm{rad/Tm}$.

Figures 2.5 and 2.6 show the calculated transmission and Faraday rotation. The first multilayer consists of 40 layers and the second of 84 layers.

One can see the formed stopband around 570 nm. It is 40-45 nm wide and transmission drops two orders of magnitude in the first case (Fig. 2.5) and three

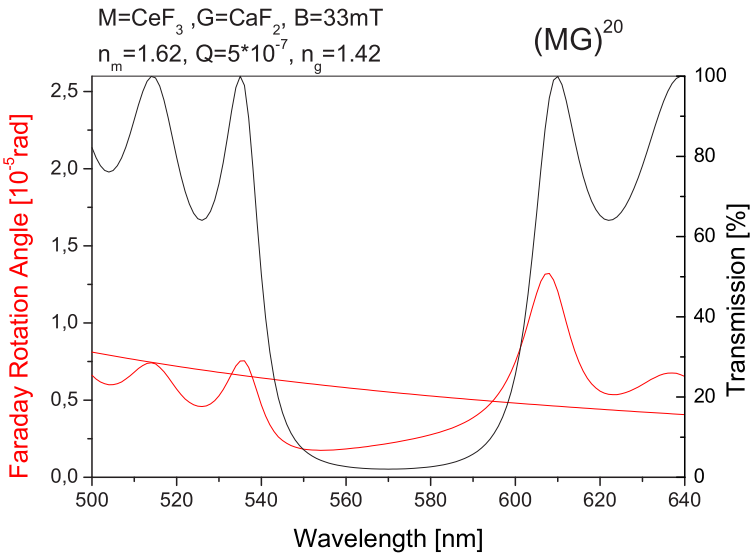

Figure 2.5: *Simulation: Faraday effect and transmission in periodic multilayers. The multilayer consist of forty layers, paramagnetic (M) CeF_3 ($n_m = 1.62$) and purely dielectric layers (G) CaF_2 ($n_g = 1.42$) in alternation $(MG)^{20}$. The applied magnetic field $B = 33\,mT \longrightarrow$ magneto-optic parameter $Q = 5 \cdot 10^{-7}$. The thickness d of the two building layers is chosen such that $n_m \cdot d_m + n_g \cdot d_g = \frac{\lambda_B}{2}$ (here: $\lambda_B = 570\,nm$, $d_m = 89.5\,nm$, $d_g = 89.4\,nm$). The flat red curve is the Faraday rotation of the paramagnetic material in one thick layer with a thickness that is the sum of the twenty paramagnetic layers.*

in the other case (Fig. 2.6). The border of the stopband is steeper the more layers there are in the structure. The spectral width goes with the refractive index contrast.

Outside the stopband both the transmission signal and that of the Faraday rotation show some oscillatory behavior. This is due to the finite thickness of the multilayer slack. The thicker the sample the sharper and closer together are the oscillations.

By comparing the usual Faraday rotation by that in the multilayer, one observes that the pure signal gets somehow modulated by the multilayer structure in a very similar way to how the transmission is modulated by it. For example, the Faraday rotation is low when transmission is low, especially inside the stopband. The difference is in the degree. For an exponential fall in transmission I observe a linear fall in Faraday rotation.

However, the most striking difference is the asymmetry in the spectral signal, whereas the transmission is perfectly symmetric around the Bragg wavelength[3].

In both configurations the Faraday rotation is stronger on the high wavelength side of the stopband than on the low wavelength side. The effect is more pronounced for Fig. 2.6, in which there are more layers involved.

[3]more strictly on an energy scale instead of the plotted wavelength dependence

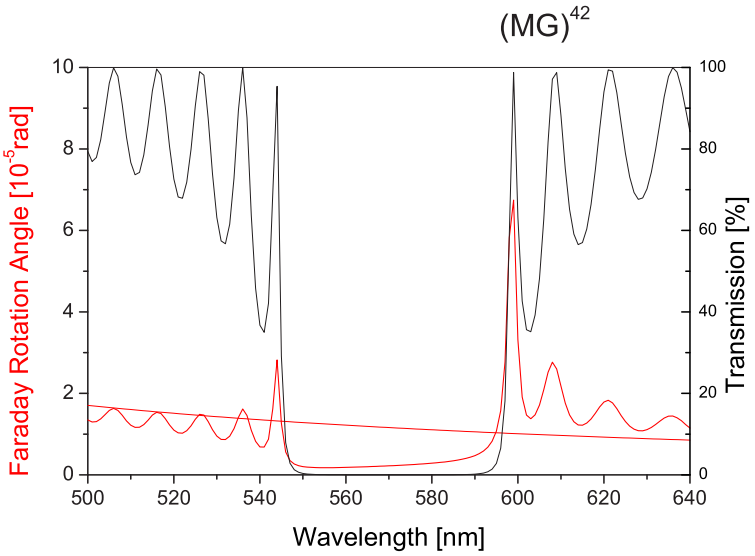

Figure 2.6: *Simulation: Faraday effect and transmission in periodic multilayers. Parameters are the same as in Fig. 2.5, apart from an increased layer number:* $(MG)^{42}$.

discussion

Now the questions arise, why is Faraday rotation modulated in a similar way as the transmission is? Why is Faraday rotation low, when the transmission is low? And most importantly, why is it asymmetric around the stopband, whereas transmission it not?

The asymmetry comes from light being more or less concentrated in energy[4] in the material with the higher or lower dielectric constant. The components were chosen to have also different Verdet constants. This could be checked by inversing the refractive index contrast and keeping the same Verdet constant contrast. The result of such a simulation is that the high and low wavelength behavior is indeed interchanged.

The interesting part of the simulation is that one has an increased Faraday rotation per length for certain wavelengths than in a homogeneous medium. Can that be improved further by a slightly changed structure? I have checked on introducing defects into the structure here below.

2.6.1 Defects

In order to introduce a defect, I kept everything as before except for some structural modifications. The new structure is of the form $(MG)^9M^2(GM)^9$ (Fig. 2.7) and $(MG)^{20}M^2(GM)^{20}$ (Fig. 2.8).

Such defects result in a *defect mode*[5] at a wavelength right in the middle of the

[4] in form of standing waves

[5] a possible state in an otherwise zero density of states

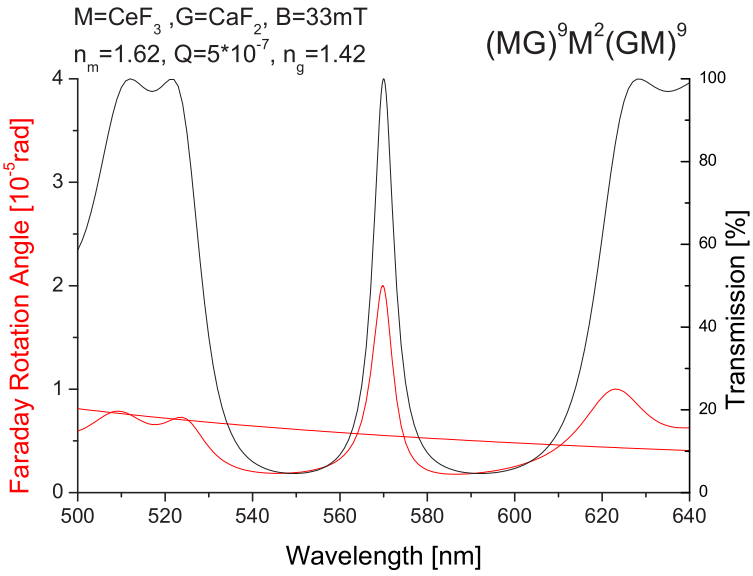

Figure 2.7: *Simulation: Faraday effect and transmission in periodic multilayers with a defect. Parameters are the same as in Fig. 2.5, apart from a modified layer structure* $(MG)^9M^2(GM)^9$.

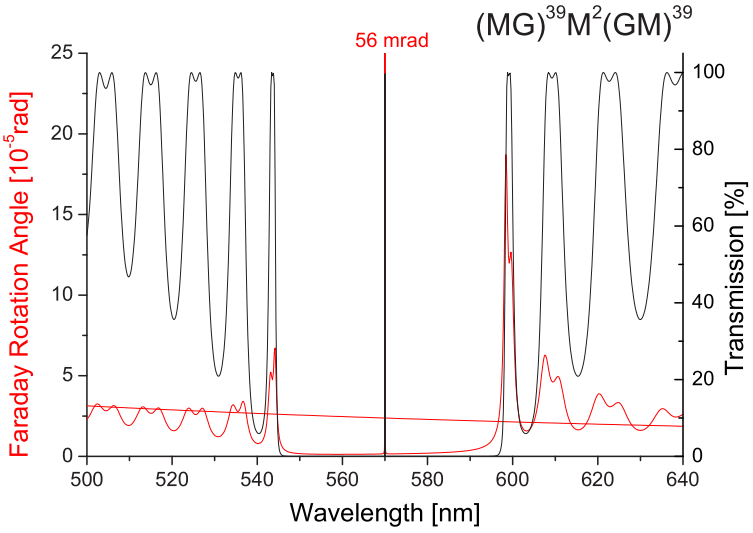

Figure 2.8: *Simulation: Faraday effect and transmission in periodic multilayers with a defect. Parameters are the same as in Fig. 2.5, apart from a modified layer structure* $(MG)^{20}M^2(GM)^{20}$.

stopband. Again the number of layers involved determines the sharpness of such a mode. The defect mode makes it possible for light to go through the crystal at this wavelength and transmission is almost 100 %. The Faraday rotation is also higher than for surrounding wavelengths and in fact it can become quite pronounced: 56 mrad in Figure 2.8 for the Bragg wavelength $\lambda_B = 570\,\text{nm}$. This represents an

increase of a factor of 200 with respect to a single layer of an equivalent thickness.

However, sharp defect modes will not be easy to realize in real structures, where one inevitably has to deal with random defects connected to the growing mechanism. It will certainly result in some smearing out of such a very sharp peak as those mentioned above; the one in transmission, for example, has a FWHM[6] of only 0.1 nm.

2.6.2 Inside a defect mode

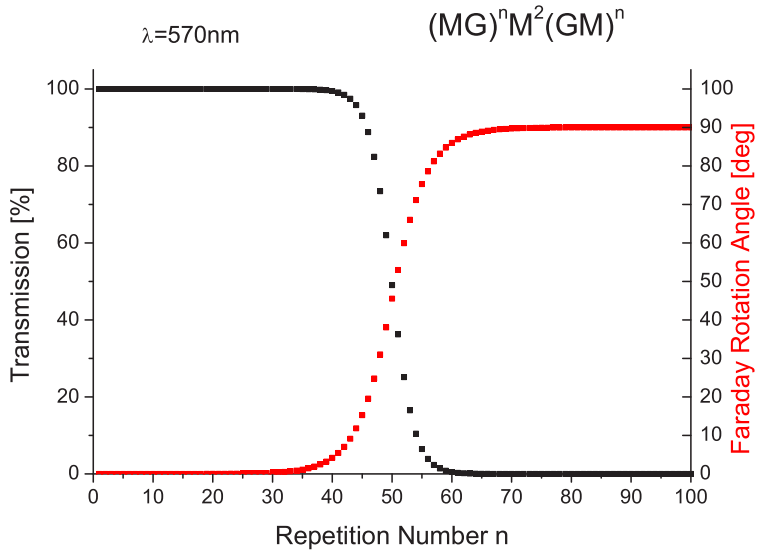

Figure 2.9: *Simulation: Faraday effect and transmission in periodic multilayers for a defect mode ($\lambda = 570\,nm$) as a function of the repetition number n for a structure of the kind $(MG)^n M^2 (GM)^n$. Material Parameters are the same as in Fig. 2.5.*

If more and more layers are added to the structure, the Faraday rotation angle for my defect mode increases. In Fig. 2.9 is plotted the Faraday rotation and transmission for a defect mode ($\lambda = 570\,\mathrm{nm}$) as a function of repetition number n in a structure of the kind $(\mathrm{MG})^n\mathrm{M}^2(\mathrm{GM})^n$.

For low repetition numbers the Faraday rotation angle is increasing exponentially. Transmission is almost 100 %. For higher repetition numbers the rotation angle asymptotically approaches the value of 90 deg. At the same time the transmission is rapidly falling to zero.

At what repetition number the transition takes place depends also on the applied magnetic field. Figure 2.10 shows the field dependence for various repetition numbers. In each case the Faraday rotation angle approaches the 90 deg mark.

Why is it not possible in my defect mode to exceed the 90 deg and why is the transmission going down?

[6]Full Width at Half Maximum

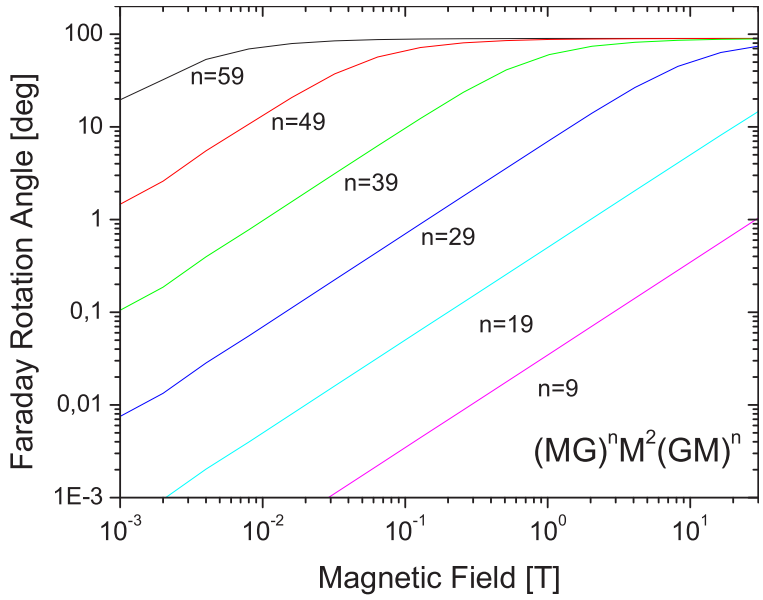

Figure 2.10: *Simulation: Faraday effect in periodic multilayers with a defect as a function of the magnetic field, $\lambda = 570$ nm.*

2.6.3 Defect mode splitting

Here, I look at such a defect mode in more detail.

It was chosen here to switch to another pair of materials: an magnetic film of bismuth substituted yttrium iron garnet (Bi-YIG) and a dielectric film of fused silica (SiO_2). The effect is merely a change of the magneto-optic parameter, that takes values of $Q = 4 \cdot 10^{-4}$. Such a high value is experimentally difficult to achieve with the preceding pair of composites. You would need both a large number of layers and a high magnetic field (compare Fig. 2.10).

Bi-YIG has a refractive index of 2.30 at 1550 nm, and SiO_2 $n = 1.52$ [IF97]. The same defect structure was used as before: $(MG)^9 M^2 (GM)^9$, with the respective layers thicknesses $d_m = 168.3$ nm and $d_g = 255.5$ nm, giving a defect mode wavelength of $\lambda_B = 1550$ nm.

Figure 2.11 shows the transmission, the Faraday rotation, as well as the ellipticity in a very small spectral range around the defect mode. Figure 2.12 shows the same for a slightly increased number of layers. What can be seen is, that Faraday rotation again peaks in the middle of the defect mode and does not exceed the 90°-mark. However, the transmission splits into two nearby peaks, even more pronounced in Fig. 2.12. The ellipticity indicates, that the two distinct modes are in the circularly polarized states.

In fact, with the above information it is no longer helpful to talk about a Faraday rotation inside the defect, because one no longer is dealing with linearly polarized light. The only exception is the exact middle position, but this is also the position where the transmission tends to zero. Outside the defect mode however, the ellipticity is quickly going to zero, indicating a fully linearly polarized light beam.

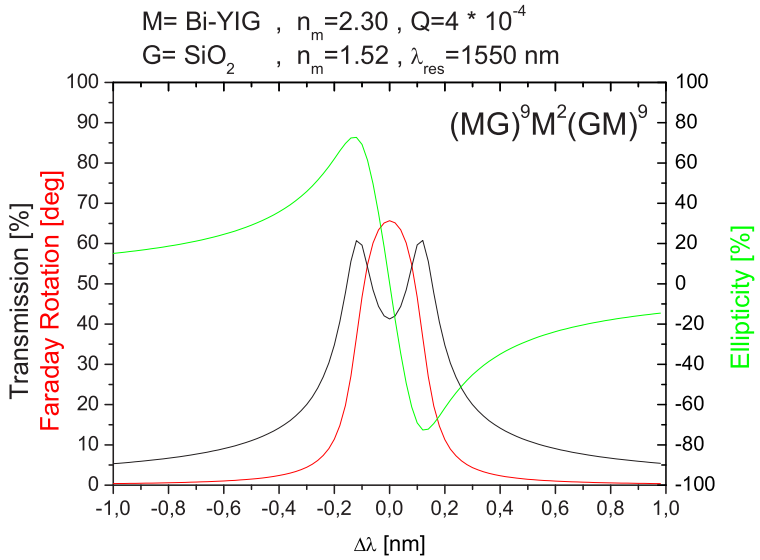

Figure 2.11: *Simulation: Faraday effect and transmission in periodic multilayers with a defect. The multilayer has a structure of the form* $(MG)^9M^2(GM)^9$. *The layer* M *is a magnetic layer of bismuth substituted yttrium iron garnet (Bi-YIG)* ($n_m = 2.30$) *and a dielectric layers* (G) *of* SiO_2 ($n_g = 1.52$). *The magneto-optic parameter takes the value* $Q = 4 \cdot 10^{-4}$. *The thickness* d *of the two building layers is chosen such that* $n_m \cdot d_m + n_g \cdot d_g = \frac{\lambda_B}{2}$ *(here:* $\lambda_B = 1550\,nm$, $d_m = 168.3\,nm$, $d_g = 255.5\,nm$*).*

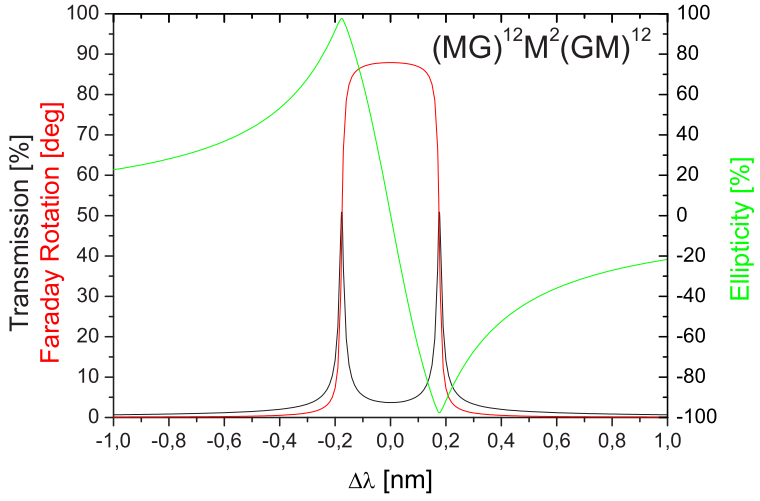

Figure 2.12: *Simulation: Faraday effect and transmission in periodic multilayers with a defect. Parameters are the same as in Fig. 2.11, apart from an increased layer number:* $(MG)^{12}M^2(GM)^{12}$.

But still, the question why the Faraday rotation can not exceed the 90°-mark remains unanswered. For more elucidation some more simulations had been per-

formed, discussed here below.

2.6.4 Resonance

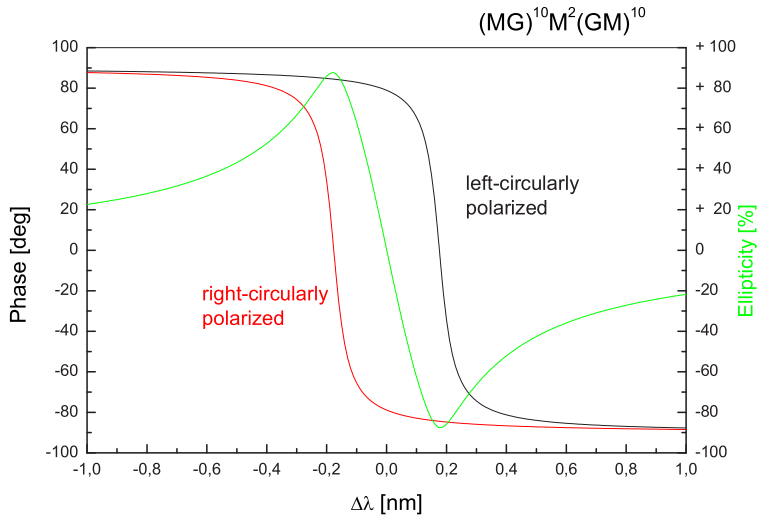

Figure 2.13: *Simulation: phase and ellipticity in periodic multilayers with a defect. Parameters are the same as in Fig. 2.11, with a slightly different number of layers: $(MG)^{10}M^2(GM)^{10}$. Instead of showing the Faraday rotation for linearly polarized light, the graph shows two curves, that indicate the phase states of the two circular modes.*

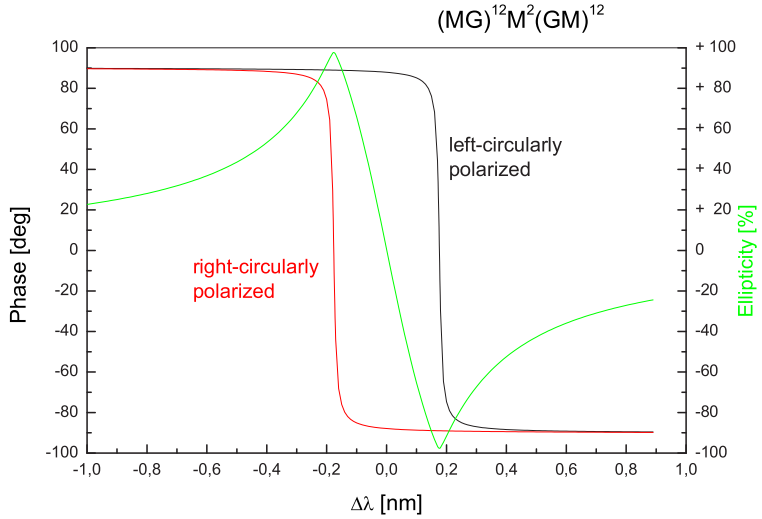

Figure 2.14: *Simulation: phase and ellipticity in periodic multilayers with a defect. Parameters are the same as in Fig. 2.13, apart from an increased layer number: $(MG)^{12}M^2(GM)^{12}$.*

Simulation have been performed for the two circularly polarized modes separately. In that case is does not make sense any more to talk about a Faraday rotation, nevertheless the phases of those waves are affected by the magneto-optical properties in the medium.

Figures 2.13 and 2.14 show the development of that phase around the defect mode. Since the initial phase can be chosen arbitrarily (here: +90° for each of them), only the relative phase shift is of importance. The figures show that for both the phase changes from +90° to -90° when crossing through the defect. They cross the 0°-mark at the positions, that were determined by the respective transmission peak in the figures 2.11 and 2.12. The transition is sharpest in the latter case.

What was observed corresponds in fact to the characteristic phase shift of all resonances, that changes its by 180°in going from one side of the resonance to the other side. For exact resonance the phase shift is 90°.

So, the reason, why Faraday rotation takes the value of 90°is when the two modes have fully split and the wavelength is in between. Then only one circular mode has changed by 180°, so that a linearly polarized beam, that is the sum of two circularly polarized modes, turns 90°around. Somewhat outside the resonance the phases of both circular modes are not changed; the linear polarization state is kept the same. For the case, that the wavelength matches a resonance frequency for one mode, the beam becomes completely circular polarized.

2.7 Faraday rotation in photonic crystals: the experiment

2.7.1 Sample preparation

For the experiment colloidal crystals consisting of an fcc packing of silica spheres [BGG+97] were used. The crystals were 1 mm thick and were several square millimeters large. Two different crystal batches, differing in sphere size ($d = 280$ nm and 294 nm) with stopbands around 573 nm and 630 nm in the [111] direction, respectively, were examined.

Fig. 2.15 depicts the typical transmission spectrum. The voids between the spheres were filled with a saturated glycerol solution of dysprosium nitrate. The dysprosium absorption peaks are likewise visible in Fig. 2.15.

This transparent liquid has a refractive index of $n = 1.484$ at 573 nm and a relatively high Verdet constant of $V = -22$ rad/Tm, which makes it much more sensitive to the applied magnetic field. In comparison, fused silica has a V of +3.48 rad/Tm at 632.8 nm [MRV92]. The beads, which are the building blocks of the employed PBGs, are made up of silica clusters of 10-30 nm in size that assemble into bigger spheres with a diameter around 300 nm. The lower refractive index $n = 1.415$ of the beads – to be compared to $n = 1.460$ for fused silica – means these spheres are porous and filled with air and small amounts of penetrated liquid. This will result in an even lower V, since the V of the liquid has opposite sign and the V of air is practically zero. The wavelength dependence of V is according to Eq. (2.14) $V = \frac{V_0}{\lambda^2 - \lambda_0^2}$, here with $\lambda_0 = 171$ nm, $V_0 = 6.6 \cdot 10^6$ rad/Tm [Düc98]. In

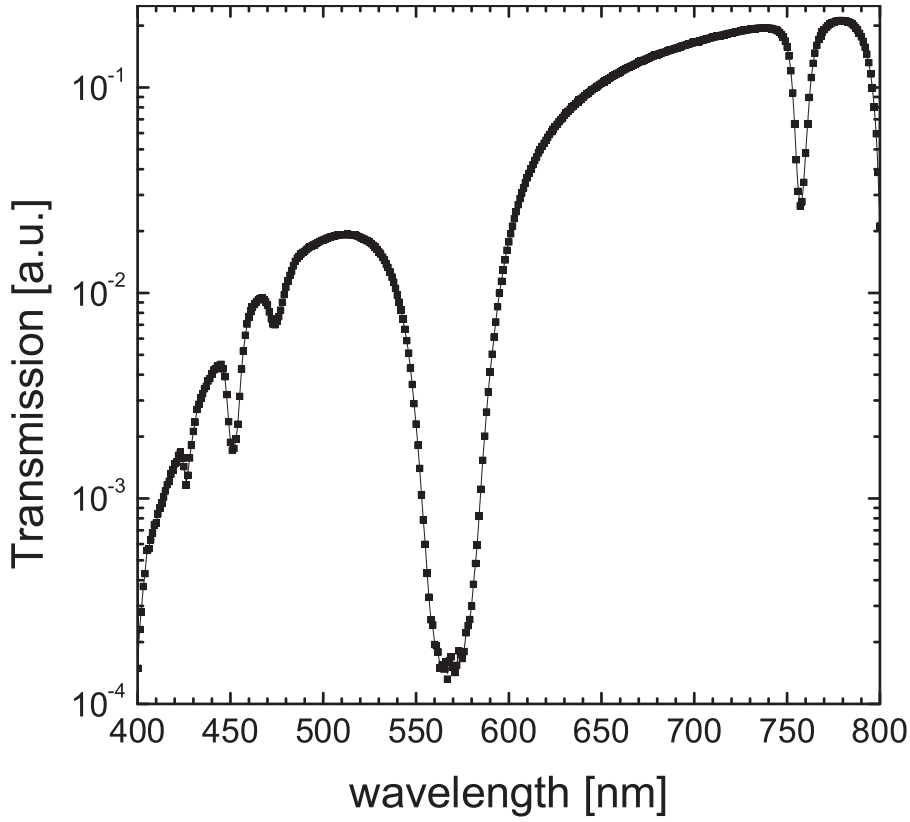

Figure 2.15: *Transmission spectrum of my impregnated silica photonic crystal measured with a commercial spectrometer showing a stopband around 570nm. The impregnating liquid is a glycerol solution saturated with dysprosium nitrate. Several dysprosium absorption peaks to the right and left of the stopband can be found as well. ($d = 280\,nm$, $l = 1\,mm$, $\lambda_B = 573\,nm$, $n_{liquid} = 1.484, \Delta n = 0.070$)*

comparison, the influence of the magnetic field in silica is negligible.

It is important to note that despite the advances made in recent years in fabricating PBGs, defects – especially stacking faults – still put certain limits on the optical quality [VAB+00]. By choosing only a small dielectric contrast between the liquid and the silica spheres, scattering at the defects is less pronounced and measurements in transmission become feasible.

2.7.2 Experimental setup

The experimental setup to measure the Faraday effect in photonic crystals is shown in Fig. 2.16.

A linearly polarized light beam enters the sample parallel to the crystal's [111] direction, which is also parallel to the magnetic field. To allow for phase sensitive detection, an alternating magnetic field at a frequency of 70 Hz is applied. A tunable dye laser serves as a coherent light source and supplies me with sufficient power near the stopband where the transmission is low. Care must be taken to

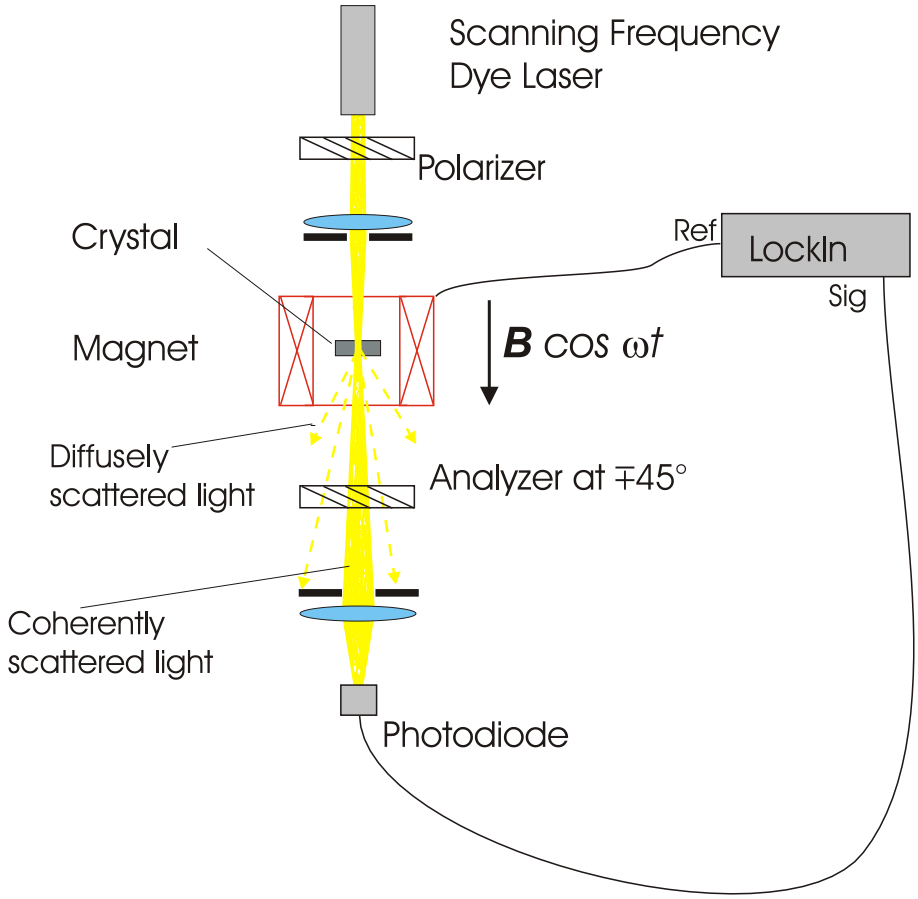

Figure 2.16: *Experimental setup to measure Faraday effect in photonic crystals.*

find a position on the crystal with few defects, so that there is a clear coherent transmission dominating the diffusely scattered background. The rotation angle variations are translated into intensity variations by an analyzer at $\pm 45°$ with respect to the polarization direction. They are detected by means of a silicon photo diode. The effective Verdet constant V_{eff} of a sample with thickness d subject to a magnetic field given by $B = B_0 \sin \omega t$ is determined by:

$$V_{eff}(\lambda) = \frac{1}{B_0 d} \frac{U_{AC}(\lambda)}{U_{DC}} \tag{2.50}$$

The voltage U_{DC} is the time-averaged voltage photo diode signal and U_{AC} is the alternating part as measured by the lock-in amplifier.

Switching the analyzer's angular position from $+45°$ to $-45°$ changes the phase of the alternating part by $180°$. Background noise can be significantly reduced by taking the average of the absolute values for both values.

2.8 Faraday rotation measurements

2.8.1 Transmission and Faraday rotation

In Fig. 2.17 is shown the measured Faraday effect of the impregnated crystal. The

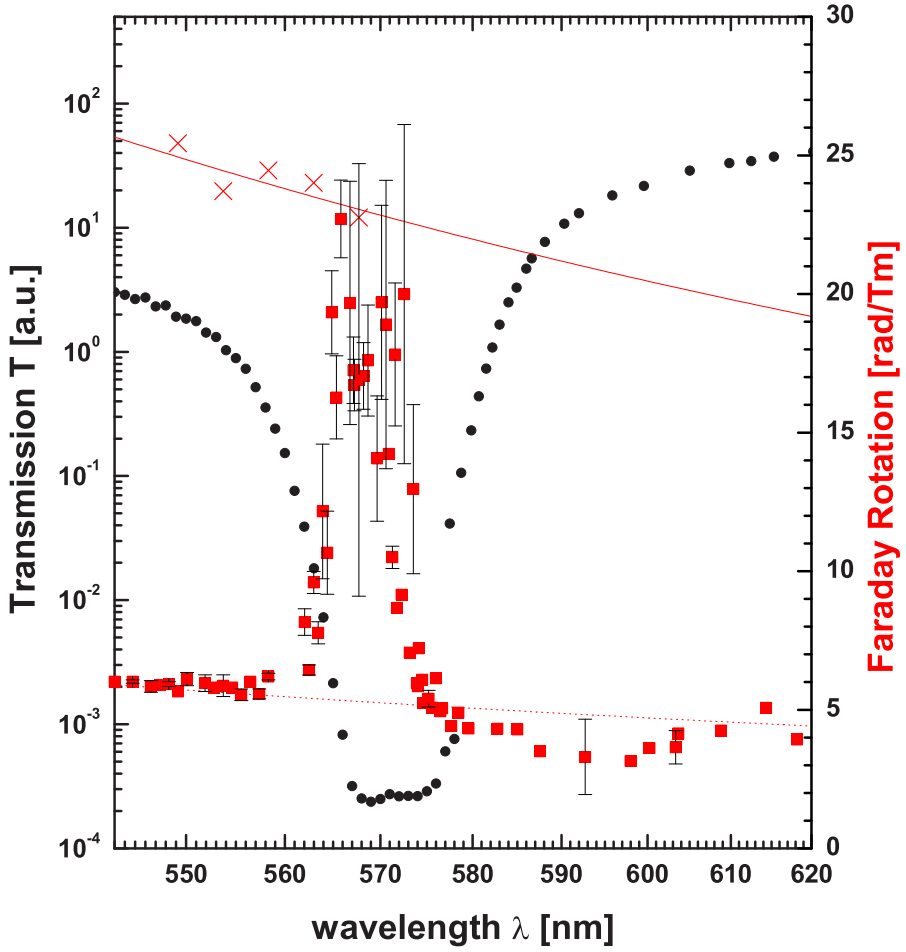

Figure 2.17: *Transmission of laser light (circles) and Faraday rotation (squares) spectra of an impregnated silica photonic crystal ($d = 280\,nm$, $l = 1\,mm$, $\lambda_B = 573\,nm$, $V_{liquid}(\lambda_B) = -22\,rad/Tm$, $n_{liquid} = 1.484$,B=33.5 $mT \rightarrow Q \approx 1 \cdot 10^{-7}, \Delta n = 0.070$). The upper line indicates the corresponding Faraday rotation of the pure liquid (crosses are measurements) and results in the lower dotted line when corrected with the filling fraction inside the PBG.*

transmission of laser light through the crystal is likewise depicted. Since the laser has a rather small aperture the measured stopband is narrower and deeper than in Fig. 2.15, for which I used a commercial spectrometer. The PBG is characterized by the diameter of the beads of $d = 280\,\text{nm}$ resulting in a Bragg wavelength of $\lambda_B = 573\,\text{nm}$ (when filled with glycerol solution). The refractive index contrast is $\Delta n = +0.070$. A value of $Q \approx 1 \cdot 10^{-7}$ is produced by a magnetic field of $B = 33.5\,\text{mT}$.

The value for the effective Verdet constant outside the stopband corresponds to the value of the liquid (crosses and nearby fitted line), corrected for the volume fraction f of liquid in the crystal and resulting in the lower dotted line, which seems to fit the Faraday rotation outside the stopband reasonably well. Inside the stopband, however, the Verdet constant increases drastically. Note that there is hardly any change observed in the Faraday effect near the stopband when transmission already falls by several orders of magnitude.

The results of a second sample ($d = 295\,\mathrm{nm}$, $l = 1\,\mathrm{mm}$, $\lambda_B = 630\,\mathrm{nm}$, $V_{liquid}(\lambda_B) = -12.5\,\mathrm{rad/Tm}$, $n_{liquid} = 1.489, B = 36.4\,\mathrm{mT} \rightarrow Q \approx 6 \cdot 10^{-8}, \Delta n = 0.075$) are plotted in Fig. 2.18.

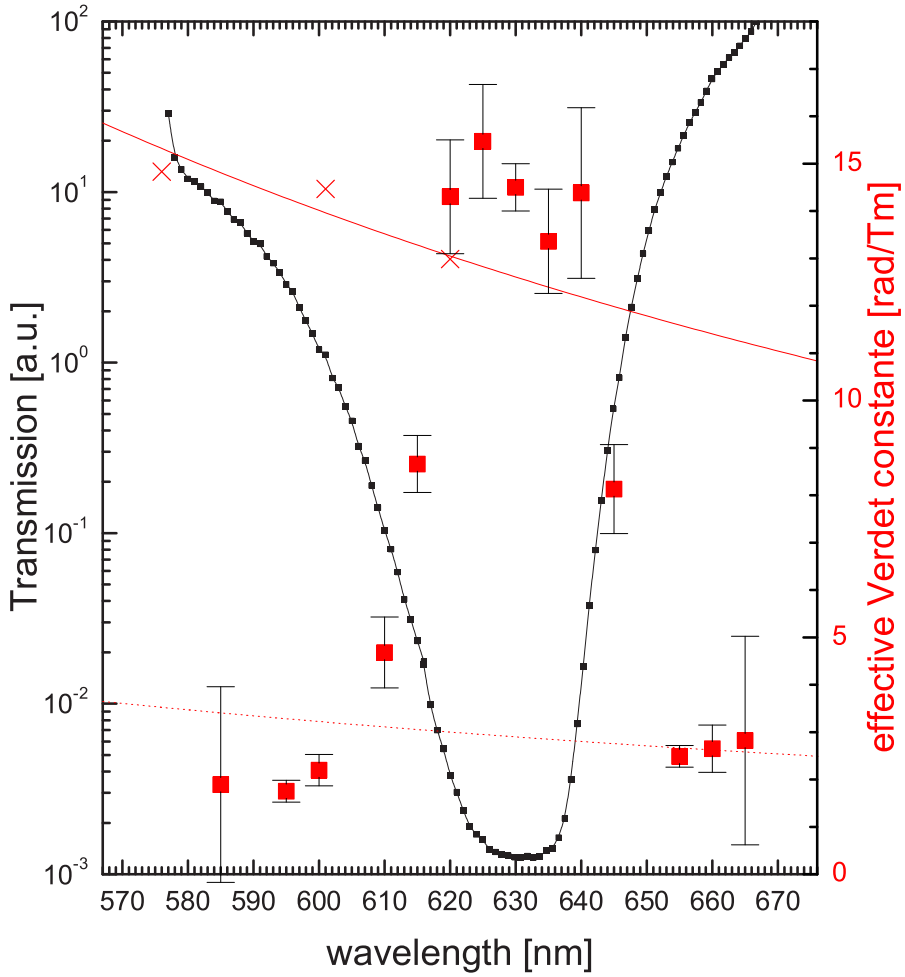

Figure 2.18: *Faraday rotation and transmission of a second PBG: ($d = 295\,nm$, $l = 1\,mm$, $\lambda_B = 630\,nm$, $V_{liquid}(\lambda_B) = -12.5\,rad/Tm$, $n_{liquid} = 1.489, B = 36.4\,mT \rightarrow Q \approx 6 \cdot 10^{-8}, \Delta n = 0.075$). Legend as in Fig. 2.17.*

Both types of my PBG exhibit the same characteristic spectral dependence. This is strong evidence that the periodicity is at the origin of the enhancement, and not imperfections of the crystal.

2.8.2 Effective medium

The Verdet constant outside the stopband takes the values of a simple effective medium associated with the two composites (indexed by a and b):

$$V_{eff} = V_a \cdot f_a + V_b(1 - f_a) \tag{2.51}$$

This seems to be quite a good rule of thumb for opals. In principle, this homogenization technique can be justified only for wavelengths large compared to the microscopic structures as was seen for the dielectric constant in random media [BS95].

Effective medium theories exist for periodic media [SKB96, RMSS98] and for magneto-optical quantities [YSK97], but they fail to show the simple relation that is observed by me.

It seems as if the effect of resonant scattering quickly vanishes outside the matching wavelength and that even more so for the Faraday rotation than for the Transmission.

It is remarkable that in opal-based photonic crystal structures (built of either silica or polymer balls) the same simple effective medium approximation - although it should not be necessary applicable to such a densely packed system of scatterers - proves to be applicable. It describes well the effective refractive index n_{eff} appearing in the expression for the Bragg wavelength λ_B, as determined from optical reflectance or transmission measurements:

$$\lambda_B = l\sqrt{n_{eff}^2 - \sin^2\theta} \tag{2.52}$$

$$n_{eff} = n_a f_a + n_b\,(1 - f_a) \tag{2.53}$$

l is the lattice constant, here in the (111)- direction of hexagonally close packed spheres of diameter d it takes the form $l = \sqrt{\frac{8}{3}}d$.

For experiments showing that this relationship indeed describes the Bragg wavelength rather well, see, e.g., [MBM+99, MBL+99, RMT+99] for silica-based opals and [PX99, XGP99] for solid-state opals built of polymer beads. Or, if not exactly the above simple approximation, then some rather similar one (for the given conditions) as shown in [VSvB+96, MWLV99] where colloidal crystals of polymer particles in aqueous medium were studied.

2.9 Magnetic circular dichroism measurements

motivation

In the last section, Faraday rotation measurements showed a resonance around the middle of the stopband. Interesting is now to see whether there is any effect not only in birefringence, but also in dichroism. However, one has to be careful when talking about dichroism in the case that is investigated here. Dichroism is a difference in absorption, but here one has to deal with a lack of transmission, that might differ for the two polarization states.

For electronic transitions, a resonance in Faraday rotation is always accompanied by a resonant behavior (peak or two opposing peaks with a value of zero in between) of the absorption and of the Faraday ellipticity, which is resulting from magnetic circular dichroism (MCD) (s. Sec. 2.3.2). The lineshape is depending whether one has the diamagnetic of paramagnetic type. The resonance here is the result of the photonic band gap structure. Should one expect an analogy to the resonance from electronic transitions?

Has the magnetic field a direct influence on the spectral width of the stopband?

setup

The MCD measurements were performed with a modified Faraday rotation setup (Fig. 2.16). To have initially circularly polarized light a $\lambda/4$-plate was placed between the laser and the sample. The analyzer was removed, so that the photo diode signal directly reflected the transmission. Like for the Faraday rotation measurements, an alternating magnetic field was applied along the (111) direction of the crystal and parallel to the light beam. The photo diode signal was fed into a lock-in amplifier for phase sensitive detection.

method

In Sec. 2.3.2 it was mentioned that the refractive index becomes complex [see Eq. (2.15)] if absorption is present. The refractive index Eq. (2.16) splits into two values for each of its circular eigenmodes in the medium. Expressed in terms of the magneto-optical parameter $Q = Q' + iQ''$ and with $n = \sqrt{\varepsilon(1 \pm Q)}$ one gets in a first order development

$$n_\pm = n_0 \pm \frac{n_0}{2}\sqrt{Q'} + i\left(\kappa_0 \pm \frac{\kappa_0}{2}\sqrt{Q''}\right) \tag{2.54}$$

with $\hat{n}_0 = n_0 + i\kappa_0$ being the mean complex refractive index for zero field.

The photo diode detects the intensity I of the transmitted light wave, which depends on the polarization state

$$I_\pm = I_0 \exp\left(-2\frac{\omega}{c}(\kappa \pm \frac{1}{2}\sqrt{\epsilon Q''})d\right) \tag{2.55}$$

$I_\pm$ is the intensity for right- and left-circularly polarized light respectively and I_0 the intensity for zero field. By altering the magnetic field $B \to -B$ the MCD is also changing sign, with the effect that $I_+ \to I_-$ and vice versa [7].

The phase sensitively detected signal AC from the lock-in divided by the mean DC-value, as measured directly from the photo diode, gives

$$\alpha = \frac{AC}{DC} = \frac{I_+ - I_-}{I_0} = -\frac{\omega n_0}{c}\sqrt{Q''}\,d \tag{2.56}$$

[7] To avoid a possible misunderstanding, I would like to emphasize here that it is not the polarization that is interchanged, but only the functions; I_+ then describes the left-circular polarization mode and I_- the left-circular one.

By measuring α, Q'' can be calculated using

$$Q'' = \left(\frac{c}{\omega n_0 d}\right)^2 \alpha^2 = \left(\frac{\lambda}{2\pi\, n_0\, d}\right)^2 \alpha^2, \tag{2.57}$$

with λ being the vacuum wave length of the incident light.

The sign of Q'' is determined by the phase of the lock-in signal and the incident polarization state. I define here Q'' of positive sign for an incoming right-circular polarization and for a signal phase of 0°.

results

Measurements were taken at characteristic points of the spectrum: in the center of the stopband, on the edges and completely outside the stopband. In each case, MCD was found to be smaller than the corresponding detection limits.

That means that $Q'' < 10^{-14}$ outside the stopband and $Q'' < 10^{-6}$ in the center of the stopband.

In another notation $\hat{n} = n \pm \delta n + i(\kappa \pm \delta\kappa)$, the detection limits can be stated as $\frac{\delta\kappa}{\kappa B} = 10^{-6}\,\mathrm{T}^{-1}$ outside and $\frac{\delta\kappa}{\kappa B} = 10^{-2}\,\mathrm{T}^{-1}$ in the center of the stopband. It was made the approximation of $\kappa \approx 1\mathrm{m}^{-1}$ for the low-loss SiO_2 .

The lock-in signal at a detection frequency of 2ω were also effectively zero.

conclusion

It has to be concluded that there is no measurable effect of MCD going linear or quadratically with B.

2.10 Summary and conclusion

Magneto-spatial dispersion can take an interesting form in photonic crystals that are subject to magnetic fields. It was pointed out that the magnetic properties of photonic crystals can still be considered a rather unexplored field.

The problem was at first looked into theoretically. A method based on the transfer matrix method was developed to simulate the magneto-optical properties of a multilayer slab, which can be considered as a one dimensional photonic crystal.

The simulations suggested the Faraday effect to behave dispersion-like around the stopband of 1d photonic crystals, with two opposing peaks forming on the edges of the stopband. The Faraday rotation vanishes in the center of the stopband. The width and height of those peaks is governed by the number of layers and the refractive index contrast.

Huge Faraday Rotation and state splitting was calculated in defects and a phase shifting that follows those observed around resonances.

The Faraday rotation of 3D photonic crystals has been measured. The samples had been impregnated with a Faraday-active liquid. The Faraday rotation outside the stopband follows the spectral behavior of the pure liquid multiplied by its volume fraction. Inside the stopband, the Faraday rotation is enhanced by up to a factor of five.

The origin of this remains to be identified since no existing theory explains this behavior. Qualitatively, internal reflections are the most likely origin. The results are quite different in their line shape from those expected after the performed simulations in one dimension.

The measurements of magnetic circular dichroism showed no significant effect on the transmitted light for both linear or quadratic dependence on the magnetic field. This is a surprising result and means that the observed resonant behavior of the Faraday rotation is not accompanied by Faraday ellipticity. It also means, that the fields applied are not sufficient to change the spectral width of the stopband.

A sound three dimensional theory that allows for magnetic fields should be developed for wave scattering in photonic crystals. Such a theory would help to understand the processes behind the peaking of the Faraday rotation. It should be determined if the effect can be further amplified, since it could then be useful in the fabrication of compact optical isolators.

Chapter 3

Chiral Symmetry Breaking in Photo-Crystallization

3.1 Introduction

Chiral symmetries and the breaking of such symmetries have recently become reinvigorated as a field of research, in which physics is making close contact to chemistry and biology.

For example, for many biologically active drugs, one of the enantiomers has a desired biological effect while the other does not, or is even toxic. Due to this reason, pharmaceutical manufacturers are required to test the physiological effects of each enantiomer and produce enantiomerically pure drugs. Synthesization of purely homochiral substances is still a challenging technological undertaking.

Further, the origin for the homochirality of life is still undecided. One possible explanation is connected with the magneto-chiral anisotropy.

This recently discovered magneto-optical effect can also be attributed to magneto-spatial dispersion, and appears in the development of the dielectric function in Eq. (1.25). It is only present in chiral media.

Magneto-chiral anisotropy can generate a small excess of a certain handedness (enantiomeric excess). The generated excess is usually very small.

It was decided to look for a mechanism of amplification. In this chapter it will be shown that crystallization under influence of irradiation (photo-crystallization) provides such an amplification.

It is demonstrated here in the crystallization of $\alpha - NiSO_4 - 6 \cdot H_2O$.

3.2 Chirality

Chirality[1] means *handedness* and applies to objects that lack mirror symmetry, as is the case for the left and the right hand of the human body. It means that a

[1] In the community of particle physicists, chiral symmetry is often called what is here referred to as *time-reversal symmetry*. Moreover, they rather apply the term *parity* instead of what is here termed chirality.

chiral object exists in two states, one *right-handed* and the other *left-handed*, quite commonly employed are also the Greek words Levo (right) and Dextro (left).

The two configurations are called *enantiomers*. Enantiomers are interconverted by *space inversion*. By contrast they conserve their 'sense' by time reversal or any spatial rotation. The symmetry connected to this conservation law is the *chiral symmetry*. Objects that are not chiral are *achiral*.

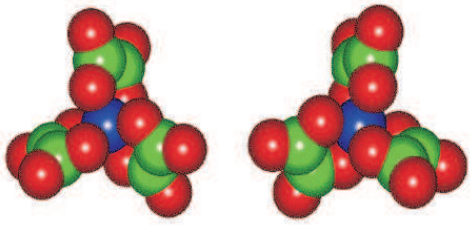

Figure 3.1: *a chiral molecule:* $Cr(ox)_3$

All helices are chiral, but not everything chiral looks like a helix. Mathematically, an object is chiral if it is not invariant under space inversion.

Chiral objects can be found of any size, from elementary particles to galaxies. In this thesis, chiral objects can be molecules or whole crystals, circularly polarized light beams or even constructions like an unpolarized light beam, which can be represented by a time-odd wave vector $\mathbf{k}$, subject to a parallel magnetic external field $\mathbf{B}$, which is a time-odd pseudo vector.

The interaction between chiral objects can be split into two parts, one that is selective on the handedness of the object and one that is not. Because of the opposite nature of the two possible kinds of handedness, the enantio-selective part of the interaction has a different sign for the two possible configurations.

3.3 Optics and magneto-optics of chiral systems

Sec. 2.3 already treated the basic magneto-optical effects. Phenomenologically similar optical effects are treated in this section. However, they result from completely different origins. Even without the presence of a magnetic field, light is undergoing rotations in its polarization, if it is traveling in chiral media.

This section describes optical activity and the magneto-chiral anisotropy, a higher order effect. Some symmetry aspects are considered and discussed further down. And at the end, nickel sulfate, the actual chiral system on which the work has been performed, is presented.

3.3.1 Optical activity

Optical activity is found in all chiral media. For light traveling along the helix axis, it manifests itself in different refractive indices n_+ and n_- for the two circular polarization states, and can be classified as *natural circular birefringence* (NCB).

For absorbing media one has to deal with differences of absorption coefficients for each normal mode, which in turn are related to the imaginary part of the refractive index κ_+ and κ_-, with $\hat{n} = n + i\kappa$. This is called *natural circular dichroism* (NCD).

Linearly polarized light of wavelength λ becomes elliptical by traveling along the optical axis over a distance d. The major axis is oriented at the angle θ:

$$\theta = \frac{\pi d}{\lambda}(n_- - n_+) \tag{3.1}$$

and its ellipticity ψ is:

$$\psi = \frac{\pi d}{\lambda}(\kappa_- - \kappa_+) \tag{3.2}$$

The origin behind optical activity is to be found in the helical structure of the molecules in a chiral media. Qualitatively spoken, the electrons are constrained to move along those helices.

For wavelengths corresponding to the pitch of such helices the approximation of a spatially uniform electromagnetic field is no longer valid and *spatial dispersion* has to be taken into account. Spatial dispersion was discussed in Sec. 1.8. Eq. (1.23) says that in this case the dielectric tensor is a function of the wave vector $\hat{\varepsilon}(\omega, \mathbf{k})$.

In the expansion Eq. (1.25) the dielectric tensor without an external magnetic field in chiral media becomes:

$$\varepsilon_{ik}(\omega, \mathbf{k}) = \varepsilon_{ik}(\omega) + \alpha_{ikl}(\omega)k_l \tag{3.3}$$

The case with the lowest symmetry of the system is that of a biaxial crystal with an arbitrary wave direction. In such a case natural optical activity is only a small perturbation of the ordinary effects of birefringence and dichroism.

For isotropic bodies or for uniaxial crystals and waves traveling in the direction of that optical axis, optical activity is at the origin of circular birefringence and dichroism. For the two $\pm$-circular eigenmodes Eq. (3.3) reduces to a skalar relation:

$$\varepsilon_\pm(\omega, \mathbf{k}) = \varepsilon(\omega) \pm \alpha^{d/l}(\omega)k \tag{3.4}$$

where $\alpha^d(\omega) = -\alpha^l(\omega)$ refers to the right (d) - or left (l) -handed media.

The connection to the Eqs. (3.1)-(3.2) can be done with the help of Eqs. (1.10)-(1.12).

3.3.2 Magneto-chiral anisotropy

The magneto-chiral anisotropy (MChA) was only recently discovered. This new optical effect has as its main characteristic the independence on the light's polarization. The magneto-chiral anisotropy is described in some detail in the pioneering work of Ernst Raupach [Rau02].

It is observed as a spatial anisotropy in the luminescence [RR97], refraction [KW98, VGF+01], absorption [RR98] and photochemistry [RR00] of chiral media subject to a magnetic field. The analogous effect for electronic magneto-transport in chiral conductors has also been reported [RFW01, KR02].

The origin behind the magneto-chiral anisotropy (MChA) is the existence of magneto-spatial dispersion (s. Sec. 1.10). From the expansion Eq. (1.25) one gets for chiral media:

$$\varepsilon_{ik}(\omega, \mathbf{k}, \mathbf{B}) = \varepsilon_{ik}(\omega) + \alpha_{ikl}(\omega)k_l + \beta_{ikl}(\omega)B_l + \gamma_{ikl}(\omega)k_l B_l \tag{3.5}$$

For high symmetry chiral media like gases, liquids, or uniaxial crystals, this leads to a dielectric constant $\varepsilon_{\pm}(\omega, \mathbf{k}, \mathbf{B})$ for the $\pm$-circular eigenmodes, propagating parallel to the symmetry axis, of the form:

$$\varepsilon_{\pm}(\omega, \mathbf{k}, \mathbf{B}) = \varepsilon(\omega) \pm \alpha^{d/l}(\omega)k \pm \beta(\omega)B + \gamma^{d/l}(\omega)\mathbf{k} \cdot \mathbf{B} \tag{3.6}$$

where $x^d(\omega) = -x^l(\omega)$ refer to right (d) - and left (l) -handed media. The material parameters α, β and γ are in general complex valued, where α and β describe natural - and magnetic optical activity respectively and γ describes MChA. The equation above needs to have the required symmetries as detailed in table 3.1 to be in accordance with the underlying physical laws.

	$\mathbf{k}$	$\mathbf{B}$	$\mathbf{k} \cdot \mathbf{B}$	ε	α	β	γ
C	+	−	−	+	+	−	−
P	−	+	−	+	−	+	−
T	−	−	+	+	−	−	+
CP	−	−	+	+	−	−	+
CPT	+	+	+	+	+	+	+

Table 3.1: *Behavior under the main symmetry operations: inversion of Charge(C), Parity(P), Time(T) and combinations*

The essential features of MChA, as expressed by Eq. (3.6), are (i) the dependence on the relative orientation of $\mathbf{k}$ and $\mathbf{B}$, (ii) the dependence on the handedness of the chiral medium (enantioselectivity), and (iii) the independence of the polarization state of the light.

3.3.3 Nickel sulfate hexahydrate

chemical structure

Nickel sulfate hexahydrate crystallizes in two possible polymorphs, the α- and the β-phase. The β-phase has a monoclinic crystal structure and is achiral. The α-phase has a tetragonal crystal structure (Fig. 3.2) and presents two enantiomeric configurations.

The crystal structure (Fig. 3.3) comprises layers of $Ni(OH_2)_6^{2+}$ and SO_4 groups connected by a network of hydrogen bonds within the layers and less strongly in between the layers.

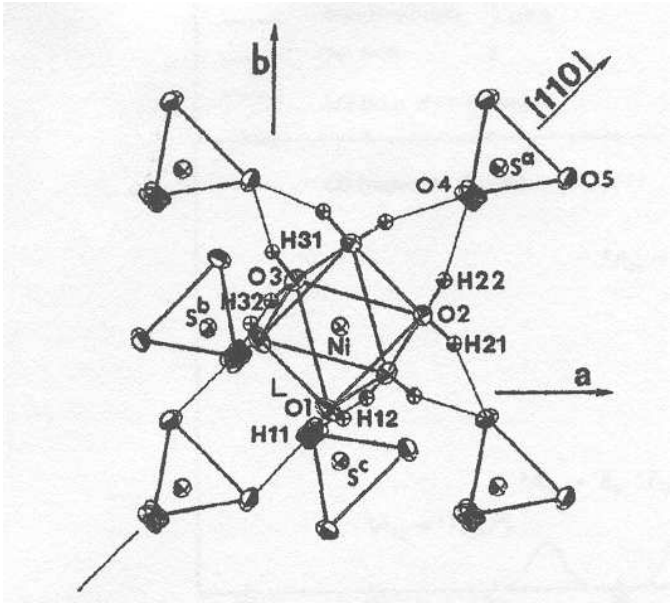

Figure 3.2: *Structure of* $\alpha - NiSO_4 \cdot 6H_2O$. *Shown is the (001) projection of the* $Ni(OH_2)_6^{2+}$ *group with all the nearest sulfate groups connected by hydrogen bonds (from:[SGK87]).*

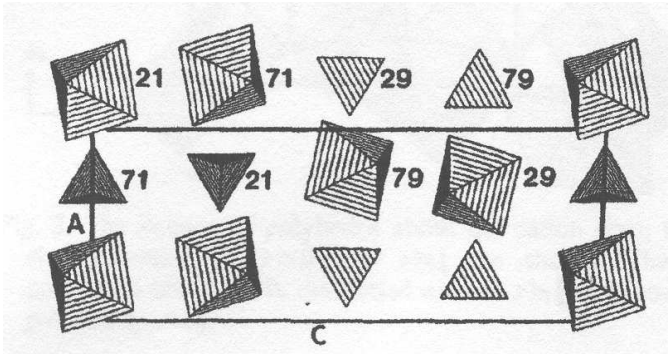

Figure 3.3: *Tetrahedra of* $\alpha - NiSO_4 \cdot 6H_2O$. *(010) projection of* NiO_6 *and* SO_4 *polyhedra (from [AF88]).*

optical and magneto-optical properties

In the range of optical frequencies, nickel sulfate hexahydrate has two main electronic transitions. They are influenced by a chiral crystal field at the position of the Ni^{2+} ions. Fig. 3.4 shows measured values for absorption, NCD and MCD. There is an absorption peak around 690 nm and another one around 1180 nm due to the corresponding electronic transitions.

The peak anisotropy values for NCD are $g_{NCD} = \left(\frac{\Delta A_{NCD}}{A}\right) = 0.11$ (1180 nm) and $g_{NCD} = 0.03$ (690 nm). Values for the MCD peaks are $g_{MCD} = \left(\frac{\Delta A_{MCD}}{A}\right) = 7.5 \cdot 10^{-4}\mathrm{T}^{-1}$ and $g_{MCD} = 8.6 \cdot 10^{-4}\mathrm{T}^{-1}$. $\Delta A = A_+ - A_-$ is the difference in absorption for the two $\pm$-circular eigenmodes and $A = \frac{1}{2}(A_+ + A_-)$ is the mean

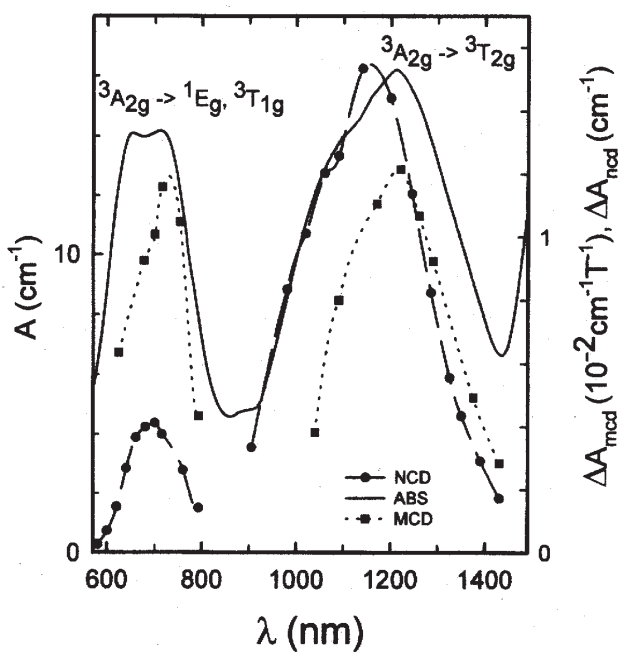

Figure 3.4: *Absorption (ABS), natural(NCD) and magnetic circular dichroism (MCD) of* $\alpha - NiSO_4 \cdot 6H_2O$ *(from [RR98]).*

value.

Fig. 3.5 shows the measurements of E. Raupach [Rau02] for the magneto-chiral dichroism (MChD) around 1300 nm with a peak value of $g_{MChD} \approx 2.5 \cdot 10^{-4}\mathrm{T}^{-1}$.

3.4 Photo-crystallization

3.4.1 Chiral symmetry breaking in crystallization

In the production of crystals that exist in form of two possible enantiomers, the result is usually a racemic mixtures of both. Yet, spontaneous chiral symmetry breaking does occur in crystallization processes and can actually be triggered by certain catalysts. It has been shown recently for example, that stirring in a solution at the time of nucleation does lead to secondary nucleation and is thus inducing a form of auto-catalysis [KBD+93, KLA99] that is then leading to a spontaneous breaking of the chiral symmetry. A controlled symmetry breaking, where the sign of the enantiomeric excess (EE) can actually be chosen, can be achieved by adding chiral seeds, or as is the approach here, by circularly polarized light. The latter is only possible if natural optical activity is present (and of important size) in the constituents.

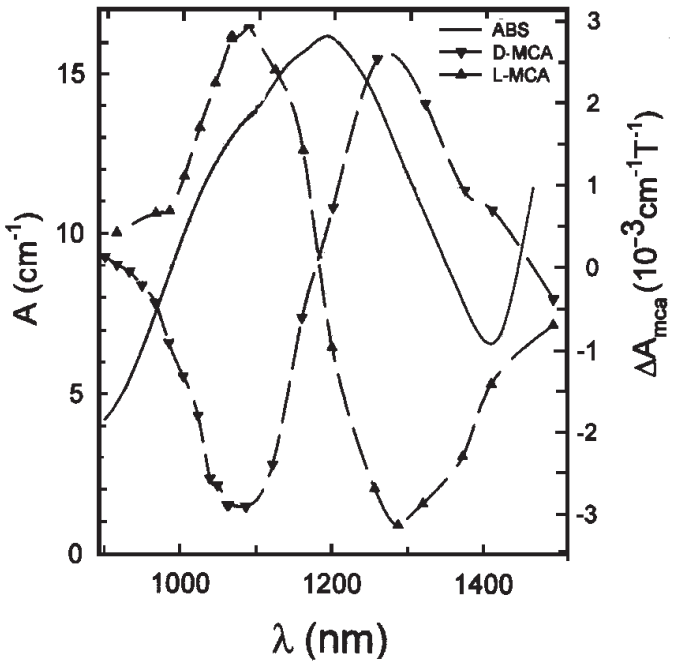

Figure 3.5: *Absorption and magneto-chiral dichroism of* $\alpha - NiSO_4 \cdot 6H_2O$ *(from [Rau02]).*

3.4.2 Crystallization from solutions

Here I describe the usual techniques to grow crystals [PRK69]. The widest used technique is the growth from solutions, because those can be handled more easily than melts or gases. The different mechanisms to produce a supersaturation and the spontaneous nucleation and the subsequent growth into a macroscopic crystal rely on cooling, solvent evaporation, or on convection.

Crystallization by cooling of the solution or by solvent evaporation are the most straightforward methods, they can be easily realized, since one only needs a thermostatted crystallizer to control the temperature. In the former case, the solution has to be cooled[2]systematically in order to keep a certain supersaturation. The constantly changing temperature is a disadvantage and creates a *non-steady-state condition*. In the latter case, a difference between the rates of evaporation of the solvent and the solute is used to alter the solution's concentration. Usually, it is sufficient to allow the vapor formed above the solution to escape. This method is also creates non-steady-state conditions.

If crystallization should be done under *steady-state conditions*, the methods employed are thermal convection, concentration convection, forced convection, etc. In the case of different temperatures in parts of the crystallizer, a temperature gradient is established and produces convection in the solution. The temperature distribution can be kept steady and the volume, where the crystallization actually takes place, can be restricted.

[2]better: directed toward lower solubility

Methods working under steady-state conditions generally produce crystals of higher quality. They also have the advantage that the involved processes can be described more easily by equilibrium thermodynamical formulas. This can be important in the longer run for the problem treated here, where the physics needs to be modeled and the model eventually verified.

3.4.3 The experiment

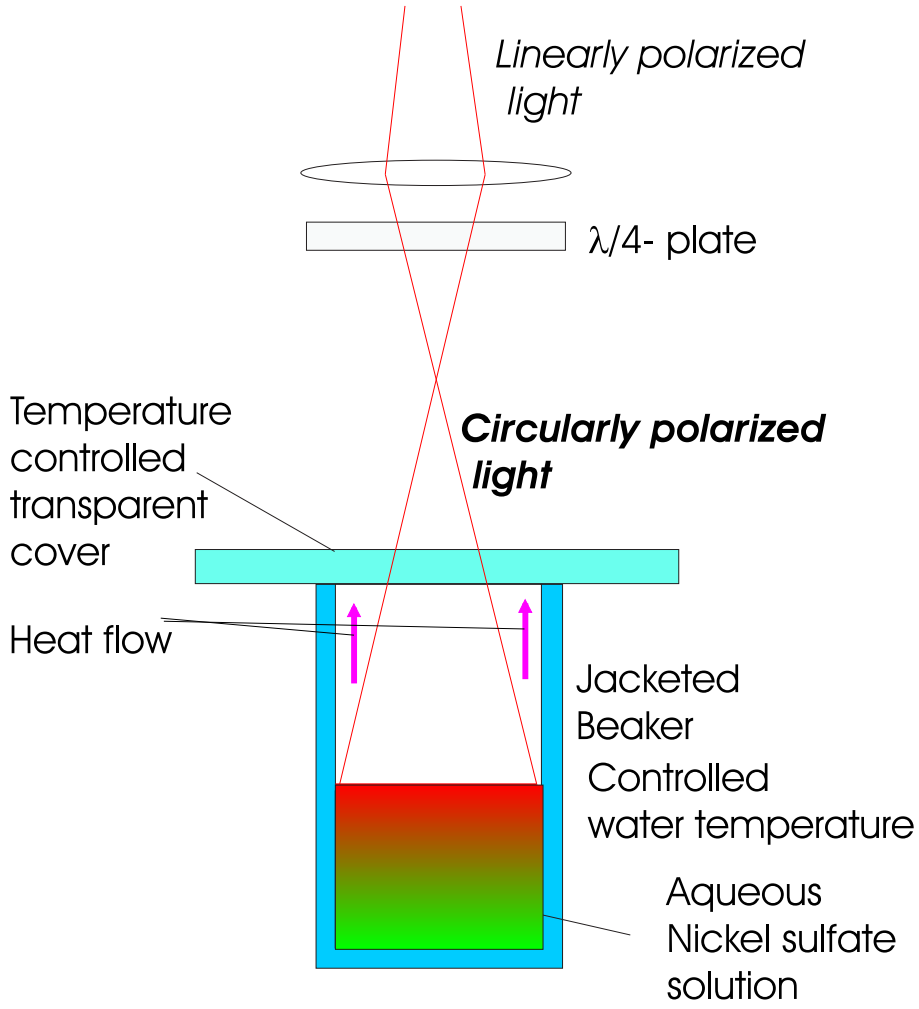

Figure 3.6: *Crystallization setup for chiral symmetry breaking with circularly polarized light.*

the photo-crystallization setup

Fig. 3.6 shows the employed photo-crystallization setup. A saturated nickel sulfate aqueous solution is put in a jacketed beaker whose temperature is controlled by a programmable water bath. The solution's surface is illuminated with circularly polarized light that is absorbed within the first millimeters. I use a linearly polarized beam from a Titan-sapphire laser tuned to a wavelength of 950 nm. A

$\lambda/4$-plate is used to turn the polarization circular. Optionally, I have a jacketed cover on top of the beaker, whose temperature can be controlled separately by an independent water bath. Without cover, free evaporation of the solvent is additionally contributing to the crystallization.

preparing the solution

I used commercially available nickel(II) sulfate hexahydrate powder (1 kg, 99 % purity), a product of Aldrich. The magneto-optics of its α-polymorph is described in detail in Sec. 3.3.3.

A solution was prepared by mixing 58 g of nickel sulfate with 40 ml of deionized water, corresponding to a concentration of $c_{NiSO_4} = 1.45$ M. The solute is dissolved completely at temperatures near 90 °C, then the solution is slowly cooled down to a temperature of 60 °C, where the solution approaches its saturation level. It is then filtered for micro particles and poured delicately into the jacketed beaker.

Under normal atmospheric pressure, nickel sulfate is forming crystals in its morphological α-phase at temperatures between 53 °C and 32 °C. The crystals have a decaeder or hexaeder (truncated pyramid) form and present an optical symmetry axis perpendicular to the base rectangle. They are dark green and are partially transparent.

beta-crystals

Above 53 °C nickel sulfate crystallizes in its morphological β-phase. The β-phase is of a lighter green color, is not transparent and has no chiral symmetry. The production of β-crystals is therefore not desired in this experiment. If, nevertheless, some β crystals can be found, then the solution has started to crystallize while still too hot. Once formed, the β-crystals continue their growth below 53 °C and then only a small number of α-crystals will be found in the resulting batch. Waiting long enough for the solution to cool to the appropriate temperature is necessary before pouring it into the beaker.

oil films

If oil films were used (s. Sec. 3.5.3), they were poured onto the settled solution at this stage. The oils have to be preheated in order to avoid an immediate triggering of nucleation. It should also be put on in a gentle way, so that the surface of the solution is not too much disturbed.

crystallization program

The crystallization is controlled over the temperature of the water bath. The program started with a phase of constant temperature (50 °C for at least 30 min.) in which the solution had time to settle. In the crystallization phase the temperature was slowly lowered to 33 °C over a time of 14 hours. For a shorter time span the resulting crystal size is generally too small for the cleaving that is required by the analyzes process. The temperature was then kept at 33 °C before the crystals

were taken out of the recipient. The cover was programmed to descend from 50 °C to 30 °C in 5 min and then more slowly in 8 h to 20 °C.

temperature gradient

To assure that a maximum number of nucleations take place in the region, where irradiation power is high, the surface is held at a temperature of some degrees lower than the rest by allowing a net flow of heat upward through a temperature controlled transparent cover. In the case of free evaporation of the solvent, the cooling of the surface is much more pronounced and takes only place close to the surface. Moreover, the evaporation rate is not easily controllable.

surface tension and critical mass

The crystallites are growing at the surface under the influence of light. Once they have exceeded the critical mass (s. Sec. 3.6 and Fig. 3.19) the influence of light is no longer necessary and they will continue to grow. Eventually, they will fall to the bottom of the beaker, where they continue to grow until the crystallization program is stopped.

various perturbations

In order to assure a minimal disruption of the crystallization procedure and to look for sources of systematic errors, various perturbation have to be taken into account. Numerous perturbations are possible for an open recipient, for instance, changes in the surrounding air humidity and a changing flow of air can lead to varying evaporation rates. More control over these parameters–as well as over dust–is obtained by putting the crystallizer in a desiccator. But even for a closed recipient, there are still moments during preparation when the solution is exposed to those influences. Additionally, problems of fogging and condensation on the cover have to be dealt with for closed recipients. Most efficient to suppress fogging and evaporation as a whole was the application of an oil film on the surface of the solution. Still, the oil films themselves can have an influence on the solution.

3.4.4 Analysis

cleavage

Each crystal of the batch has to be cleaved before one can determine its handedness. For practical reasons, only crystals of a decent size can be cleaved. For a fixed solution volume this limits the number of useful crystals.

Nickel sulfate crystals easily split perpendicular to the optical axis. An orientation along the optical axis is then simply the direction perpendicular to the surface of a cleaved crystal.

natural circular dichroism

The discrimination between the two enantiomers is possible by measuring the crystals natural circular dichroism (NCD). One has to measure the absorption for the two circular polarization modes of the light. If right-circularly polarized light is more absorpted than left-circularly polarized light, the crystal is right-handed, and vice versa. Compared to the overall absorption, NCD is of the order of 4% in nickel sulfate for a wavelength of 632 nm. The difference can not be seen simply by eye, and the analysis can become extremely time consuming if the polarization has to be changed by hand for each crystal.

PEM-setup

Fig. 3.7 shows the setup to analyze a number of crystals more quickly. It uses

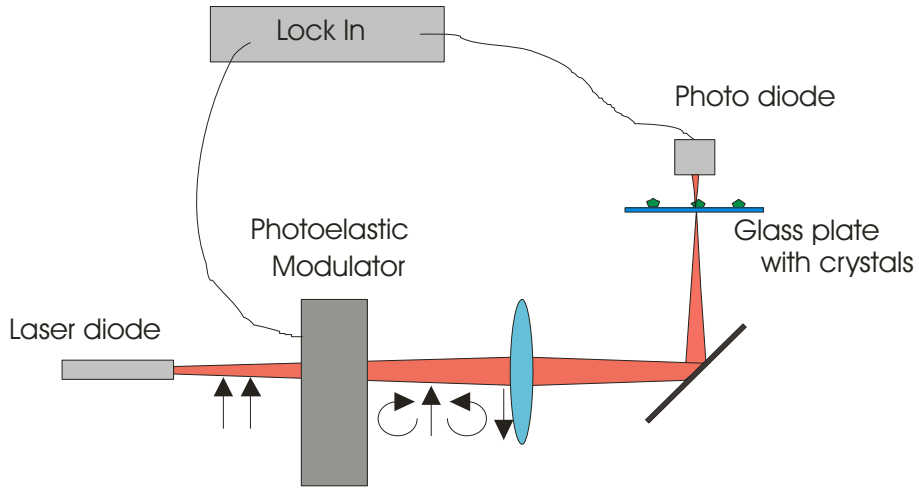

Figure 3.7: *Setup to analyze crystal chirality. A photo-elastic modulator transforms linearly polarized light into circularly polarized light oscillating between the right- and left-circular polarization states (as indicated by the arrows) at a frequency of 30 kHz.*

a photo-elastic modulator (PEM) at a frequency of 30 kHz. Linearly polarized light has its polarization altered by the PEM. It oscillates between right- and left-circular polarization. The light then enters a nickel sulfate crystal and is partially absorbed while traveling along the optical axis. The transmitted light is phase sensitively detected by a lock-in amplifier. The sign of the lock-in signal indicates the handedness of the analyzed crystal. Thus I can distinguish between the two enantiomers. This process only takes a few seconds, a considerable improvement to the former measurement method. The order of magnitude can be estimate by the thickness of the crystal along the optical path in the case of any doubt about the absolute value.

limitations

But even this PEM method is not fast enough to analyze large numbers of crystals. Large numbers are ultimately necessary in order to reduce the large error margins inherent in my crystallization method. The major bottleneck is the fact that every single crystal has to be cleaved and oriented by hand. Another problem is the need for sufficient size of the crystals. This necessitates a rather long crystallization time. However, a method that is able to collectively measure the handedness of a whole batch has not yet been found.

definition of enantiomeric excess

The enantiomeric excess in a batch was defined as

$$\frac{\Delta N}{N} = \frac{N_D - N_L}{N_D + N_L}. \tag{3.7}$$

Thus, if the number of left-handed crystals N_D is equal to the number of right-handed crystals N_D (racemic mixture), the excess $\Delta N/N$ is zero. It is +1(-1) for a batch contenting only right-(left-)handed crystals.

statistics

The standard deviation is $1/\sqrt{N}$.

The additional systematic errors connected with the preparation can be quite important! One should follow strictly a chosen procedure in always the same way to limit as much as possible its unquantifiable influence.

3.5 Measurements and discussion

3.5.1 Enantiomeric excess as a function of light ellipticity

Tab. 3.2 shows the result of a first group of analyzed crystal batches. The particular experimental conditions (s. Sec. 3.4.3) for these early measurements were that of an open recipient allowing for free evaporation of the solution. Laser light (950 nm) is illuminating continuously the recipient from above. The solution was not prefiltered and no oil films were present. The crystallization procedure consists of only two steps: i) filling of the jacketed beaker at a temperature of 55°C, ii) slowly cooling down of the solution to 30°C over 16h.

By means of a $\lambda/4$-plate the polarization state of the light could be changed from right-circularly polarized over linearly polarized to left-circularly polarized light, continuously. Figure 3.8 shows graphically the observed dependence of the enantiomeric excess on the angular position ϕ of the $\lambda/4$-plate. A fitted sinus function (matching probability: 72%) is plotted next to the data points for comparison.

The ellipticity ψ is a sinus function of ϕ: $\psi = \sin(\phi/2)$. The same data as in Fig. 3.8 as a function of ellipticity is plotted in Fig. 3.9 and appears to be of a linear dependence in a first approximation.

ellipticity	angle of $\lambda/4$-plate	ΔN	N	$\frac{\Delta N}{N}$ in %	$\pm\frac{1}{\sqrt{N}}$ %
+1	-45	-149	267	-56	6
+0,866	-30	-16	24	-66	20
0	0	2	92	+2	10
-0,866	+30	+1	31	+3	18
-1	+45	+79	121	+65	9

Table 3.2: *A first group of analyzed batches; Nickel sulfate concentration in initial solution:* $c_{NiSO_4} = 58\,g/40\,ml$*, free evaporation, irradiation wavelength* $\lambda_i = 950\,nm$*, irradiation power:* $P_i = 500\,mW$

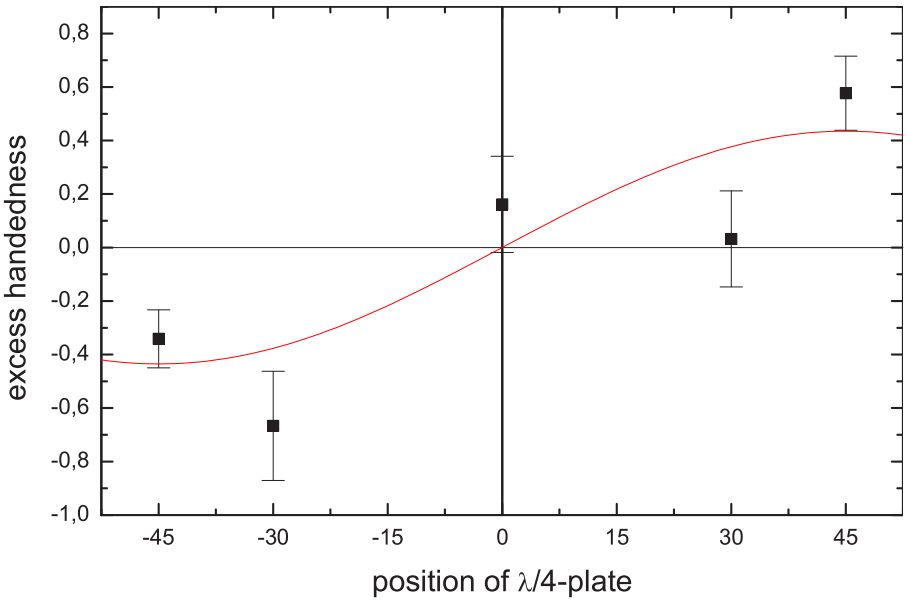

Figure 3.8: *Enantiomeric excess as a function of the angle of the* $\lambda/4$*-plate (plotted from Table 3.2).* $c_{NiSO_4} = 58\,g/40\,ml$*; free evaporation; irradiation wavelength* $\lambda_i = 950\,nm$*; irradiation power:* $P_i = 500\,mW$*. The line is a sinus plot* $(y = A\sin(\phi/2))$ *fitted to the data points (coefficient of determination :* R^2*=72%)* [a].

[a] *The coefficient of determination is the percent of the variation that can be explained by the regression equation.*

As one can see, the enantiomeric excess reaches high values within reach of the complete elimination of one handedness. The excess is changing sign when going from left-circularly to right-circularly polarized light and is zero for linearly-polarized light.

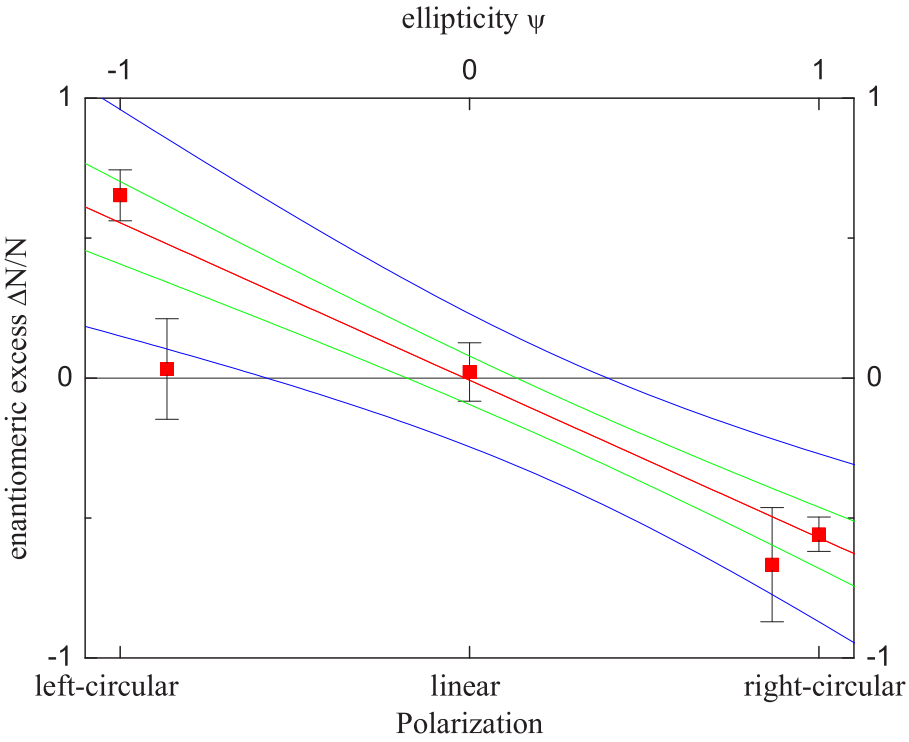

Figure 3.9: *The enantiomeric excess as a function of the ellipticity of the light (from Table 3.2)* $c_{NiSO_4} = 58\,g/40\,ml$*; free evaporation; irradiation wavelength* $\lambda_i = 950\,nm$*; irradiation power:* $P_i = 500\,mW$.

3.5.2 Enantiomeric excess under varying experimental conditions

The measurements presented above were 'quick shot' measurements that turned out to yield astonishingly pronounced results. The next steps involved looking for improvements in the choice of various experimental parameters.

changed concentration

One immediately turns the attention to the preparation of the saturated nickel sulfate solution, where one could play with its concentration c_{NiSO_4}. The effect of a changed concentrations lies in a modification of the solution's initial saturation level. There should be no crystallization before the solution has settled in the recipient, this means the concentration has to be sufficiently low. But the concentration should also be sufficiently high in order to grow sufficiently large crystals, that use most of the temperature interval for growing[3]. It would be worthwhile to look for an analysis method that could do with smaller crystals (s. Sec. 3.4.4).

Experiments with a concentration c_{NiSO_4} changed to $56\,g/40\,ml = 1.40\,M$ were tried in order to reduce the percentage of batches showing no significant excess,

[3]It was not practical to increase the already long crystallization time.

which could be due to 'accidents' triggering the crystallization. The persistent share of 'accidental' batches proved that they could not be as easily controlled as initially suspected.

cover

A weak point of my first experimental design was the free evaporation, which is sensitive to possibly changing conditions of the outer environment, like varying air humidity, temperature changes and falling dust particles. To eliminate these influences, a transparent cover was put on top of the jacketed beaker. The first measurements of that kind were disappointing, since no excess could be observed any more. By comparison to the evaporating system, it was found that the solution's surface should be colder than the bulk to favor nucleation in that part. In order to control this, a jacketed cover was used, whose temperature could be controlled separately from the beaker. Enantiomeric excesses were observed when holding the cover at temperatures that were at least 10 °C lower with respect to the beaker.

fogging

The lower temperature of the cover had the disadvantage that one had condensation of water from the hot solution on its surface. Eventually droplets form and hinder the light to reach the surface with full intensity. One effect is that light is partly scattered out of the desired optical path. Another one is that the droplets work as lenses and create an intensity pattern on the surface of the solution. Both effects are undesired. Unfortunately, it is impossible to completely avoid the formation of those droplets in humidity conditions of 100 %.

Nevertheless, a film of *Sigma Coat (Aldrich)* on the cover's surface helps to improve conditions for some minutes.

Another way is the application of oil films as discussed in the next subsection.

pre-filtering In order to avoid premature nucleation from dust particles the solution was filtered. The pore size was chosen in the μm range.

infilling procedure Infilling of the hot solution into the beaker should be done very carefully to avoid premature nucleation from turbulences and evaporation in a still open recipient. I used a flexible tube, which was held between the cover and the beaker and allowed for a laminar fluid flow.

importance of the first minutes It is clear from the above explanations that the first few minutes are the most important in the production of an enantiomeric excess. It might even be possible to switch of the laser after that initial stage. Unfortunately, there is so far no clear-cut proof for that. The inherently large systematic error made tests in that direction not entirely convincing.

3.5.3 Influence of oil films

The fruitless efforts to find efficient ways of blocking the fogging of the cover in conditions of near 100 % air humidity let me look for ways that block the evaporation on the surface of the solution. Oil films show the necessary transparency and adapt smoothly to the surface even with very little material.

However, one needs to be careful in the choice of oil, especially in case of organic ones. They are often chiral. Since an interaction of the nucleation process at the surface layer with the oil molecules can not be excluded, this would disrupt my experiment. Therefore, I started my search with synthetic oil[4].

ellipticity	ΔN	N	$\frac{\Delta N}{N}$ in %	$\pm\frac{1}{\sqrt{N}}$ %
1	-11	23	-48	21
0	0	10	0	32
-1	+9	23	+39	21

Table 3.3: *A second group of analyzed batches;* $c_{NiSO_4} = 56\,g/40\,ml$; $\lambda_i = 950\,nm$; $P_i = 200\,mW$.

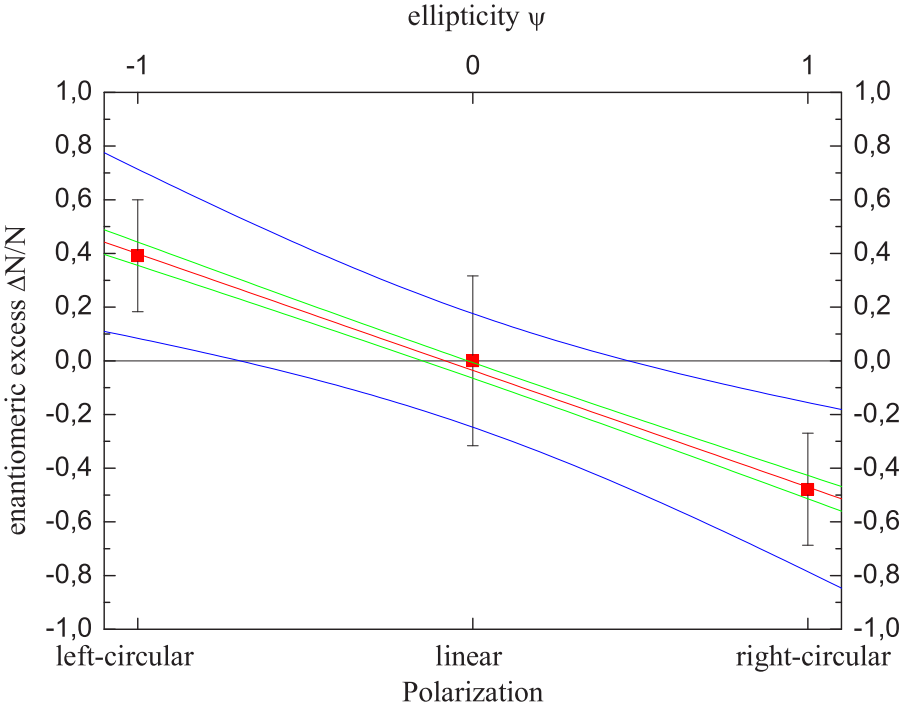

Figure 3.10: *The enantiomeric excess as a function of the ellipticity of the light (from Table 3.3)* $c_{NiSO_4} = 56\,g/40\,ml$; $\lambda_i = 950\,nm$; $P_i = 200\,mW$.

[4]It is still possible for some to have chiral components, but then they should at least consist of a racemic mixtures of both enantiomers.

ellipticity	ΔN	N	$\frac{\Delta N}{N}$ in %	$\pm\frac{1}{\sqrt{N}}$ %
+1	-28	38	-74	16
0	-10	40	-25	16
-1	15	47	+32	15

Table 3.4: *A third group of analyzed batches;* $c_{NiSO_4} = 58\,g/40\,ml$; $\lambda_i = 950\,nm$; $P_i = 500\,mW$.

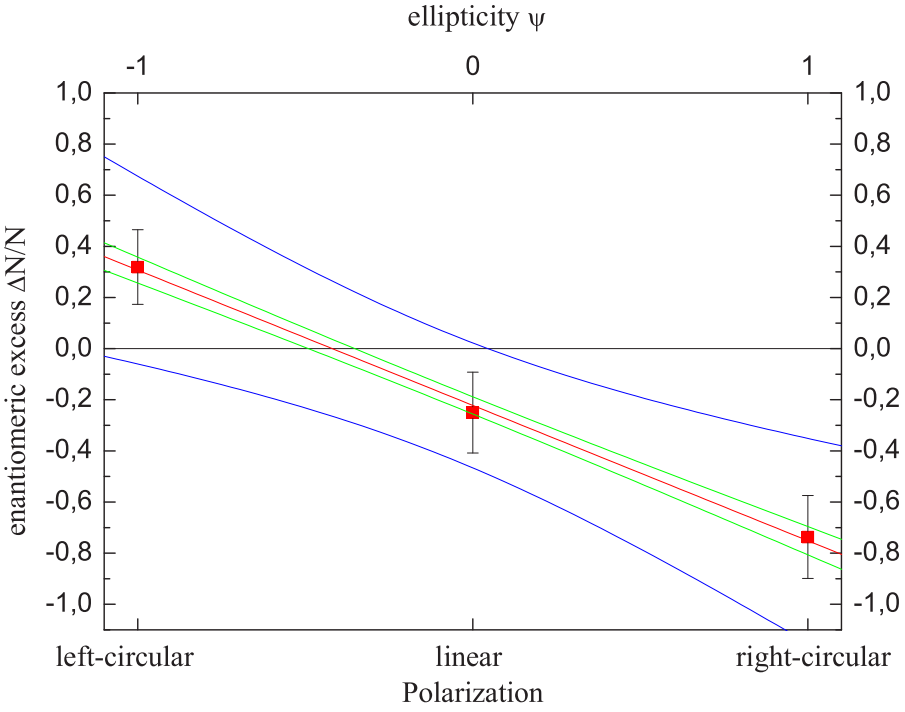

Figure 3.11: *The enantiomeric excess as a function of the ellipticity of the light (from Table 3.4)* $c_{NiSO_4} = 58\,g/40\,ml$; $\lambda_i = 950\,nm$; $P_i = 500\,mW$.

One oil was poly(dimethyl) siloxane 200® fluid a product from Aldrich. Its chemical structure is $[-Si(CH_3)_2-]_n$, it has a viscosity of 50 cstokes and a density of n_D^{20}=0.96 g/ml

There seems to be an offset in the enantiomeric excess generated by the siloxane oil film (s. Fig. 3.11).

Figure 3.12 shows contradictory results with siloxane as the oil film, and the work with it was therefore discontinued.

Another oil was liquid paraffin (n_D^{20}=0.88 g/ml, product of Merck).

Figure 3.13 shows no detectable excess. It has to be concluded that liquid paraffin is also not useful. Is it eliminating somehow the light's influence by changing the polarization state?

The check is done by measuring any optical activity of the oil. There was no

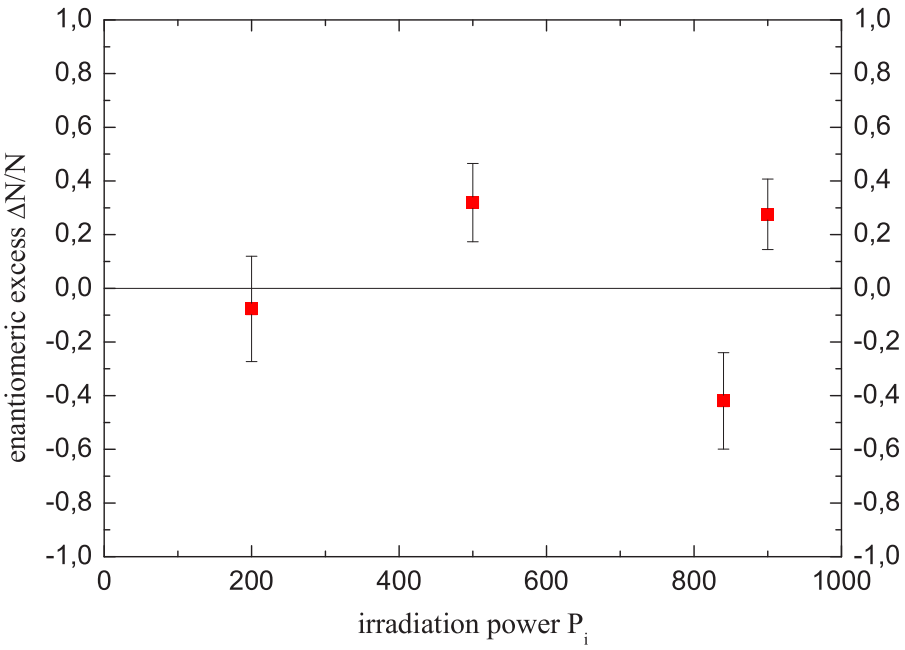

Figure 3.12: *The enantiomeric excess as a function of irradiation power of the light (from Table 3.5) with oil film on top.* $c_{NiSO_4} = 56\,g/40\,ml$*; oil film: poly-(dimethyl)siloxane 200 fluid;* $\lambda_i = 950\,nm$*; right-circularly polarized light.*

Batch	power mW	ellipticity	ΔN	N	$\frac{\Delta N}{N}$ in %	$\pm\frac{1}{\sqrt{N}}$ %	oil
T	500	+1	-28	38	-74	16	siloxane
V	500	0	-10	40	-25	16	siloxane
S	500	-1	15	47	32	15	siloxane
W	200	-1	-2	26	-8	20	siloxane
X	840	-1	-13	31	-42	18	siloxane
Y	500	-1	0	8	0	35	paraffin
Z	900	-1	-2	40	-5	16	paraffin
AA	900	-1	16	58	28	13	siloxane

Table 3.5: *several more batches* $c_{NiSO_4} = 56\,g/40\,ml$*; under various oil films;* $\lambda_i = 950\,nm$*;*

significant optical activity in both types of oil in the optical regime measured with two crossed polarizers. It was presumed that there were no drastic changes to that in the near infrared region.

By contrast, liquid paraffin has a small absorption peak at 925 ± 25 nm, $A_{max} = 0.05$, $A_{950nm} = 0.01$. There is no significant absorption for siloxane oil: $A_{950nm} = 0.002$, small peak at 910 ± 15 nm, $A_{max} = 0.08$.

This explains to some extent the reduced excess in Fig. 3.10 and the absence of an excess in Fig. 3.13.

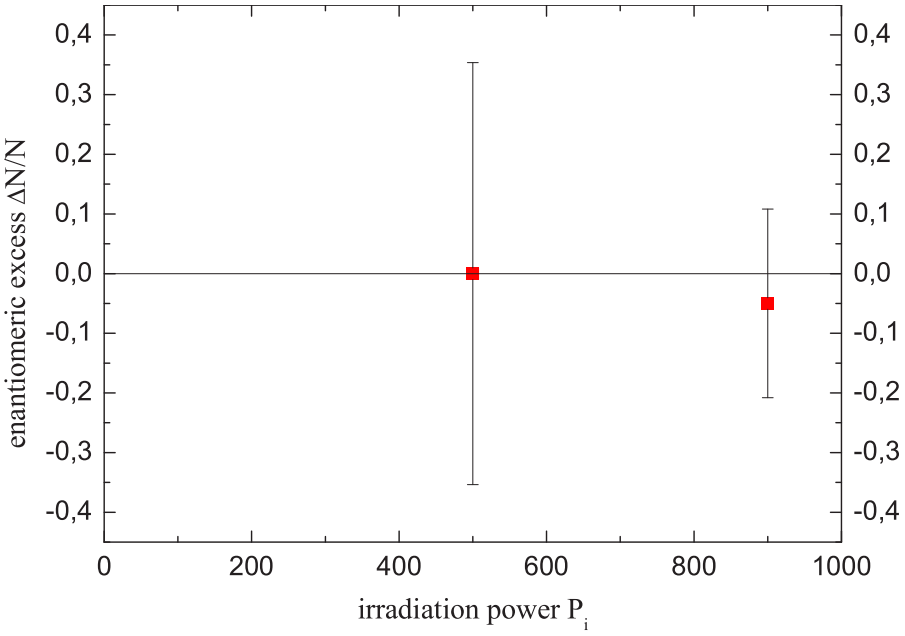

Figure 3.13: *The enantiomeric excess as a function of irradiation power (from Table 3.5) under a liquid paraffin oil film.* $c_{NiSO_4} = 56\,g/40\,ml$*; oil film: liquid paraffin;* $\lambda_i = 950\,nm$*;*

What actually has been showing some optical activity was the plastic top of the jacketed cover in its first version, thus explaining the offset present in Fig. 3.10. It was therefore replaced by glass.

3.5.4 Enantiomeric excess as a function of light power

Is is of some importance to know how the irradiation power quantitatively influences the enantiomeric excess. Whether it is a linear dependence, an exponential one, or some other form, will give an important hint to the microscopic interaction of the light with the forming nuclei.

Table 3.6 compares data for two different values of incident light power.

power mW	ellipticity	ΔN	N	$\frac{\Delta N}{N}$ in %	$\pm\frac{1}{\sqrt{N}}$ %
200	+1	+1	15	+7	26
500	+1	+9	23	+40	21

Table 3.6: *Comparison of two batches with varying light power;* $c_{NiSO_4} = 58\,g/40\,ml$*; free evaporation;* $\lambda_i = 950\,nm$*; right-circularly polarized light.*

By looking at the errors bars in Fig. 3.14, one can see that they do not allow for a detailed analysis of the power dependence of the enantiomeric excess. Nevertheless, there are hints that the process needs a minimum laser power to produce

a significant excess.

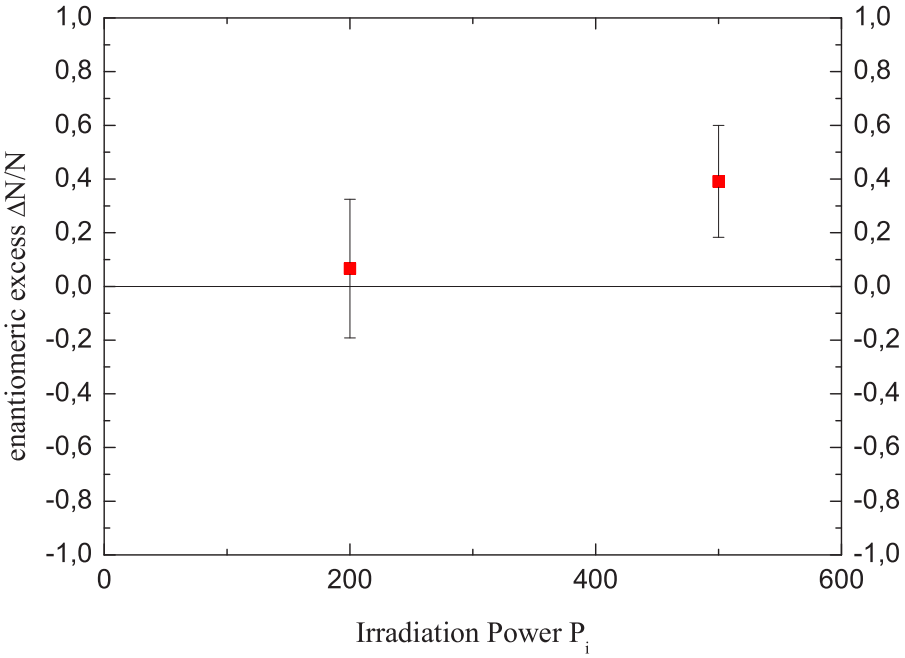

Figure 3.14: *The enantiomeric excess as a function of irradiation power (from Table 3.6).* $c_{NiSO_4} = 58\,g/40\,ml$*; free evaporation;* $\lambda_i = 950\,nm$*; right-circularly polarized light.*

Once the crystallization process is better under control, a complete power dependence would be useful to better understand the mechanism behind this chiral symmetry breaking.

3.6 Constructing a model

This large excess originates from a rather small difference in absorption for circularly polarized light of the two enantiomers (natural circular dichroism) of nickel sulfate crystals, which is of the order of 10 % at 950 nm (see Fig. 3.4).

In this section, I propose a mechanism that may be responsible for the observed enantiomeric excess.

3.6.1 Phase diagram of a solution

The physical system to describe is a solution, i.e., the solvent and the solute. They are in constant interaction and are characterized by their concentration and chemical structure. These interactions are sensitive to external influences, such as temperature, pressure, etc..

getting a feeling for the solution's state

The most critical point of the experiment lies in determining the right state of the solution. In order to make excesses of the observed magnitudes possible, the right preconditions have to be arranged within a certain precision. A delicate choice is the positioning of a proper crystallization point in the solubility diagram (see Fig. 3.15) near the saturation limit.

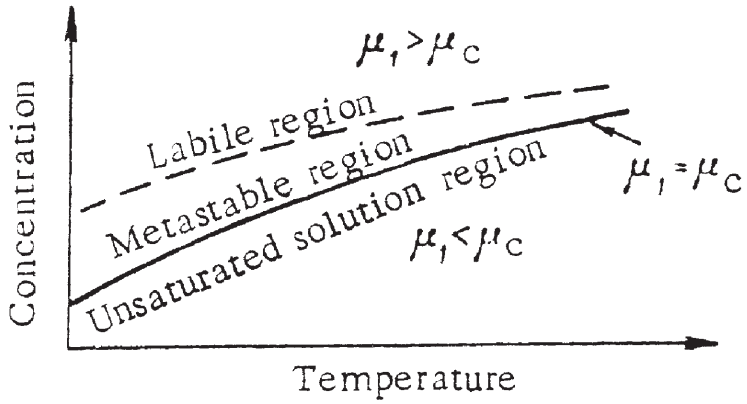

Figure 3.15: *The phase diagram of a solution (from: [PRK69]).*

positioning in the solubility diagram

The phase diagram (Fig. 3.15) is divided into three different zones: the *unsaturated* zone and two zones where the solution is *saturated*, one *labile* the other *metastable*. The solution should be in the metastable state. In the labile state crystallization does occur spontaneously and is therefore not controllable. In the unsaturated region any crystallite in the solution is dissolved.

A solution in the metastable region is characterized by the fact that the probability of a spontaneous nucleation taking place is considerable. In most of the times, however, the probability of an existing crystallite to dissolve is also still very high. In fact, a formed nucleus rarely exceeds in its growth the critical size. Any trigger, however, be it a dust particle or those fluctuations, has a certain small chance to push a crystallite beyond its critical size.

So, if the solution is in such a state and the temperature is lowered subsequently, one enters the labile zone, where crystallites above the critical size will continue to grow.

That means, that the limit has to be crossed sufficiently slow.

In my case now, I have two possible states for a crystallite: a left- and a right-handed form.

3.6.2 Nucleation, crystallization and the choice of handedness

In the process of growth from a tiny nucleus of a few molecules to a full grown crystal of macroscopic size, there is somewhere the choice between a right-handed or a left-handed form.

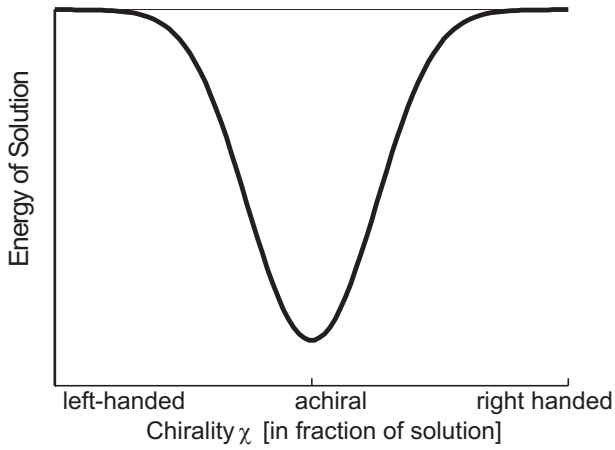

Figure 3.16: *Free energy of an unsaturated solution as a function of its chirality (enantiomeric distribution).*

Imagine first the opposite case of a crystal getting dissolved in the solvent. The solution is supposed to be unsaturated. Such a situation is presented in Figure 3.16 in form of the free energy of the solution as a function of its chirality.

For the unsaturated solution the energy is minimal if completely achiral, that means, with no formed, chiral crystals in it. Any crystal be it right- or left-handed added to the solution tends to this minimum; it gets dissolved. Without any special arrangement the energy curve will be completely symmetric around the achiral point. The precise form of the energy curve, however, remains elusive.

The reverse process of a crystallite being formed out of the solution can be depicted by inversing the picture of Fig. 3.16 to Fig. 3.17. This time the solution

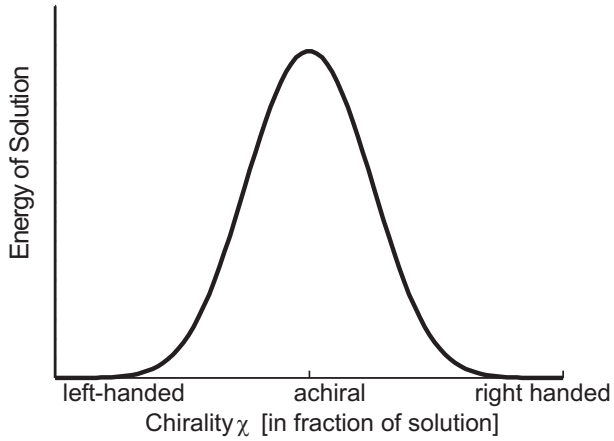

Figure 3.17: *Free energy of a supersaturated solution (labile region) as a function of its chirality.*

is supersaturated. The starting point is the achiral state in the middle of the figure. In order to minimize its energy the solution will spontaneously produce crystals, and due to the symmetry, it will do so in equal proportions[5] of left- and right-handed ones. In a strict way the solution as a whole is then still achiral, but can be divided into chiral subgroups with opposite handedness.

If the solution is now in a metastable phase, crystallization needs a trigger. The situation is depicted in Figure 3.18. Small fluctuations around the achiral

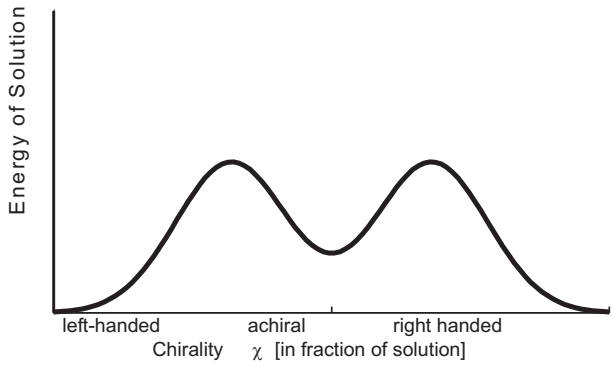

Figure 3.18: *Free energy of a supersaturated solution (metastable region) as a function of its chirality.*

state, implying the formation of very small nuclei, will not result in full grown macroscopic crystals, but will go back into the solution. Only if these nuclei exceed the so called 'critical size' (s. Fig. 3.19) will they tend toward a continuous growth.

The energy barrier can only be crossed by high fluctuations (in temperature, concentration, pressure, etc.) or external triggers that modify the local equilibrium. Those external triggers can be dust particles, stirrers, etc. and even a light

[5] within the range of the statistics in this stochastic process

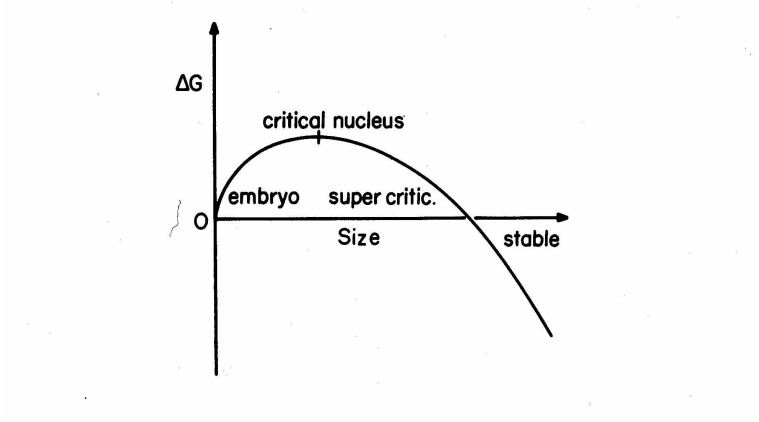

Figure 3.19: *The critical size of a nucleus: free energy ΔG versus size.(from: [PRK69])*

source directed onto the solution. How is the light interacting with the solution then?

3.6.3 The influence of polarized light

The light is essentially absorbed after entering the solution's surface. The absorption coefficient depends on the light wavelength and the penetration depth is typically a few millimeters. The energy of the beam is ultimately transformed into heat. This in turn increases the solubility[6] in the surrounding area.

Nickel sulfate now exhibits natural circular dichroism. This means the amount of energy absorbed per unit length is asymmetric with respect to handedness for circularly polarized light. The enantiomer which absorbs more light has a lower probability to cross the critical nuclei size in the initial nucleation stadium. It is more likely to dissolve due to a local elevation of temperature. If the point of stability of the solution is wisely chosen, one ends up with an enantiomeric excess. This situation is depicted in Figure 3.20.

$$E(\chi, I) = (I_+ - I_-)(a + b\chi) + E(\chi, I = 0) \tag{3.8}$$

$$b/a = \Delta\varepsilon''/\varepsilon'' \tag{3.9}$$

Eq. (3.8) describes the free energy E of the solution in such a metastable state as a function of chirality χ and irradiation intensity I. The two possible polarization states of the light are distinguished by indexes as I_+ and $-I_-$. The free energy of the solution without any irradiation present is $E(\chi, I = 0)$. It depends on the saturation level and has the approximated form as shown in the Figs. 3.16-3.18. The material parameters describing the used solute are a and b. These are closely related to $\Delta\varepsilon''$ and ε'' in the way shown in Eq. (3.9). Here is were the anisotropy

[6] true for most solutions including aqueous nickel sulfate, but other solutions exist where solubility is falling with temperature.

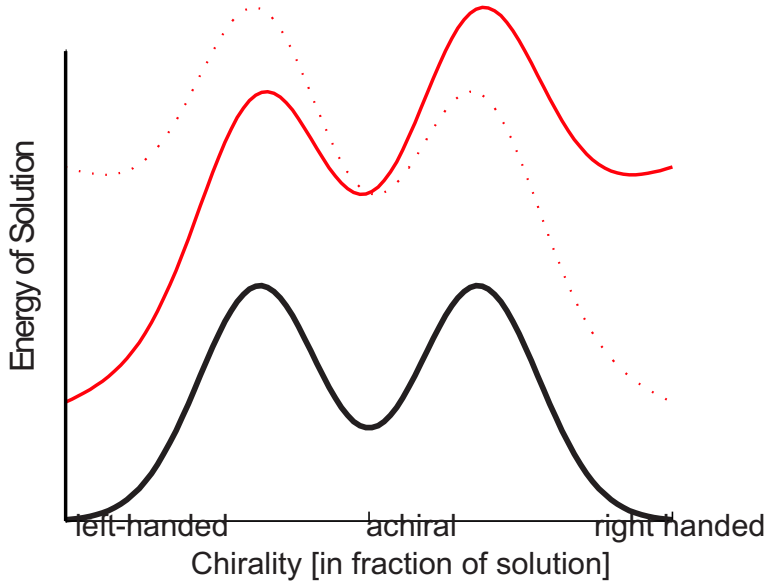

Figure 3.20: *The influence of absorpted light that is circularly polarized on the free energy of the solution. The solid and dotted lines have opposite handedness. An anisotropy is introduced by natural circular dichroism. The effect is portrayed exaggerated in scale.*

enters. Whereas $\varepsilon'' = \Im(\varepsilon)$ merely describes the absorption that is independent of the polarization, $\Delta\varepsilon''$ takes into account any dichroism.

For right-circularly polarized light, the energy difference between a right-handed crystal to that of a left-handed crystal can be stated as

$$\Delta E_+ \equiv \Delta E(I = I_+) \equiv E(\chi = 1, I = I_+) - E(\chi = -1, I = I_+) \quad (3.10)$$

$$= I_+ * 2b = 2a\frac{\Delta\varepsilon''}{\varepsilon''} I_+ \quad (3.11)$$

The material parameter $a = a(\lambda)$ depends on the wavelength and the strength of NCD in the medium.

The actual probability $P_\pm$ that an enantiomeric excess in right-handed(+) or left-handed(-) crystals results, depends also on the mean energy fluctuations $< |E_F| >$ that are already present in the system:

$$P_\pm = \exp\left(-\frac{< |E_F| >}{|\Delta E_\pm|}\right) \quad (3.12)$$

3.7 Photo-crystallization with unpolarized light

After having demonstrated the amplification mechanism inherent in photo-crystallization, where a small absorption difference of a few percent due to NCD is translated into an enantiomeric excess of several 100% of one enantiomer with respect to the other, one could now explore an amplification of MChA with the same mechanism.

3.7.1 Existence from symmetry arguments

Left- or right-circularly polarized light provided the initial preference for one enantiomer and the suppression of the other. With unpolarized light the system would not be able to distinguish between one handedness or the other. In a formal way, introducing an axial vector that couples to the vector describing the incident light would result in a helix. A magnetic field constitutes such an axial vector and, if coupling to the light, would then define a handedness in the system. That such a coupling exist has indeed been proved by the recent observation of magneto-chiral anisotropy (s. Sec. 3.3).

The effect shows the symmetries required (s. Tab. 3.1) and it is indeed independent on the polarization. Its magnitude, however, is generally very small.

With the knowledge gathered to far, it can already be estimated that photo-crystallization under magnetic fields will probably produce a measurable enantiomeric excess.

3.7.2 Estimating orders of magnitudes

The principal question here is how strong a magnetic field is needed to observe an enatiomeric excess: 10 T, 100 T, or 1000 T?

The anisotropy factor g related to magneto-chiral dichroism (MChD) is of the order of $g \approx 10^{-4}\mathrm{T}^{-1}$ around a resonant transition in $NiSO_4$, so for 1 T it is several hundred times smaller than the anisotropy resulting from NCD with $g \approx 3 \cdot 10^{-2}$ at a resonance peak.

To induce roughly the same excess by MChD as by NCD, hundreds of Tesla would then be necessary. This is technically impossible for static laboratory fields. The excess one could expect for a field of about 10 T and with an amplification factor of 100 is about 10^{-2}. That means you need good statistics to resolve a few percent. The number of analyzed crystals N in a batch should fulfill the condition $\frac{1}{\sqrt{N}} \ll 1\%$, or $N \gg 10000$. With the current analytical method this is out of reach by a factor of 10-100.

By pushing the limits to feasible 40 T and amplification regime of > 200 (that have already been seen sporadically) and by making a major effort in analyzing a high number of crystals, the observation of chiral symmetry breaking from magneto-chiral anisotropy becomes a feasible but still rather challenging undertaking.

3.7.3 Experimental design

In principle, the modifications to the photo-crystallization setup are clear (Fig. 3.21). The $\lambda/4$-plate has to be removed and perhaps replaced by a depolarizer. The whole crystallizer is then placed inside a magnet.

But normally, and especially in the case of high fields, room inside the magnet is restricted. One way would be to use a small crystallizer, but the solution's volume becomes then insufficient to produce a decent number of crystals of a decent size. A better way would be to change the crystallization method and to separate the

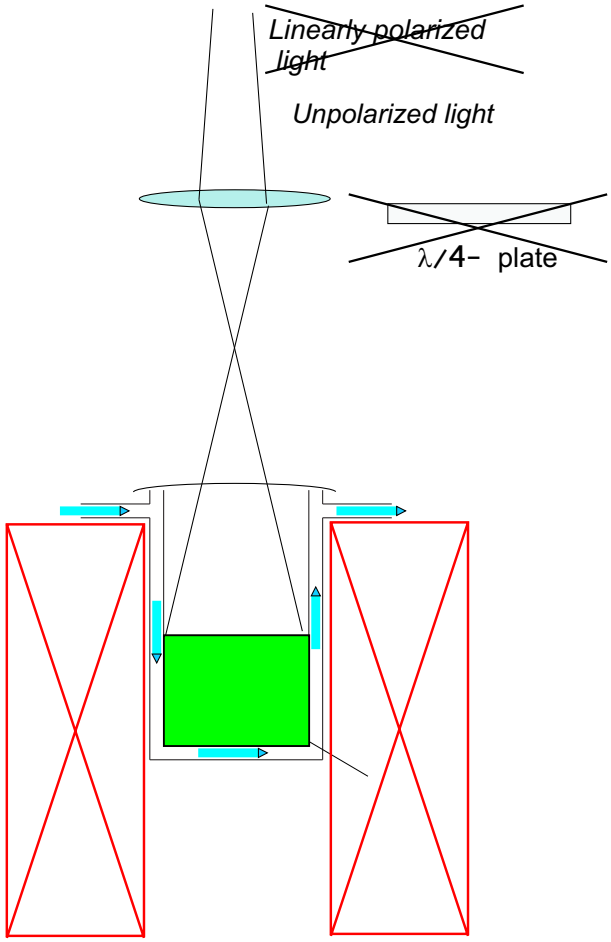

Figure 3.21: *schematic: photo-crystallization in a magnetic field.*

initial nucleation step from the subsequent step of growing those crystallites into macroscopic objects.

For that, a reservoir of the solution is placed completely outside the magnet. By means of tubes, there should be a circulation installed from the reservoir to a place inside the magnet that is illuminated with the laser light, perhaps from an optical fiber. Here the temperature should be lower than in the rest of the circuit, so that the solution becomes supersaturated and nucleation then becomes more probable. The so produced seeds would then be transported back into the reservoir, where they continue to grow even under a little higher temperature.

3.8 Summary and conclusion

It was observed that circularly polarized light produces a large enantiomeric excess in the crystallization of chiral crystals. The usually observed chiral symmetry is broken in such a system. The circularly polarized light falling perpendicular on the surface of the solution thus constitutes a chiral object that is interacting with the forming chiral crystallites at or near the surface of the solution.

A qualitative description was proposed and the observations were shown to be consistent with the developed model. The model suggest that because of NCD the local temperature is different around left- or right-handed crystallites, which in turn leads to different probabilities of continued growth or of going back into the solution. Those probabilities change exponentially as a function of temperature difference in regions where the solution is supersaturated and metastable. A relation was given that expresses the free energy as a function of irradiation intensity and chirality of the solution. The model explains the mechanism of amplification of any anisotropy present in a medium.

However, a multitude of perturbations present in the employed method of crystallization, and the high criticality around the initial phase of nucleation, introduce considerable uncertainties. They result in an overall (systematic) error in the measurements, that limits a more quantitative description. More time and considerable resources are necessary for a major improvement of the crystallization design before more detailed measurements can be envisioned.

Nevertheless, it was firmly established, that photo-crystallization inherently constitutes a powerful amplification mechanism. It can be predicted that the same mechanism should equally enhance the effects of the magneto-chiral anisotropy. In contrast to circularly polarized light, the chiral object interacting with the chiral medium then consist of unpolarized light in combination with a longitudinal magnetic field.

In the following chapter, another amplification mechanism is shown to exist for the amplification of the magneto-chiral anisotropy.

Chapter 4

Magneto-Chiral Anisotropy in Bragg Scattering

4.1 Introduction

In chapter 3 I had looked for a mechanism that amplifies the effects of the magneto-chiral anisotropy. The ultimate experiment of producing a measurable enantiomeric excess by means of photo-crystallization with unpolarised light and subject to a magnetic field has yet to be done. The amplification mechanism used there had too many critical elements.

Nevertheless, in chapter 2 it was shown that a photonic band gap, acting as a Fabry-Pérot resonator, has the power to amplify the Faraday rotation when the light is in resonance with the structure.

In fact, the magneto-chiral anisotropy in luminescence and absorption experiments are intrinsically resonant with electronic transitions in the medium.

If one can find now a material that has both a chiral structure and a photonic band gap, one could check the predicted effect in another way. Such a system is genuinely interesting to study, because of an almost complete absence of this special case in the literature.

In this chapter it is shown that cholesteric liquid crystals (CLC) have the desired symmetries. There exists theoretical work [Eri00] in which such a resonant effect is already predicted. It is proved here experimentally that light scattering in cholesteric liquid crystals shows strongly resonant magneto-chiral anisotropy near the Bragg resonance. The optical transmission of unpolarized light was found to depend linearly on an external longitudinal magnetic field and on the handedness of the medium.

4.2 Cholesteric liquid crystals

Liquid Crystals

For certain organic materials the transition from the solid to the liquid state has some intermediate phases. These intermediate phases are characterized by

mechanical and symmetry properties that lie somewhat between those of a liquid and those of a crystal. That is why they are called *liquid crystals*.

They have been extensively studied and are known for their exceptional optical properties. Applications involving liquid crystals are found in everyday life and most famously in the form of *liquid crystal displays*.

They can be separated into several classes: *nematics*, *smectics*, and *cholesterics*. The latter are in fact only a distorted form of the nematic phase.

Nematics are anisotropic liquids, in a certain temperature interval the molecules are aligned preferentially along one direction. At higher temperatures they become isotropic, like conventional liquids, and at lower temperatures they crystallize.

For handbooks on liquid crystals, see [KH80, DGG+98].

Cholesterics

Cholesteric liquid crystals (CLC) arise out of proper nematics, if a chiral molecule is dissolved in the liquid. Cholesterics show a helical structure in their collective molecular orientation (see Fig. 4.1). The structure is periodic along the helical axis and the spatial period p is called the *pitch*(see Fig. 4.2).

The pitch can take positive or negative values, corresponding to right- and left-handed helices. Its magnitude depends on the material, which is often a mixture of two ingredients. It is very sensitive to temperature and other external parameters.

The orientation of the axis is in principle arbitrary, but can be influenced by applying appropriate boundary conditions. Cholesteric single crystals can be obtained in films of around 10-1000 μm. In between two polished glass plates, parallel to each other, the cholesteric liquid crystal will tend to orient his helical axis perpendicular to the surfaces.

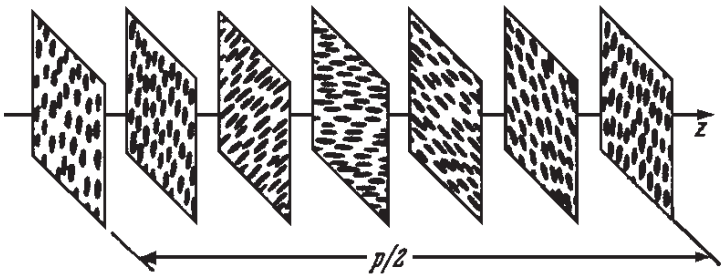

Figure 4.1: *The chiral structure of cholesteric liquid crystals (from: [KH80]).*

a chiral medium with a photonic bandgap

If light is falling on such a slab, it will experience Bragg-like scattering. Since the optical properties are modulated periodically along the pitch, I have here a one dimensional photonic crystal. The Bragg condition for light traveling along the helical axis can be stated as:

$$np = m\lambda \quad , \quad m = 1, 2, ... \tag{4.1}$$

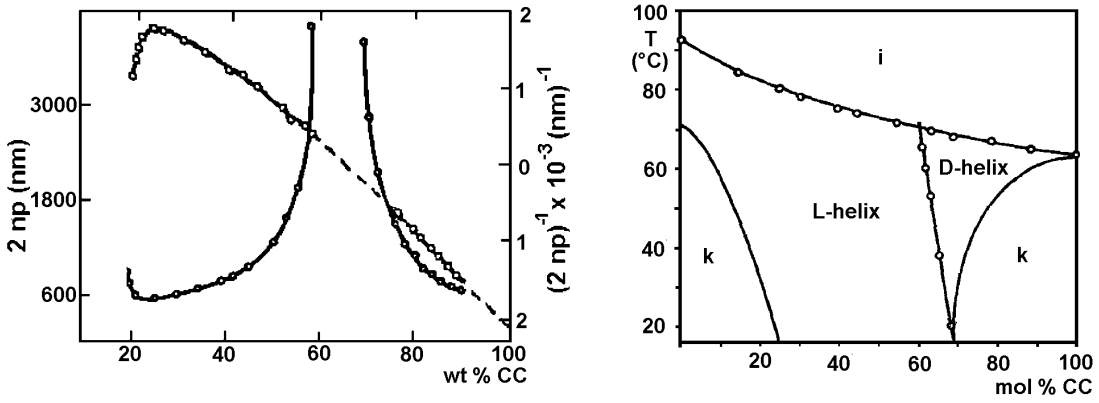

Figure 4.2: *Phase Diagram of the mixture of Cholesteric Liquid Crystals. Left: Pitch depending on weight parts of constituents. Right: Crystallization Phase depending on temperature and mole parts of constituents (from [KH80]).*
The pitch - and therefor the position of the photonic band gap - can be chosen over a wide range in these CLC-mixtures (left). Both kinds of handedness can occur, as shown in the phase diagram on the right hand side.

If the wavelength inside the medium λ/n corresponds to the pitch p, this gives rise to Bragg reflections. Thus, around this Bragg wavelength a photonic band gap opens up. However, the photonic band gap present in ChLCs has the important peculiarity that it is only present for one circular polarization mode and completely absent for the other. Only the circular mode for which the electrical pattern is identical in shape to the cholesteric helix is reflected, the other mode is transmitted without any significant reflection (s. Fig. 4.3).

So both of the symmetries that I was looking for - chirality and a photonic stopband - are combined in this material.

4.3 Resonant magneto-chiral anisotropy

In this section the magneto-chiral anisotropy under resonant conditions is discussed. In particular, the focus is on resonance due to Bragg scattering and on cholesteric liquid crystals as the scattering medium.

resonance as a means for amplification

How does a resonance works as a mechanism for amplification? What happens in a resonator?

In a resonator energy is continuously send around two or more states. For example, in an optical resonator the energy of a wave flows around from one mirror to the other and back again in a circular way. For the resonance frequency the wave doing one roundtrip will find exactly the same phase state from its start and can thereby constructively interfere with itself. Is there a constant flow into the resonator, the energy contained can quickly accumulate and reach high values,

especially if leaks are small. If the leaking corresponds exactly to the inflow, one has approached a saturation. In the optical case, a wave that has entered the resonator is performing some roundtrips, before it leaves the resonator.

The transmitted light is the part that has *leaked* from the structure. One could thus talk of a *lifetime* τ or of the number N of *roundtrips* performed.

$$\tau = \frac{1}{\Gamma} \tag{4.2}$$

$$N = \frac{\tau c}{2 n_{eff} d} \tag{4.3}$$

Γ stands here for the *decay rate* and describes the damping, whereas n_{eff} is the effective refractive index, c the velocity of the wave and d the resonator length.

Bragg scattering

In the case of Bragg scattering the mirrors are replaced by interfaces throughout the whole length of the resonator. The incident plane wave is partially scattered at each layer. The resonance wavelength is given by the Bragg condition.

In chapter 2 I found that the Faraday rotation increases in the photonic crystal structure. This result was a direct consequence of multiple scattering inside the structure, similarly to a Fabry-Pérot resonator. This phenomenon can be interpreted as an amplification of Faraday rotation due to resonance:

$$\theta_{res} \approx 2N\theta \tag{4.4}$$

For CLCs a layer contains one spatial period, with which the optical properties are modulated: $L = \pi/q$, with q being the pitch of the helical structure.

resonance and MChA

What evidence do I have that such an amplification would also work out for the magneto-chiral anisotropy? At first sight it seems that such an enhancement is not possible, because the MChA changes sign between forward and backward traveling waves. This means that the effect cancels out.

Now this is true only, when looking at it in a first order approximation. A peaking in the effect of MChA could reappear in the presence of tiny perturbations. A wave having done one full roundtrip should in principle meet his starting point with a phase difference of 180 ° and interfere destructively with it. However, a tiny perturbation could lead to an additional phase shift, the interference of both waves is then not completely destructive. Due to the resonant character a however tiny amount of constructive interference can end up to a full measurable peak. The exact spectral position of such a peak would then depend on the specific defects of a given sample, but have to be around the resonant region, albeit with a smaller linewidth than would be expected from a first order effect at the resonance.

Measurements will help to clarify those questions that for now appear a bit speculative. But let me look first at intrinsically resonant systems, namely absorption and luminescence.

magneto-chiral anisotropy in absorption and luminescence

From the literature one finds that MChA is much larger in luminescence and absorption experiments than is the case for experiments in refraction.

The MChA luminescence and absorption experiments measure the imaginary part $\Im(\gamma)$ and are intrinsically resonant with electronic transitions in the medium.

Fairly large effects, with relative anisotropies up to $10^{-3}\,\mathrm{T}^{-1}$ were reported [RR97]. In contrast, in the non-resonant MChA refraction experiments, which measure the real part $\Re(\gamma)$, only refractive index anisotropies of $10^{-10}\,\mathrm{T}^{-1}$ were found [KW98, VGF+01]. For both cases, the observed orders of magnitude agree with those predicted by simple models.

existing theory

Eritsyan [Eri00] calculated the transmission through a cholesteric liquid crystal in a magnetic field parallel to the helix axis for wavelengths close to the cholesteric Bragg resonance. In this work, only the α and β terms of Eq. (3.6) were taken into account, but nevertheless a strongly resonant transmission anisotropy of the order of $10^{-4}\,\mathrm{T}^{-1}$ was predicted. It had already been pointed out that in absorption [RR98] and photochemistry [RRTM00], these two terms together can lead to a cascaded form of MChA , proportional to $\alpha \cdot \beta$, which has phenomenologically the same properties as the genuine MChA that is proportional to γ. The experimental verification of the existence of such a resonant enhancement of MChA in Bragg scattering is the subject of this chapter.

4.4 Sample preparation and experimental setup

After having gained some insight into resonant MChA and cholesteric liquid crystals, one can now proceed with the design of the experiment. This section will show how the samples were prepared and describes the experimental setup.

the sample cells

The sample cells consisted of two glass plates separated by a spacer with a thickness between $10\,\mu$m and 1 mm. The cells were filled with the LC mixture in the isotropic phase. Alignment of the helix axis perpendicular to the plates was obtained by gently shearing the plates or by a capillary flow of the isotropic phase between the glass plates. Since I worked in the visible wavelength range, the good crystalline quality could be easily verified by visual inspection.

the mixture

Two different mixtures of cholesteryl chloride (ChCl) and cholesteryl oleyl carbonate (ChOC) (Sigma-Aldrich) were used, one with a left-handed helix (1:3 ChCl/ChOC) and one with a right-handed helix (4:1 ChCl/ChOC), at temperatures of 300 K and 350 K respectively.

Figure 4.3 shows the transmission difference between left- and right circularly polarized light, for a left- and a right handed sample. The maxima in the circular

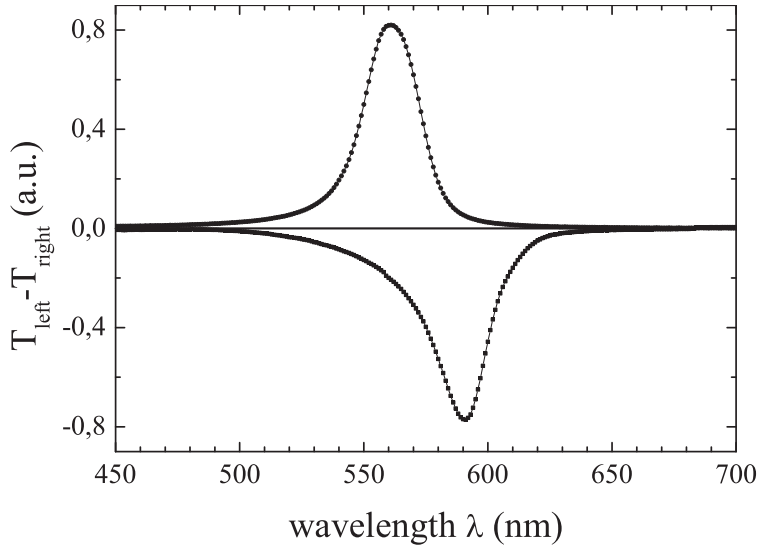

Figure 4.3: *Difference in Transmission between left- and right circularly polarized light for two different CLC mixtures (both ChOC-ChCl, in different weight ratios). Top: left-handed CLC (weight-ratio 3:1) at room temperature; Bottom: right-handed CLC (weight-ratio 1:4) at 350 K. The peaks coincide with the Bragg resonance.[Düc03]*

differential spectra coincide with the Bragg resonances of the respective ChLCs.

the setup

The experimental setup is depicted in Figure 4.4.
The magneto-chiral anisotropy of the prepared ChLCs was measured by applying an alternating magnetic field of about 0.5 T parallel to the helix axis. Unpolarized, incoherent light from a lamp, filtered by interference filters with a typical transmission bandwidth of 10 nm, was guided to the cell by means of an optical fiber (diameter 1 mm, numerical aperture 0.45). The light transmitted through the CLC parallel to the magnetic field direction was collected by a similar fiber, which guided it to a photo multiplier tube. The magnetic-field-induced transmission changes were phase-sensitively detected by a lock-in amplifier.

the magnet

The magnet used was a small home-made one, capable of creating alternating fields of the order of 1 T peak to peak. The poles of the magnet had been drilled through to allow optical fibers entering and leaving parallel to the field direction. The current ($I_{AC} \sim 1$ A) was supplied by a home-made amplifier triggered to the reference frequency of lock-in, which was $f = 28.5$ Hz.

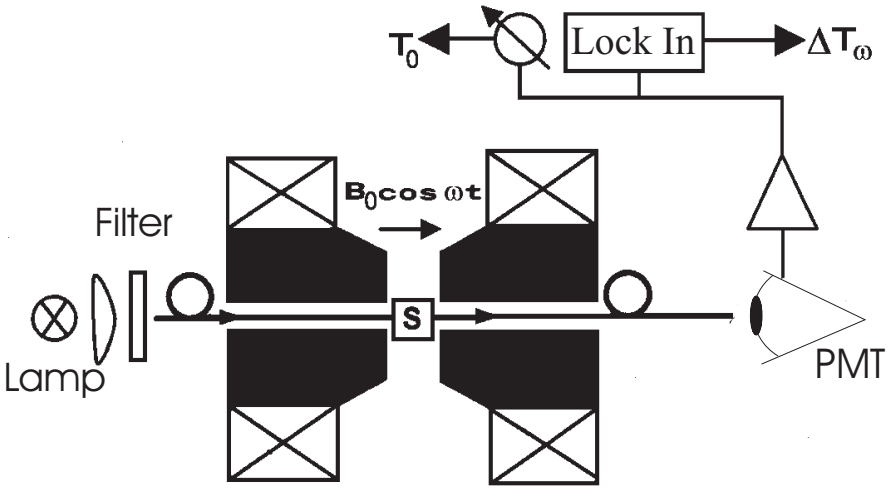

Figure 4.4: *Schematic setup of the magneto-chiral anisotropy measurement. Filtered light is guided through an optical fiber (∅ 1 mm, numerical aperture NA = 0.47) to the CLC. Transmitted light is collected by a similar light guide and detected by a photomultiplier tube (PMT). The alternating magnetic field is applied parallel to the axis connecting the fibers.*

the sample holder

The sample cells were placed inside a holder made of copper that can also be employed to control the temperature of the sample (high heat capacity and heat conductivity). For that end, the copper plate was connected to a programmable water bath. Thick pieces of Teflon were put between the sample holder and the magnet to reduce the heat flow. Sample temperatures could thus be controlled within an interval of less than 0.1°C.

measuring the anisotropy

I define the relative transmission anisotropy Δt as

$$\Delta t \equiv \frac{T(B) - T(-B)}{T(B) + T(-B)} \tag{4.5}$$

$T(B)$ is the transmission of light through the sample with the magnetic field parallel to the helix axis. $T(-B)$ is for an antiparallel magnetic field.

The value of Δt is determined by dividing the AC-signal of the lock-in signal, $T(B) - T(-B)$ which is a function of the amplitude of the AC magnetic field, by the DC-signal arriving at the multiplier tube. The DC-signal stays constant during the measurement within a few percent of its value. The AC-signal is averaged over typically 1000 s.

$$\eta = B^{-1}\Delta t \tag{4.6}$$

To introduce a value for the anisotropy that is independent of the magnetic field, η was defined according to Eq. (4.6).

4.5 Measurements and discussion

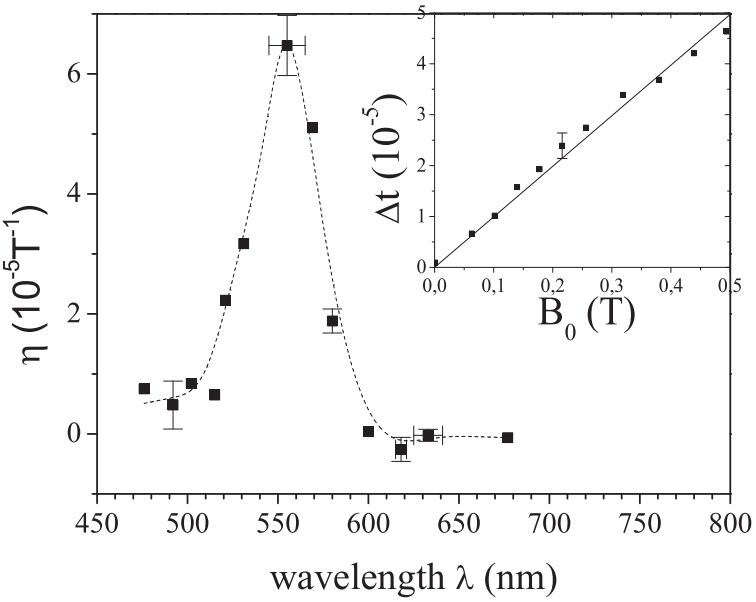

Figure 4.5: *Inset: Relative transmission anisotropy $\Delta t = \eta B$ versus magnetic field for a left-handed sample of 500 µm thickness consisting of 1:3 ChCl/ChOC at room temperature. The main figure shows the wavelength dependence of the normalized relative transmission anisotropy η for a left-handed sample of 500 µm consisting of 1:3 ChCl/ChOC at room temperature (line is guide to the eye). The maximum observed corresponds approximately to the Bragg resonance of the sample.[Düc03]*

The inset of Figure 4.5 shows the relative transmission anisotropy Δt for a left-handed sample as a function of the externally applied magnetic field. A clear linear relation is found. The observed order of magnitude agrees reasonably well with the predictions by Eritsyan [Eri00] and illustrates that under resonant conditions refractive MChA can be quite strong.

By rapid cooling to liquid nitrogen temperatures, cholesteric structure could be frozen.

Approximately the same MChA as at room temperature was observed, thereby excluding magnetic realignment of the molecules as cause for the observed MChA.

The main part of Figure 4.5 shows the wavelength dependence of the MChA in form of the relative transmission anisotropy normalized for the magnetic field $\eta = B^{-1}\Delta t$ for a left-handed CLC. A clear resonance is observed that is close to the Bragg resonance. The peak shows its maximum at around 550 nm and reaches a value of $\eta \approx 6 \cdot 10^{-5}\,\mathrm{T}^{-1}$. Its FWHM[1] is about 50 nm.

[1] Full Width at Half Maximum

This is completely different from the wavelength dependence predicted by Eritsyan, which has a derivative-type line shape, with a zero-crossing at the Bragg resonance, and large and opposite values in the two opposite wings of the Bragg band [Eri00]. This large discrepancy suggests that the theoretical treatment in Ref. [Eri00] is incomplete, and that the γ terms of Eq. (3.6) play a dominant role in the observed MChA. A similar dominance of γ terms over $\alpha \cdot \beta$ terms was found in the absorption and photo-chemistry experiments [RR98, RRTM00]. Clearly, the development of a theory for light propagation in CLC involving the γ-terms of Eq. (3.6) is called for.

The wavelength dependence of MChA for a right-handed sample is depicted in Figure 4.6. The 'negative' peak corresponds to the Bragg resonance, and in comparison with figure 4.5 one can see that by changing the handedness of the medium the MChA changes its sign, as was demanded for γ in Eq. (3.6).

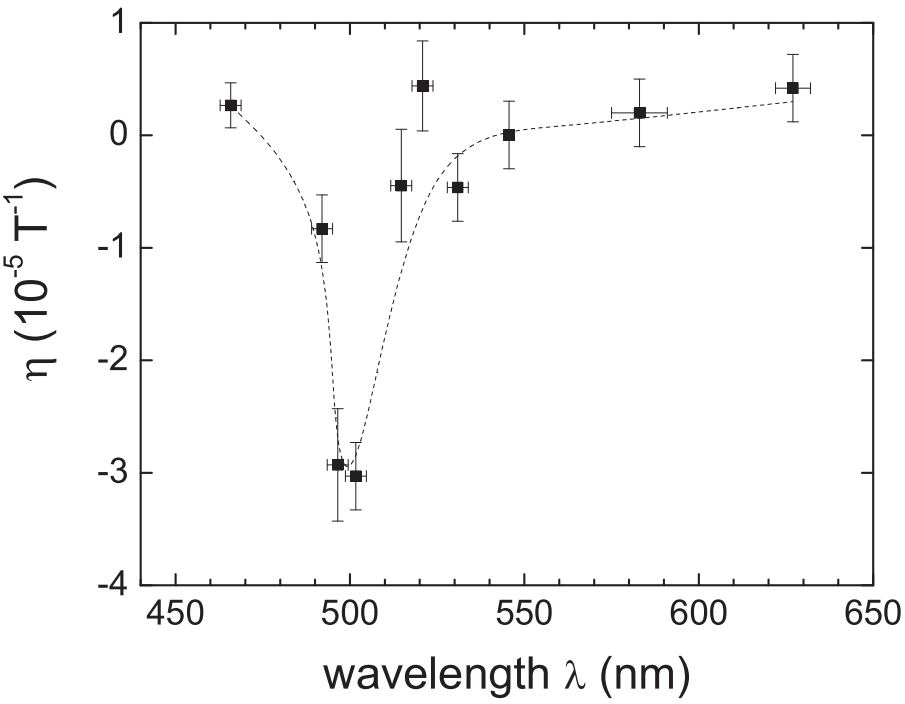

Figure 4.6: *Wavelength dependence of η for a right-handed sample consisting of 4:1 ChCl/ChOC at 350 K (line is guide to the eye). The maximum observed corresponds approximately to the Bragg resonance of the sample. The order of magnitude is similar to that in Figure 4.5, whereas the sign has changed.*

Although the samples in Fig. 4.6 and Fig. 4.3 bottom are characterized by the same parameters, they differ quite a lot in their Bragg resonance positions. This is due to the very critical dependence on concentration and temperature typical for liquid crystals and, in particular, for my right-handed samples.

Why right-handed samples are even more critical in their properties becomes clear by a look at the phase diagram as depicted on the right-hand side of Fig. 4.2. One has to mention here that right-handed samples that are more stable can easily

be found, but they would have made a comparison with my left-handed sample less straightforward.

The MChA of both types of handedness is in the same order of magnitude. Note that the two types of samples are not enantiomers (mirror images), and therefore MChA strength, linewidth, etc.[2], need not be identical. Further studies should check the relation of sample quality to the resonance response in more detail. However, as the chiroptical properties of the two types of samples are of similar magnitude but opposite sign (Fig. 4.3), the magneto-optical properties should be similar on the basis of the close chemical similarity of their components. Similar magnitudes and opposite signs should be expected for the MChA of the two types of samples, as observed.

It was further observed that MChA clearly vanishes upon approaching the cholesteric-isotropic phase transition temperature, which was at 306 K for this sample [Düc03]. This behavior confirms that the MChA is related to the collective, cholesteric super molecular structure.

Measurements in the range of 18 and 500 μm proved η to be independent of sample thickness. There is at this moment no detailed theory that allows one to draw conclusions from this observation.

The dependence of the effect on the relative orientation of $\mathbf{k}$ and $\mathbf{B}$ was investigated by simply interchanging the light source and detector at the ends of the optical fibers. Thus the flow of light is inversed ($\mathbf{k}$ to $-\mathbf{k}$). It was found that the anisotropy Δt (phase-sensitively measured with respect to an alternating magnetic field B) changes sign, whereas the absolute value was not effected. This proves the dependence of η on the scalar product of $\mathbf{k} \cdot \mathbf{B}$.

4.6 Summary and conclusion

In summary, cholesteric liquid crystals were singled out for their unique symmetry properties. They are suitable systems to verify the existence of a mechanism capable of significantly amplifying the effects of magneto-chiral anisotropy.

The amplification mechanism was resonant multiple scattering inside the cholesterics due to the existence of a photonic band gap. A high optical activity is present in such systems because of their helical structure.
The experiment consisted of an unpolarized light beam in combination with an externally applied parallel magnetic field hitting a cholesteric liquid crystal and traveling along its helical axis. The anisotropy was measured in transmission.

It has been shown that the normalized transmission anisotropy η in cholesteric liquid crystals peaks for wavelengths near the Bragg wavelength. Its sign clearly depends on the handedness of the medium. The signal was found to be proportional to the vector product of the applied magnetic field and the incident wave vector. The results presented here clearly prove the existence of a resonant enhancement of MChA. The theoretical description by Eritsyan (Ref. [Eri00]) was found to be incomplete.

[2] strength and linewidth are presumably connected to the sample quality that in turn influences the resonance response

The observations suggest that it should be possible to observe MChA in Bragg scattering of unpolarized, or linearly polarized X-rays by chiral crystals. Thereby one could obtain specific chiral information of crystal structures, as an alternative to X-ray natural circular dichroism measurements by use of polarization modulation of synchrotron radiation [APT+98].

Overall Summary and Conclusion

New phenomena in magneto-optics

The effects of spatial dispersion and applied magnetic fields on the propagation of light through media lead to interesting optical phenomena such as the Faraday effect and optical activity and are known for a hundred years. Further interesting and important effects can still be found in our days, which is the case for the magneto-chiral anisotropy, where a combined effect of spatial dispersion and magnetic fields, namely magneto-spatial dispersion, act together.
At the origin of new optical effects is usually the breaking of a fundamental symmetry. An external magnetic field breaks the time reversal symmetry and the chiral symmetry is broken in optically active substances.
New optical effects are also discovered in photonic crystals. In those materials a spatial modulation of the dielectric constant breaks a continuous translational symmetry into a discrete one. This may result in the opening up of a photonic band gap.
In this thesis I studied systems, where some or all of the mentioned symmetries have been broken. The combination of broken symmetries resulted in interesting new magneto-spatial phenomena.

Magneto-optics of photonic crystals

The magneto-optics of photonic band gap materials is still lacking groundbreaking experimental and theoretical investigations.

In one dimensional photonic crystals, for which I have performed numerical simulations, I observed a Faraday rotation spectrum that has a derivative-type shape with peaks of opposing signs at the edges of the stopband. Strongly resonant Faraday rotation was calculated around specially designed defect modes. For high magnetic fields the Faraday rotation saturates in the resonant mode and the peaks splits up in two as the polarization degeneracy is lifted.

The main observation in this part was the measurement of the Faraday rotation of three dimensional photonic crystals. The crystals were impregnated with a Faraday-active liquid. The Faraday rotation outside the stopband follows the spectral behavior of the pure liquid multiplied by its volume fraction. Inside the stopband, the Faraday rotation is enhanced up to a factor of five. Qualitatively, internal reflections are the most likely origin. A fully three dimensional scattering theory needs to be developed in order to understand the observations quantitatively.

Photo-crystallization

A small enantiomeric excess can be generated by magneto-chiral anisotropy. The generated excess is usually very small, which drove us to look for a mechanism of amplification. I have shown that crystallization under influence of irradiation (photo-crystallization) provides such an amplification, which was demonstrated here in the growth of $\alpha - NiSO_4 - 6 \cdot H_2O$.

The produced enantiomeric excess reaches high values within reach of the complete elimination of one handedness. The excess is changing sign when going from left-circularly to right-circularly polarized light and zero for linearly-polarized light. This large excess originates from a rather small natural circular dichroism of my crystals, which is of the order of 8%.

I interpret my results in the way that the enantiomer that absorbs more light has, in such conditions, a lower probability to cross the critical nuclei size in the initial nucleation stadium. It is more likely to dissolve due to a local elevation of temperature. A necessary condition is the delicate choice of a proper crystallization point in the solution's phase diagram near the saturation limit.

In principle, the same amplification mechanism can be used to enhance the effects of the magneto-chiral anisotropy. The enantioselectivity would then be provided by a magnetic field in combination with unpolarized light. However, a multitude of perturbations present in the used method of crystallization and the very criticality around the initial phase of nucleation make a quick experimental observation of this expectedly much smaller effect unlikely. Future efforts should start with a major investment in crystallization equipment and a change to a steady-state crystallization method. It would also be wise to separate the place of nucleation from the place of growth of already formed crystallites in order to control both processes independently.

Resonant magneto-chiral anisotropy

In this part is was shown that cholesteric liquid crystals are almost ideal systems to exhibit large effects of magneto-spatial dispersion. They somehow combine the two preceding parts in so far as they are both chiral and have the periodic translational symmetry that result in a photonic band gap.
The main observation was that magneto-chiral anisotropy takes large values in cholesteric liquid crystals, that can be observed in the transmission of light that is traveling along the optical axis and parallel to an externally applied magnetic field. The mechanism responsible for such a huge amplification was identified as resonant Bragg scattering. A complete theoretical treatment is still missing. A promising project could involve the simulation of the effect in cholesteric liquid crystals with a modified version of the transfer matrix method developed in chapter two of this thesis.
Specific chiral structure information should be extractable from resonant magneto-chiral anisotropy measurements, using the Bragg scattering at the crystal lattice planes.

Deutsche Zusammenfassung

Neue Phänomene in der Magneto-Optik

Die Effekte von räumlicher Dispersion und von äußerlich angelegten Magnetfeldern auf die Lichtausbreitung in Materie führen zu interessanten optischen Phänomenen wie etwa der Faraday Effekt oder die optische Aktivität und man kennt sie bereits seit hundert Jahren. Weitere interessante und wichtige Effekte können selbst unserer Tage noch gefunden werden, wie das etwa der Fall der magnetochiralen Anisotropie ist. Hier arbeiten räumliche Dispersion und Magnetfelder zusammen, und man kann somit von magnetisch-räumlicher Dispersion sprechen. Den Ursprung neuer, optischer Effekte ist gewöhnlich in einer fundamentalen Symmetriebrechung zu suchen. So bricht ein äusseres Magnetfeld die Zeitumkehrsymmetrie und die Spiegelsymmetrie ist in optisch aktiven Substanzen verletzt (Chiralität).
Neuartige optische Effekte werden neuerdings auch in photonischen Kristallen entdeckt. In diesen Materialien wird durch eine räumliche Modulation der dielektrischen Konstante eine kontinuierliche Translationssymmetrie in eine diskrete Translationssymmetrie gebrochen. Das Öffnen einer photonischen Bandlücke kann so erzielt werden.
In dieser Dissertation habe ich Systeme untersucht, in denen einige oder alle der genannten Symmetrien gebrochen sind. Die Kombination der Symmetriebrechungen resultierten in interessanten, neuen Phänomenen, die der magnetisch-räumlichen Dispersion zugerechnet werden können.

Die Magneto-Optik photonischer Kristalle

Die Erforschung der Magneto-Optik photonischer Kristalle ist noch unberührtes Gelände und es mangelt an weitreichenden Untersuchungen, seien sie experimenteller als auch theoretischer Natur.

In dieser Arbeit wurden numerischen Simulationen an eindimensionalen photonischen Kristallen durchgeführt. Das berechnete Spektrum der Faraday Rotation zeigt eine Form, die der Ableitung einer Lorentzfunktion ähnelt. So findet man an einem Ende des Stoppbandes ein Maximum, während man am anderen Ende ein Minimum beobachtet. Die Faraday Rotation wird in speziell entworfenen Defektmoden stark resonatorisch. In hohen Magnetfeldern sättigt der Faraday Effekt in der Resonanzmode und der Peak spaltet auf. Die Polarisationsentartung ist somit aufgehoben.

Das zentrale Ergebnis in diesem Teil der Arbeit war die erstmalige Messung

des Faraday Effektes von dreidimensionalen photonischen Kristallen. Die Kristalle waren mit einer Faraday-aktiven Flüssigkeit imprägniert worden. Die Faraday Rotation außerhalb des Stoppbandes folgt dem spektralen Verlauf der reinen Flüssigkeit multipliziert mit ihrem Volumenanteil. Innerhalb des Stoppbandes steigen die Werte der Faraday Rotation bis auf das Fünffache. Qualitativ sind interne Reflektionen als deren Ursprung zu sehen. Die Entwicklung einer vollständigen dreidimensionalen Streutheorie ist für eine quantitative Analyse unabdingbar.

Photokristallisation

Mit Hilfe der magnetochiralen Anisotropie kann man einen enantiomerischen Überschuss erzeugen. Da der erzeugte Überschuss normalerweise sehr gering ausfällt, haben wir uns auf die Suche nach einem Verstärkungsmechanismus gemacht. In dieser Arbeit habe ich gezeigt, dass die Photokristallisation, d.h. eine Kristallisation unter Lichteinfluss, solch eine Verstärkerfunktion beinhalten kann. Dies wurde hier im Wachstum von Nickelsulfatkristallen ($\alpha - NiSO_4 - 6 \cdot H_2O$) demonstriert.

Der somit erzielte enantiomerische Überschuss ist sehr hoch und kommt in den Bereich der fast vollständigen Beseitigung einer Händigkeit. Wechselt man den Polarisationszustand des Lichtes von links-zirkular zu rechts-zirkular so schlägt der erzeugte Überschuss auf die andere Händigkeit um. Kein statistisch signifikanter Überschuss wird mit linear polarisiertem Licht erzielt. Eine ursprünglich eher kleine ($\sim$ 8%) Anisotropie in Form der vorhandenen optischen Aktivität kann somit auf eine grosse ($\sim$ 80%) Anisotropie in Form erzeugter Händigkeit verstärkt werden.

Ich interpretiere mein Ergebnis in dem Sinne, dass dasjenige Enantiomer, welches unter den gegebenen Bedingungen mehr absorbiert, eine niedrigere Wahrscheinlichkeit aufweist die kritische Nukleusgröße zu überschreiten. Eine Erhebung der lokale Temperatur macht ein Auflösen wahrscheinlicher. Die Wahl des Kristallisationspunktes im Phasendiagramm der Lösung ist bei unserer Methode allerdings sehr kritisch.

Im Prinzip kann derselbe Verstärkungsmechanismus auch auf die magnetochirale Anisotropie angewendet werden. Die Enantioselektivität würde dann mit Hilfe von Magnetfeldern und unpolarisiertem Licht erfolgen. Ein baldiger experimenteller Nachweis ist jedoch wenig wahrscheinlich, da der erwartete sehr viel kleinere Effekt von den vielfältigen Störungen und insbesondere von der äußerst kritischen Initialphase des Kristallisationsprozesses überschattet werden dürfte. Zukünftige Anstrengungen sollten mit einer bedeutenden Investition in der Kristallisationsausrüstung starten und einer Kristallisationsmethode der Vorzug gegeben werden, in der gleichmässige Bedingungen gewährleistet werden können. Es wäre ebenfalls klug, die anfängliche Nukleation vom weiteren Wachstumsprozess örtlich zu trennen, da dann beide Prozesse voneinander unabhängig kontrollierbar würden.

Die Magneto-chirale Anisotropie in Resonanz

In diesem Teil habe ich gezeigt, dass cholesterische Flüssigkristalle ideale Sys-

teme in der Hinsicht sind, dass dort sehr große magnetisch-räumliche Dispersionseffekte beobachtet werden können. Die drei untersuchten Symmetrien sind dort allesamt gebrochen: sie haben eine chirale Struktur und haben ein verbotenes photonisches Energieband entlang der optischen Achse und sie sind empfindlich auf äußerlich angelegte Magnetfelder. So habe ich beobachten können, dass die magnetochirale Anisotropie in cholesterische Flüssigkristallen sehr hohe Werte annimmt. Dies wurde in Transmissionsmessungen des Lichts entlang der optischen Achse der Kristalle und parallel zum äußeren Magnetfeld beobachtet. Der Ursprung dieser enormen Verstärkung wurde in der resonanten Braggstreuung gefunden. Die bisher vorhandenen theoretische Behandlungen in diesem Bereich sind allesamt unvollständig.

Ein Erfolg versprechendes Projekt könnte darin bestehen, die im zweiten Kapitel entwickelte Simulationsmethode in einer modifizierten Version auf cholesterische Flüssigkristalle anzuwenden. Des Weiteren sollte es mit Hilfe der resonatorischen magnetochiralen Anisotropie möglich sein spezifische Informationen über die chirale Struktur von Kristallen zu erhalten, indem man Bragg Streuung an den Kristallebenen ausnützt.

Bibliography

[AF88] R. J. Angel and L. W. Finger. Polymorphism of nickel sulfate hexahydrate. *Acta Crist.* , C44:1869–73, 1988. 57

[APT+98] L. Alagna, T. Prosperi, S. Turchini, J. Goulon, A. Rogalev, C. Goulon-Ginet, C. R. Natoli, R. D. Peacock, and B. Stewart. X-ray natural circular dichroism. *Phys. Rev. Lett.* , 80:4799, 1998. 91

[BGG+97] V. N. Bogomolov, S. V. Gaponenko, I. N. Germanenko, A. M. Kapitonov, E. P. Petrov, N. V. Gaponenko, A. V. Prokofiev, A. N. Ponyavina, N. I. Silvanovich, and S. M. Samoilovich. Photonic band gap phenomenon and optical properties of artificial opals. *Phys. Rev. E*, 55(6):7619–25, 1997. 44

[BJ99] K. Busch and S. John. Liquid-crystal photonic-band-gap materials: the tunable electromagnetic vacuum. *Phys. Rev. Lett.* , 83(5):967–70, 1999. 26

[BNM+01] L. C. Botten, N. A. Nicorovici, R. C. McPhedran, C. Martijn de Sterke, and A. A. Asatryan. Photonic band structure calculations using scattering matrices. *Phys. Rev. E*, 64(4):046603, 2001. 31

[BS95] K. Busch and C. M. Soukoulis. Transport properties of random media: A new effective medium theory. *Phys. Rev. Lett.* , 75(19):3442, 1995. 49

[BZ79] N. B. Baranova and B. Ya. Zel'dovich. Theory of a new linear magnetorefractive effect in liquids. *Mol. Phys.* , 38(4):10851098, 1979. 12

[CYH95] C. T. Chan, Q. L. Yu, and K. M. Ho. Order-N spectral method for electromagnetic waves. *Phys. Rev. B*, 51(23):16635–42, 1995. 31

[DGG+98] D. Dennis, J. W. Goodbye, G. W. Gray, H. W. Spiess, and V. Vill. *Handbook of Liquid Crystals*. Wiley VCH, 1998. 14, 82

[Düc98] Georg Düchs. The inverted photonic Hall effect. Master's thesis, Univ. Würzburg, 1998. 44

[Düc03] Georg Düchs. *Scattering of Photons and Surface Plasmon Polaritons in Magnetic Fields*. PhD thesis, Univ. Konstanz, 2003. 86, 88, 90

[Eri00] O. S. Eritsyan. Diffraction reflection of light in a cholesteric liquid crystal in the presence of wave irreversibility and Bragg formula for media with nonidentical forward and return wavelengths. *J. Exp. Theor. Phys.* , 90(1):102–8, 2000. 81, 85, 88, 89, 90

[HCS90] K. M. Ho, C. T. Chan, and C. M. Soukoulis. Existence of a photonic band gap in periodic dielectric structures. *Phys. Rev. Lett.* , 65(25):3152, 1990. 23, 31

[HS96] K. R. Heim and M. R. Scheinfein. An alternative approach for magneto-optic calculations involving layered media. *J. Magn. Magn. Mater.* , 154(1):141–52, 1996. 32

[IF97] M. Inoue and T. Fujii. A theoretical analysis of magneto-optical Faraday effect of YIG films with random multilayer structures. *J. Appl. Physics*, 81(8):5659–61, 1997. 41

[JMW95] J. D. Joannopoulos, R. D. Meade, and J. N. Winn. *Photonic Crystals: Molding the flow of light.* Princeton University Press, New Jersey, USA, 1995. 26

[JVF97] J.D. Joannopoulos, P.R. Villeneuve, and S. Fan. Photonic crystals: putting a new twist on light. *Nature (London)*, 386:143–9, 1997. 12

[KBD+93] D. K. Kondepudi, K. L. Bullock, J. A. Digits, J. K. Hall, and J. M. Miller. Kinetics of chiral symmetry breaking in crystallization. *J. Am. Chem. Soc.* , 115(22):10211–6, 1993. 58

[KH80] H. Kelker and R. Hatz. *Handbook of Liquid Crystals.* Verlag Chemie, Weinheim, 1980. 14, 82, 83

[KLA99] D. K. Kondepudi, J. Laudadio, and K. Asakura. Chiral symmetry breaking in stirred crystallization of 1.1'-binaphthyl melt. *J. Am. Chem. Soc.* , 121(7):1448–51, 1999. 13, 58

[KMTE03] H. Kato, T. Matsushita, A. Takayama, and M. Egawa. Theoretical analysis of optical and magneto-optical properties of one-dimensional magnetophotonic crystals. *J. Appl. Physics*, 93(7):3906–11, Apr. 2003. 32

[KR02] V. Krstic and G. L. J. A. Rikken. Magneto-chiral anisotropy of the free electron on a helix. *Chem. Phys. Lett.* , 364(1-2):51–6, 2002. 55

[KW98] P. Kleindienst and G. Wagnière. Interferometric detection of magnetochiral birefringence. *Chem. Phys. Lett.* , 288:89– 97, 1998. 12, 55, 85

[KZ77] S. Kielich and R. Zawodny. Linear and nonlinear magneto-optical effects in materials with spatial dispersion and magnetic ordering. *Physica B*, 89:122–5, 1977. 15

[Lid03] David R. Lide, editor. *Handbook of Chemistry and Physics*. CRC Press, ISBN: 0849304849, 84th edition, 2003. 36

[LLP84] L. D. Landau, E. M. Lifshitz, and L. P. Pitaevski. *Electrodynamics of Continuous Media*, volume 8 of *Course of Theoretical Physics*. Pergamon, Oxford, 2nd edition, 1984. 14, 17

[LOT97] S.-C. Lim, J. Osman, and D. R. Tilley. Theory of a gyromagnetic Fabry-Pérot resonator. *J. Phys.: Cond. Mat.* , 9:8297–8306, 1997. 23

[LvTRS98] D. Lacoste, B. A. van Tiggelen, G. L. J. A. Rikken, and A. Sparenberg. Optics of a Faraday-active Mie sphere. *J. Opt. Soc. Am A*, 15(6):1636–42, 1998. 23

[Man99] M. Mansuripur. The Faraday effect. Optics & Photonics News, Nov. , Nov. 1999. 28

[MBL+99] H. Miguez, A. Blanco, C. Lopez, F. Meseguer, H. M. Yates, M. E. Pemble, F. Lopez-Tejeira, F. J. Garcia-Vidal, and J. Sanchez-Dehesa. Face-centered cubic photonic bandgap materials based on opal-semiconductor composites. *J. Lightwave Technol.* , 17:1975, 1999. 49

[MBM+99] H. Miguez, A. Blanco, F. Meseguer, C. Lopez, H. M. Yates, M. E. Pemble, V. Fornes, and A. Mifsud. Bragg diffraction from indium phosphide infilled fcc silica colloidal crystals. *Phys. Rev. B*, 59(3):1563–6, 1999. 49

[MRV92] E. Munin, J. A. Roversi, and A. B. Villaverde. Faraday effect and energy gap in optical materials. *J. Phys. D: Appl. Phys.* , 25:1635, 1992. 44

[MWLV99] M. Megens, J. E. G. J. Wijnhoven, A. Lagendijk, and W. L. Vos. Light sources inside photonic crystals. *J. Opt. Soc. Am. B*, 16:1403, 1999. 49

[PB71] D. L. Portigal and E. Burstein. Magneto-spatial dispersion effects on the propagation of electro-magnetic radiation in crystals. *J. Phys. Chem. Solids*, 32:603–8, 1971. 15, 21

[PK92] J. B. Pendry and A. Mac Kinnon. Calculation of photonic dispersion relations. *Phys. Rev. Lett.* , 69:2772, 1992. 23, 31

[PRK69] T. G. Petrov, E. B. Reivus, and A. P. Kasatkin. *Growing Crystals from Solution*. Consultants Bureau, New York, 1969. 59, 73, 76

[PX99] S. H. Park and Y. Xia. Crystallization of meso-scale particles over large areas and its application in fabricating tunable optical filters. *Langmuir*, 15:266, 1999. 49

[Rau02] Ernst Raupach. *The Magneto-Chiral Anisotropy.* PhD thesis, Univ. Konstanz, 2002. 55, 58, 59

[RFW01] G. L. J. A. Rikken, J. Fölling, and P. Wyder. Electrical magnetochiral anisotropy. *Phys. Rev. Lett.* , 87:236602, 2001. 55

[RMSS98] A. V. Radchik, P. Moses, I. L. Skryabin, and G. B. Smith. New effective medium approach to optical response in non-random arrays. *Thin Solid Films*, 317(1-2):446–8, 1998. 49

[RMT+99] S. G. Romanov, T. Maka, C. M. Sotomayor Torres, M. Mueller, and R. Zentel. Emission properties of dye-polymer-opal photonic crystals. *J. Lightwave. Technol.* , 17:2121, 1999. 49

[RR97] G. L. J. A. Rikken and E. Raupach. Observation of magneto-chiral dichroism. *Nature (London)*, 390:493, 1997. 12, 55, 85

[RR98] G. L. J. A. Rikken and E. Raupach. Pure and cascaded magnetochiral anisotropy in optical absorption. *Phys. Rev. E*, 58(4):5081–4, 1998. 55, 58, 85, 89

[RR00] G. L. J. A. Rikken and E. Raupach. Enantioselective magnetochiral photochemistry. *Nature (London)*, 405:932, Jun. 2000. 13, 55

[RRTM00] E. Raupach, G. L. J. A. Rikken, C. Train, and B. Malézieux. Modelling of magneto-chiral enantioselective photochemistry. *Chem. Phys.* , 261:373, 2000. 85, 89

[RvT96] G. L. J. A. Rikken and B. A. van Tiggelen. Observation of magnetically induced transverse diffusion of light. *Nature (London)*, 381:54, 1996. 23

[Sak01] Kazuaki Sakoda. *Optical Properties of Photonic Crystals.* Optical Sciences. Springer, 2001. ISSN 0342-4111. 26

[SGK87] K. Stadnicka, A. M. Glazer, and M. Koralewski. Structure, absolute configuration and optical activity of alpha-nickel sulfate hexahydrate. *Acta Crist.* , B43:319–325, 1987. 57

[SKB96] B. Sareni, L. Krähenbühl, and A. Beroual. Effective dielectric constant of periodic composite materials. *J. Appl. Phys.* , 80(3):1688–96, 1996. 49

[SKM92] N. Stefanou, V. Karathanos, and A. Modinos. Scattering of electromagnetic waves by periodic structures. *J. Physics condensed Mat.* , 4(36):7389–400, 1992. 31

[Taf95] A. Taflove. *Computational Electrodynamics: The Finite-Difference Time Domain Method.* Artech House, Boston, 1995. 31

[VAB+00] Y. A. Vlasov, V. N. Astratov, A. V. Baryshev, A. A. Kaplianskii, O. Z. Karimov, and M. F. Limonov. Manifestation of intrinsic defects in optical properties of self-organized opal photonic crystals. *Phys. Rev. E*, 61(5):5784–93, 2000. 45

[VGF+01] M. Vallet, R. Ghosh, A. Le Floch, T. Ruchon, F. Bretenaker, and J.-Y. Thepot. Observation of magnetochiral birefringence. *Phys. Rev. Lett.* , 87(18):183003, Oct. 2001. 12, 55, 85

[VSvB+96] W. L. Vos, R. Sprik, A. van Blaaderen, A. Imhof, A. Lagendijk, and G. H. Wegdam. Strong effects of photonic band structures on the diffraction of colloidal crystals. *Phys. Rev. B*, 53:16231, 1996. Erratum: Phys. Rev. E **55** (1997) 1903. 49

[XGP99] Y. Xia, B. Gates, and S. H. Park. Fabrication of three-dimensional photonic crystals for use in the spectral region from ultraviolet to near-infrared. *J. Lightwave. Technol.* , 17:1956, 1999. 49

[Yeh80] P. Yeh. Optics of anisotropic layered media: a new 4*4 matrix algebra. *Surf. Science*, 96(1-3):41–53, 1980. 31

[YSK97] C.-Y. You, S.-C. Shin, and S.-Y. Kim. Modified effective-medium theory for magneto-optical spectra of magnetic materials. *Phys. Rev. B*, 55(9):5953–8, 1997. 49

[ZK97] A. K. Zvezdin and V. A. Kotov. *Modern Magneto-optics and Magneto-optical Materials*. Studies in Condensed Matter Physics. Institute of Physics Publishing, Bristol, UK, 1997. 28, 29

Appendix A

Acknowledgments — Danksagung Remerciements — Dank U

I would like to pay tribute to Geert Rikken for the excellent supervision of this thesis and his continuing input of outstanding scientific expertise.
I am also very much indebted to Prof. Peter Wyder for the trust he put in me and his guidance.
The dissertation was performed at the Grenoble High Magnetic Field Laboratory with the financial backing of the Max Planck Society.
I wish to thank Prof. Schatz from the University of Konstanz, who kindly excepted to coexpertise this work.

In gratitude for the fruitful collaboration, I would like to thank Eugene Petrov from the Stephanov Institute of Physics in Minsk, Belarus.
I also wish to thank Willem Vos from the University of Amsterdam and Cefe López from the Material Science Institute of Madrid for their photonic crystal samples.

It is a pleasure for me to commend my dear colleagues for their stimulant vision and personality and of course their friendship: Georg Düchs, Ernst Raupach, Cornelius Strohm, Roman Kramer, Thomas Roth, Ekkehard Teske, Barbaros Özyilmaz, Enno Bibow, David Schaeffer, Ilya Sheikin, Markus Weiß, Andreas Gröger, Roland Schleser, Francisco Teran, and Jörg Hinderer.

And last but not least, let me thank my wife Loubna and my son Jazil for cheering up my private life during that time.

Appendix B

Publications

The following publications contain work performed in the context of the present dissertation:

C. Koerdt, G. Düchs, and G. L. J. A. Rikken.
'Magnetochiral anisotropy in Bragg scattering'.
Physical Review Letters **91**(7), 073902, 12 August 2003.

C. Koerdt, G. L. J. A. Rikken, and E. P. Petrov.
'The Faraday effect of photonic crystals'.
Applied Physics Letters **82**(10), pp. 1538-1540, 10 March 2003.
Also at: *Virtual Journal of Nanoscale Science & Technology* **17**(11), 17 March 2003.

There are some more publications planned:

C. Koerdt, and G. L. J. A. Rikken.
'Chiral symmetry breaking in photo-crystallization'.
unpublished.

C. Koerdt.
'Resonant Magneto-Chiral Anisotropy'.
unpublished (invited by Modern Physics Letters B to submit a Brief Review).